THE ORGANIZATION OF SPIRAL RAINBANDS

IN A HURRICANE

by

Inez Yau-Sheung Fung

.

S.B   Massachusetts Institute of Technology
(1971)

SUBMITTED IN PARTIAL FULFILLMENT
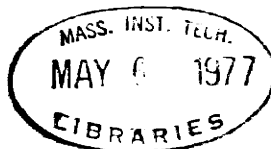OF THE REQUIREMENTS FOR THE
DEGREE OF

DOCTOR OF SCIENCE

at the

MASSACHUSETTS INSTITUTE OF TECHNOLOGY

January, 1977

Signature of Author ....
Department of Meteorology, January 1977

Certified by ....
Thesis Supervisor

Accepted by ....
Chairman, Departmental Committee on Graduate Students

THE ORGANIZATION OF SPIRAL RAINBANDS IN A HURRICANE

by

Inez Yau-Sheung Fung

Submitted to the Department of Meteorology on
20 January 1977, in partial fulfillment of the
requirements for the degree of Doctor of Science

ABSTRACT

Radar pictures of hurricanes show a characteristic and persistent (for three to four days) spiral pattern of rainbands, even though the life of individual cumulus clouds is less than two hours. These rainbands have radial wavelengths of 20 to 60 km and remain quasi-stationary relative to the storm center. In this thesis, we hypothesize that the underlying wave pattern which organizes the cumulus clouds into the observed spiral bands is a result of the Rayleigh instability of the boundary layer of the hurricane.

The steady state, axisymmetric and non-linear boundary layer flow under a hurricane-like vortex is solved numerically by the "pseudo-time-marching" method of Rivas (1975). A linear perturbation analysis is performed on the mean flow thus obtained, which possesses both radial and vertical shears. By approximating the vertical structure by three layers of constant shear, and by assuming that the spirals are tightly wound, we obtain, analytically, a dispersion relationship relating the wavenumbers and frequencies of the perturbations.

A global eigenvalue analysis of the dispersion relationship reveals that the most unstable wave has lines of constant phase which correspond well to the spiral arms observed in a hurricane. The most unstable wave is trapped both radially and vertically, and the spiral rainbands persist as long as the hurricane maintains its circulation.

Thesis Supervisor: Jule G. Charney
Title: Sloan Professor of Meteorology

DEDICATION

To

My father and my mother

ACKNOWLEDGEMENTS

TABLE OF CONTENTS

LIST OF FIGURES

LIST OF TABLES

Fig. 1.1

Radar picture of Hurricane Caroline on August 31, 1975 taken
by WSR-57 radar at Brownsville, Texas. (From film loop of
radar pictures of Caroline. Courtesy of Mr. Billy Lewis, NHEML.)

CHAPTER ONE – INTRODUCTION

Radar and satellite observations of the mature hurricane have revealed characteristically a very organized and persistent pattern of clouds. The eyewall, a ring of intense cumulus activity, circles the cloud-free eye at a radius of about 20 km, while, away from the eyewall, spiral bands of clouds extend to as far as 500 km from the storm center. Two types of spiral cloud bands are observed. Land-based radar, which looks at low-level cloud distributions, reveals individual convective cells grouped together to form spiral bands separated by clear regions. These radar bands have radial wavelengths of 20 to 60 km and widths of about half this or 10 to 30 km. The pattern of these bands, the "grand design", is fairly constant in shape, and lasts throughout the life of the mature storm. Figure 1.1 shows a picture of Hurricane Caroline taken by WSR-57 radar at Brownsville, Texas, on August 31, 1975. Because of the curvature of the earth, and the usually weaker convective activity at large distances from the center, the radarscope captures the spiral pattern only within a radius of about 200 km. There also appears to be a spiral cloud structure of larger radial wavelength, ca 200 km, which is revealed by brightness enhancement of satellite photographs of the cirrus cloud cover of the hurricane. In this thesis, we shall be concerned only with the short wavelength spiral bands, and shall refer to them as spiral rainbands.

In 1964, Charney and Eliassen demonstrated the importance of friction, together with cumulus clouds, on the growth of a hurricane depression.

Frictional convergence in the boundary layer supplies moisture to the clouds, and the clouds supply latent heat energy to the cyclone to cause its growth. In this thesis, we shall attempt to show that in a mature hurricane, it is the instability of the frictionally induced inflow into the hurricane which is responsible for the organization and persistence of the spiral rainband pattern.

1.1 KINEMATICS OF RAINBANDS

The rainbands have a very constant shape characterised by the crossing angle, which is defined as the angle which the spiral makes with a circle concentric with the storm center. The crossing angle is defined to be positive if the rainbands spiral outward anticyclonically. Senn et al. (1957) found that only a few logarithmic spiral patterns with varying crossing angles (α) are needed to fit all the bands observed on the radarscope. These log spirals are described by

$$\frac{1}{r}\frac{dr}{d\theta} = \tan \alpha = \beta\left(1 - \frac{R_0}{r}\right) \tag{1.1.1}$$

where $\beta = \tan 20°$, and R_o = radius of eyewall. An average value of the crossing angle is 15°. According to Senn et al., the patterns have from two to seven arms. Malkus et al. (1961) found that the rainbands maintain a quasi-conservative position relative to the quadrants in which they are found and do not rotate about the storm center. By comparing cloud and radar photographs of Hurricane Daisy on August 25 and 27, 1958, Malkus et al. found that the major bands of Daisy on the two days remained in approximately the same position and orientation relative to the eye.

They moved only some 10 to 20 n.m. closer to the center in two days!
However, Senn and Hiser (1959), by measuring individual echoes in a single
band and plotting their half-hourly positions, and identifying their mo-
tions as that of the band itself, found an apparent propagation radially
outwards at speeds of 4 to 30 kts. They also found that the lifetime of
an individual band is rather short — about 35 minutes, which is about
the lifetime of the echoes that compose the band. The longest-lived ones
last for about two hours. In contrast, Senn et al. (1957) observed that
the bands moved with the mean wind at 2500 feet where the radial speed is
about 2 to 4 kts.

To resolve this contradictory evidence concerning the propagation
of the rainbands, the author studied the film loop of radar pictures of
Hurricane Caroline. A sequence of six pictures of Caroline taken at ten-
minute intervals is displayed in Figure 1.2. Over the twelve hours or so
of observation, it was found that the spacings between the bands remained
nearly constant even though the bands were often irregular and fragmented.
At no time was band propagation or band generation near the center ob-
served, as when a pebble is dropped into a pond. Senn and Hiser were
tracking the migration of a specific set of radar echoes, not an indivi-
dual band. An individual band may have the appearance of propagating
outwards if the echoes which compose them travel with a velocity component
which is directed radially outwards.

1.2 RADAR ECHOES

Rainbands are made up of stratocumulus clouds, except perhaps for
the band closest to the eyewall of an intense hurricane. These rainband
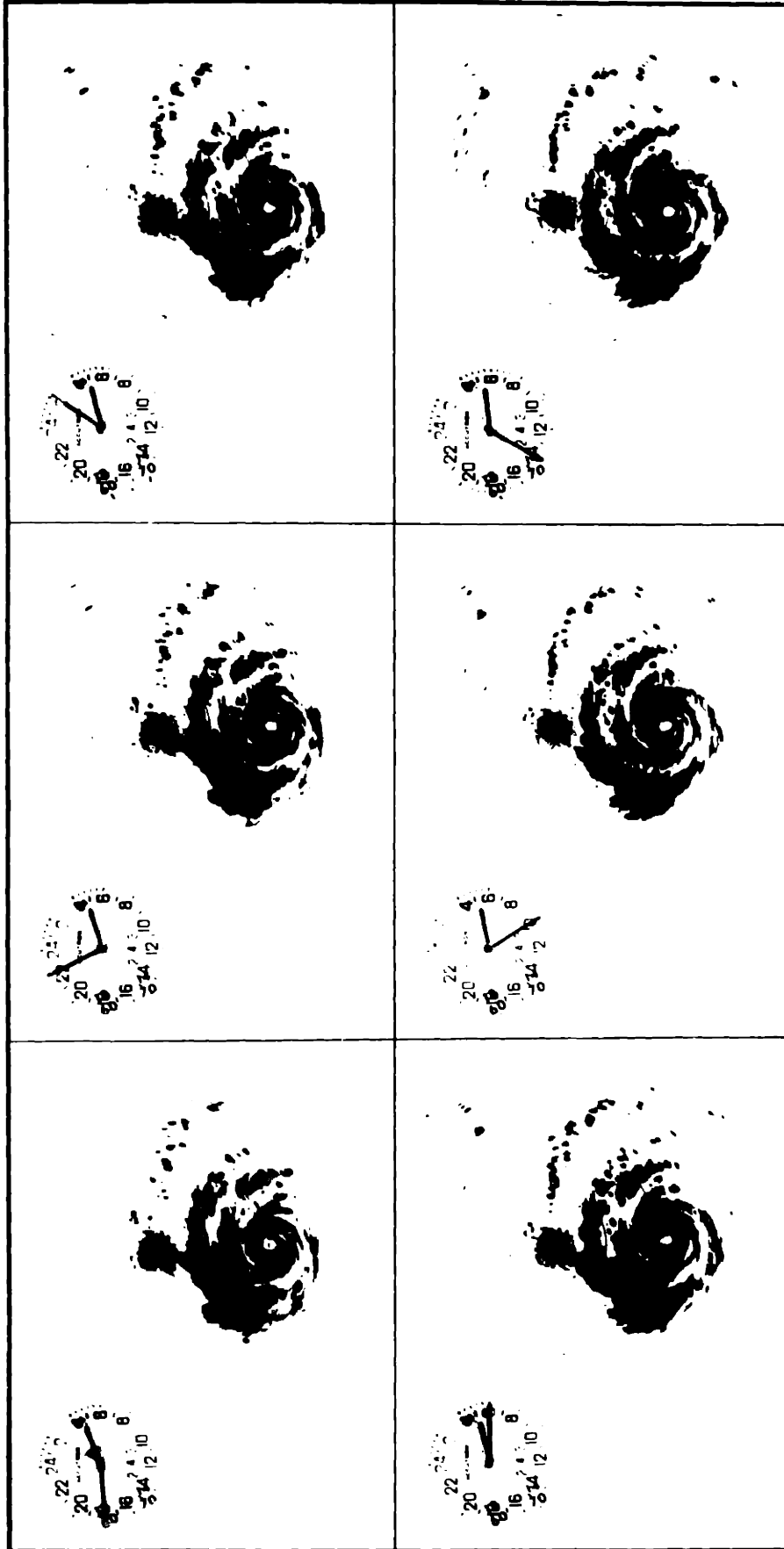
Fig. 1.2 Time lapse photographs of Hurricane Caroline on August 31, 1975. (from film loop of radar pictures of Caroline. Courtesy of Mr. Billy Lewis, NHEML.)

clouds are not very tall [Hawkins et al. (1976)]. They are generated on the upwind side of the band, and move cyclonically across the band and dissipate on the downwind side. Their speed of propagation along a band is of the order of 100 km/hr [Tatehira (1961)], giving a circumferential speed of the same order and a radial speed of 100 sin (α) km/hr or 17 km/hr for the crossing angle of 10° found by Tatehira. He attributed an apparent outward propagation of the band again to the radial propagation of the echoes.

1.3 ROLE OF LATENT HEAT

In the mature hurricane, the eyewall, a site of intense convective activity is made up of cumulonimbus towers reaching to the tropopause. Except perhaps for the rainband closest to the eyewall, however, the clouds in the outer portions of the hurricane are not very tall (Figure 1.3). Ligda (1955) found that the echoes in the rainbands were indeed stratiform in character. The numerical experiments of Kurihara (1976) and Diercks and Anthes (1976a) also showed that the artificial supression of latent heat release did not affect the formation or propagation of the gravity waves they found. Thus, although latent heat release plays an active and necessary role in the formation and maintenance of the hurricane circulation, we shall assume that its influence on the organization of the rainbands may be neglected. This is, of course, not to say that there is no feedback from the latent heat release, only that the feedback is not a dominating effect.
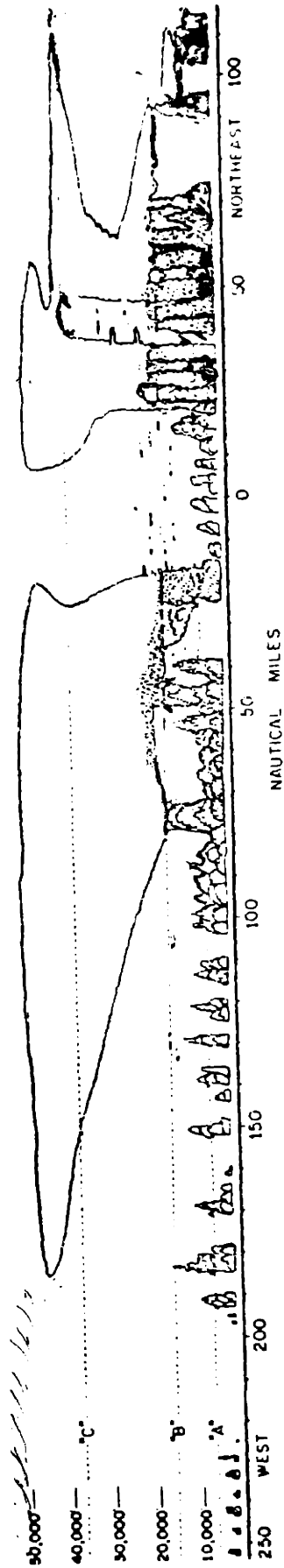
Fig 1.3   Vertical crossection through Cleo, August 18, 1958, showing cloud structure and heavier radar echos.   Note that convection is concentrated in the inner portion of the storm especially in the wall cloud around the eye.   (From La Seur, 1961.)

1.4 THEORIES OF BAND FORMATION

Early investigators of the rainbands made conjectures about their formation based on their observations:

Fletcher (1945) and Wexler (1947) suggested that the bands were cloud streets in the trade wind area or the Intertropical Convergence Zone which have "coiled into the hurricane".

Kessler and Atlas (1956) attributed the spiral bands to a banded structure in low-level horizontal convergence. This is confirmed by the analysis of Tatehira (1961). However, neither of these authors gave a cause for the convergence pattern.

Senn and Hiser (1958, 1959) suggested that "a strong vertical up-thrust at the eyewall" moving around the eye as an oscillating disturbance would create one portion of a spiral band in a given quadrant at a given time and another portion of the spiral at a later time in the next counterclockwise quadrant. Gravity wave propagation in the vortex or advection in the hurricane's outflow at cirrus levels would then provide the mechanism for the outward propagation of the spirals.

Atlas et al. (1963) envisioned the oscillating disturbance as a convective tower (plume) displaced from the eyewall. The plume in spreading downstream would trace out a spiral. They believed that an instability at the base of the melting layer would generate roll clouds like the rainbands. Contrary to the conjectures of previous investigators, they thought that it is the spiral clouds themselves which determine where the low level lifting and convergence will occur.

Because their observations showed a remarkable persistence of the rainband pattern over three days, Malkus et al. suggested a stable interaction between the convective and hurricane scale motions in such a way

that cloud regeneration occurs in a few favored locations. They did not, however, elaborate on the nature of this interaction.

Both Tepper (1958) and Abdullah (1966) presented models of gravity waves propagating along an inversion surface. They likened the formation of hurricane bands to that of squall lines in mid-latitudes. However, the interfacial waves obtained by Abdullah travel at an impossible speed — 240 km/hr.

Three-dimensional simulations of the hurricane have produced banded structures of spiral shape. Yamamoto (1963) recognized that for disturbances proportional to $e^{i(mnr + l\theta)}$, the lines of constant phase are spirals. Krishnamurti (1961), Anthes et al. (1971), Anthes (1972), Kurihara and Tuleya (1974), Mathur (1975), and Diercks and Anthes (1976a) all performed time integration experiments using elaborate multi-leveled primitive equation models which included the effects of friction and latent heat release. All their models produced spiral bands of vertical motion which appeared to originate near the storm center and propagate radially outwards. Because the smallest grid size used by these investigators was 20 km, they were unable to resolve the short-wavelength rainbands and obtained spiral bands with radial wavelengths of about 200 km. Although none of the above models explained the origins of the rainbands, they do shed some light on the nature of spiral-shaped waves in a hurricane vortex.

In experiments in which he included latent heat released by ascending moist air at 375 mb (non-convective latent heat release) in addition to convective release of latent heat above the boundary layer, Mathur (1975) obtained propagating spiral bands of upward motion which

developed where strong divergence took place in the upper troposphere of the outflow region. The bands failed to develop when the upper level heating was excluded.

Anthes et al (1971) and Anthes (1972) obtained pronounced spiral bands of upward motion at the top of the boundary layer when their hurricane model developed asymmetries in the outflow region. These bands had radial wavelengths of the order of 200 km, propagated outwards at a speed of 24 kts. and had lifetimes of 2.5 days.

Diercks and Anthes (1976a) showed that these bands were traveling gravity waves with associated strong convergence of cyclonic angular momentum in the boundary layer. When they artificially supressed latent heat release from both convective and non-convective processes, they found that the bands continued to propagate outwards, suggesting that latent heat release in the bands was a result, rather than a cause, of the convergence pattern associated with the traveling wave and hence did not play an important role in the maintenance or propagation of the bands.

Kurihara and Tuleya (1974) obtained spiral bands also of the order of 200 km wavelength which moved outwards at speeds of 50 to 100 km/hr. These bands behaved like internal gravity waves. These authors favored, but did not substantiate, the moving point source suggestion of Senn and Hiser (1959) as the generating mechanism for the bands.

Kurihara (1976) solved an eigenvalue problem for perturbations which were Archimedes spirals (with constant wavelengths in the radial direction). His basic state was a hurricane-like vortex which had shears in both the radial and the vertical directions. Kurihara found that the pattern with two arms and radial wavelength of 200 km had the fastest

growth rate. This wave grew near the center of the storm, derived its

energy from the radial shear kinetic energy of the mean wind, propagated

outward and became a neutral gravity wave. His results supported Diercks

and Anthes' numerical result that latent heat release is not important

for the formation and propagation of the spiral bands.

Diercks and Anthes (1976b) found that the formation of the spiral

bands requires rotation in the mean state, though not inertial instability.

1.5 THE PRESENT INVESTIGATION

The problem of spiral bands in a differentially rotating vortex

is not unique to the hurricane. Lin and his co-workers [see e.g. Lin and

Shu (1964), Lin (1970)] have developed the Density Wave Theory to explain

the grand design of the spiral galaxies. The central problem to these

spiral patterns is very well described by Oort (1962) as quoted by Lin

(1966) in an article concerning spiral galaxies:

> In systems with strong differential rotation, such as
> found in all nonbarred spirals, spiral features are
> quite natural. Every structural irregularity is likely
> to be drawn out into a part of a spiral. But this is
> not the phenomenon we must consider. We must consider
> a spiral structure extending over the whole galaxy,
> from the nucleus to its outermost part, and constituting
> two arms starting from diametrically opposite points.
> Although this structure is often hopelessly irregular
> and broken up, the general form of the large-scale
> phenomenon can be recognized in many nebulae.

Indeed, in a Cartesian coordinate system, any wave of the form

$e^{i(kx + \ell y - \omega t)}$ has wavefronts which are parallel straight lines making

angles of $\tan^{-1}\left(-\dfrac{\ell}{k}\right)$ with the x-axis. They propagate with a phase

speed given by $c_{ph} = \dfrac{\omega}{k}$. Similarly, then, in a cylindrical coordinate

system, any wave of the form $e^{i(\Phi(r) + m\theta - \omega t)}$, where $\Phi(r)$ is a well-behaved function of r, m is a positive integer, and ω is a constant, has lines of constant phase given by the curve

$$\Phi(r) + m\theta = constant \qquad (1.1.2)$$

which describes a spiral pattern. The pattern has m arms. The "crossing angle" α which the spiral makes with a concentric circle is given by

$$\alpha = \tan^{-1} \left[\frac{m/r}{k(r)} \right] \qquad (1.1.3)$$

where $k(r) = \frac{d\Phi}{dr}$ is the wavenumber in the radial direction. If $k(r)$ is positive, then the spiral will appear as a "trailing" spiral. If $k(r)$ is negative, while m remains positive, then the spiral is a "leading" spiral. (See Figure 1.4.) The spiral propagates in the r-direction with a phase speed given by $c_{ph} = \frac{\omega}{k}$.

In view of the above discussion, the questions to ask, then, are not why there should be spirals, but rather:

1) why the spiral which we would _expect_ in a differentially rotating hurricane should possess the wavelengths and phase speeds that are observed; and

2) why the spiral pattern should persist for periods of three days or more when the lifetime of the convective cells which compose them last for no more than two hours.

The answer does not lie in the suggestions of Fletcher and Wexler that the rainbands are cloud streets which have coiled into the hurricane. For then in the course of a day or two there would be an increasing pile-up
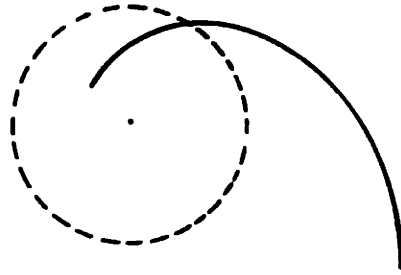
trailing spiral: $m > 0$, $k(r) > 0$
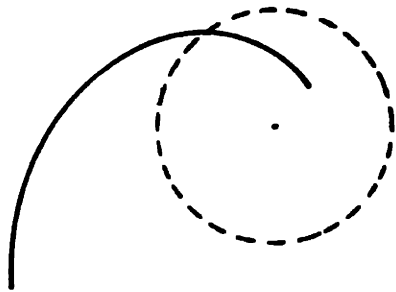
leading spiral: $m > 0$, $k(r) < 0$

Fig. 1.4   Schematic picture of trailing and leading spirals.

of cloud streets wound into or near the center of the storm. This is not observed.

Nor are the rainbands just gravity waves propagating outwards as suggested by Anthes (1971, 1972), Kurihara and Tuleya (1974), and Diercks and Anthes (1976a). These gravity waves would tend to disappear from the scene unless there were a continuous generating mechanism or a feedback process to replenish them. Moreover, the gravity wave spirals obtained by these authors have wavelengths about ten times those observed on the radarscope.

The mechanism that we propose for the explanation of both the structure and the lifetime of the spiral rainbain pattern is Rayleigh instability in the hurricane boundary layer above the sea surface. (See Lin (1955) for a discussion of Rayleigh instability.) This explanation was originally suggested by Faller (1961) who noted the similarity between the crossing angle and spacing of the rainbands and those observed in an experimental study of the instability of the laminar Ekman layer. However, further investigations by Faller (1966, 1972) were concerned with the instability of the local Ekman flow, and did not deal with the global instability of the entire hurricane boundary layer.

Because of the strong winds in the hurricane, its boundary layer structure is determined frictionally rather than convectively. Thus it possesses Ekman-like velocity profiles which have inflection points in the inflow velocity $\bar{U}$. The presence of the inflection point (or vorticity extremum) is in our case a sufficient as well as necessary criterion for instability. The inflection point then occurs in the lowest kilometer of the hurricane. The most unstable waves would have wavelengths about ten times the depth of shear across the inflection point [Rayleigh

(1-80)]. They would orient themselves to the mean flow so as to maximize the shear across the inflection point in the velocity component perpendicular to the wavefront. They would also propagate at a speed equal to the mean wind at the inflection point so that there could be most efficient extraction of energy from the mean flow.

Indeed, the average crossing angle of 15° for the rainbands agrees well with that for the most unstable wave of the local Ekman flow [Faller (1964), Tatro and Mollo-Christensen (1967)]. Also the observation that the bands move with the speed of the mean wind at 2500 feet (0.8 km) [Senn, Hiser and Bourret (1957)] supports Rayleigh instability as the generating mechanism for the rainbands.

The picture we propose for the spiral rainbands is as follows: Rayleigh instability of the hurricane boundary layer manifests itself as spiral regions of alternate upward and downward velocities. Inflowing moist air in the lowest kilometer of the hurricane then, on encountering this spiral wave pattern, rises (sinks) in the region of upward (downward) motion, forming clouds (clear regions). The spiral rainband pattern thus does not possess the same clouds throughout its three or more days of existence, but merely provides a site for cloud formation. It turns out that these waves are trapped both in the vertical and in the radial direction (see Chapter 4). Thus, even when the waves attain finite amplitude equilibrium with the mean flow (which we shall not consider in this study), the spiral wave pattern is capable of existing as long as the hurricane maintains its strength.

Chapter 2 of this thesis presents the governing equations for the basic state and the small-amplitude short-wave perturbations. The method

of multiple scales is briefly reviewed. This method allows, on the scale of variation of the phase of the waves, separation of the horizontal and vertical dependencies in the perturbation equations. The nonlinear inseparable basic state equations are solved in Chapter 3 by the Rivas scheme (1975). By employing the large Reynolds number approximation and a three-layer representation of the basic state found in Chapter 3, we obtain, in Chapter 4, the local dispersion relationship governing the frequencies and horizontal wave numbers of the waves. By applying the radial boundary conditions, the global dispersion relationship is obtained, from which we find the wave with the fastest growth rate. Finally, the wave amplitude is determined again using the method of multiple scales.

CHAPTER TWO – THE MODEL

2.1 GEOMETRY

We shall consider a stationary circular vortex on an f-plane. Its geometry is illustrated in Figure 2.1. It is semi-infinite in the vertical, bounded below by a rigid bottom, and it extends from some radius R_o radially outwards to infinity. It consists of two layers in the vertical: the upper one corresponding to the stably stratified quasi-Boussinesq interior of the hurricane, and the lower layer, its associated boundary layer. We assume that the boundary layer is neutrally stratified.

2.2 GOVERNING EQUATIONS

We shall develop the basic state and linearized equations in our model in cylindrical coordinates (r, θ, z) whose center coincides with the center of the storm. The corresponding velocity components are (u, v, w). The notation for the velocity components is illustrated in Figure 2.2.

For the sake of completeness, we shall develop the equations for a stratified boundary layer. In actual application, the frictional terms in the interior and the buoyancy terms in the boundary layer equations are neglected.

The dimensional equations for a quasi-Boussinesq fluid are:
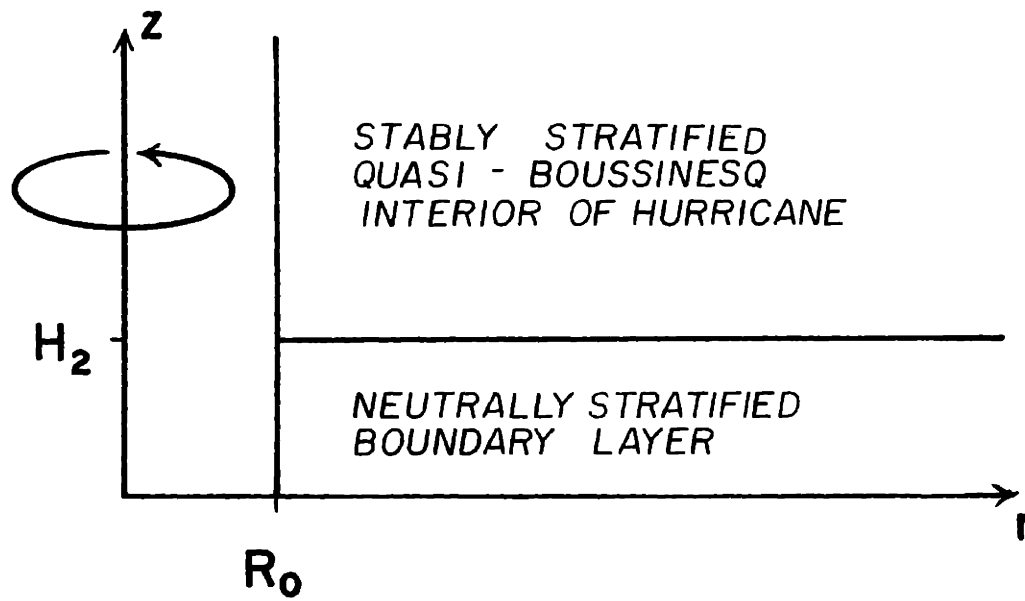
Fig. 2.1   Geometry of the model.

Fig. 2.2   Notation of coordinate system and velocity
components.

$$\frac{\partial u_*}{\partial t_*} + u_* \frac{\partial u_*}{\partial r_*} + \frac{v_*}{r_*}\frac{\partial u_*}{\partial \theta} + w_* \frac{\partial u_*}{\partial z_*} - \frac{v_*^2}{r_*^2} - f v_*$$

$$= -\frac{1}{\rho_*}\frac{\partial p_*}{\partial r_*} + \nu \nabla_*^2 u_* \qquad (2.2.1)$$

$$\frac{\partial v_*}{\partial t_*} + u_* \frac{\partial v_*}{\partial r_*} + \frac{v_*}{r_*}\frac{\partial v_*}{\partial \theta} + w_* \frac{\partial v_*}{\partial z_*} + \frac{u_* v_*}{r_*} + f u_*$$

$$= -\frac{1}{\rho_*}\frac{1}{r_*}\frac{\partial p_*}{\partial \theta} + \nu \nabla_*^2 v_* \qquad (2.2.2)$$

$$\frac{\partial w_*}{\partial t_*} + u_* \frac{\partial w_*}{\partial r_*} + \frac{v_*}{r_*}\frac{\partial w_*}{\partial \theta} + w_* \frac{\partial w_*}{\partial z_*}$$

$$= -\frac{1}{\rho_*}\frac{\partial p_*}{\partial z_*} - g + \nu \nabla_*^2 w_* \qquad (2.2.3)$$

$$\frac{\partial}{\partial t_*}(\ln \Theta_*) + u_* \frac{\partial}{\partial r_*}(\ln \Theta_*) + \frac{v_*}{r_*}\frac{\partial}{\partial \theta}(\ln \Theta_*)$$

$$+ w_* \frac{\partial}{\partial z_*}(\ln \Theta_*) = 0 \qquad (2.2.4)$$

$$\frac{\partial u_*}{\partial r_*} + \frac{u_*}{r_*} + \frac{1}{r_*}\frac{\partial v_*}{\partial \theta} + \frac{1}{\rho_*}\frac{\partial}{\partial z_*}(\rho_* w_*)$$

$$= 0 \qquad (2.2.5)$$

where

$$\nabla_*^2 = \frac{\partial^2}{\partial r_*^2} + \frac{1}{r_*}\frac{\partial}{\partial r_*} + \frac{1}{r_*^2}\frac{\partial^2}{\partial \theta^2} + \frac{\partial^2}{\partial z_*^2} \qquad (2.2.6)$$

We non-dimensionalize and linearize at the same time, with the barred quantity $\overline{(\quad)}$ representing the basic state, and the primed quantity $(\quad)'$ the perturbations. The starred quantities are dimensional, and the unstarred ones are non-dimensional.

$$t_* = \frac{D}{U} \, t$$

$$u_* = U \, (\overline{U} + u')$$

$$v_* = U \, (\overline{V} + v')$$

$$w_* = U \, (\frac{D}{L} \, \overline{W} + w')$$

$$\rho_* = \rho_o (\overline{\rho} + \rho') \tag{2.2.7}$$

$$P_* = \rho_o \, U^2 (\overline{p} + p')$$

$$\ln\Theta_* = \ln \overline{\Theta} + \frac{\theta'}{\overline{\theta}}$$

$$r_* = Dr$$

$$z_* = Dz$$

where $D = \sqrt{\nu/f}$, L = overall radial scale of hurricane

2.2.1 Scaling of r

In the hurricane, there are two radial scales. The mean hurricane circulation varies on the scale of the radius of the storm, $L \sim 500$ km ; the radial wavelength of the rainbands is only about 15 km near the eye, and about 30 to 60 km farther out. We have used $D \sim 1$ km as the scaling parameter for r_* in Equation (2.2.7), even though the wavelengths we are interested in are at least ten times D. This is consistent with

Rayleigh's (1880) prediction that wavelength (λ) of the most unstable wave is related to the depth of the shear region (b) (In Rayleigh's notation, $\lambda = 8b$). In this problem, the depth of the shear is of the order of the boundary layer depth D.

To separate these two scales, we introduce the method of multiple scales (See Nayfeh (1973), Chapter 6, for detailed discussion). The method of multiple scales is a generalization of the WKB method which is applicable only to ordinary differential equations.

Instead of using the one radial coordinate r (which is scaled by D), we introduce two new radial coordinates r_0 and r_1 :

$$r_1 = \epsilon r \; ; \qquad r_0 = \frac{1}{\epsilon} \Phi(r_1) \tag{2.2.8}$$

where $\epsilon = \frac{D}{L} \ll 1$, and $\Phi(r_1)$ is to be determined from the analysis.

Then,

$$\frac{\partial}{\partial r} = \frac{\partial r_0}{\partial r} \frac{\partial}{\partial r_0} + \frac{\partial r_1}{\partial r} \frac{\partial}{\partial r_1}$$

$$= \frac{1}{\epsilon} \frac{d\Phi}{dr_1} \frac{dr_1}{dr} \frac{\partial}{\partial r_0} + \epsilon \frac{\partial}{\partial r_1}$$

$$= \frac{d\Phi}{dr_1} \frac{\partial}{\partial r_0} + \epsilon \frac{\partial}{\partial r_1}$$

We define $k(r_1) \equiv \frac{d\Phi}{dr_1}$ and $|k(r_1)| \sim O(1)$, so that

$$r_0 = \frac{1}{\epsilon} \int_{R_0}^{r_1} k(r_1') \, dr_1' \tag{2.2.9}$$

and

$$\frac{\partial}{\partial r} = k(r_1) \frac{\partial}{\partial r_0} + \epsilon \frac{\partial}{\partial r_1} \tag{2.2.10}$$

Then a quantity $q(r, \theta, z, t)$ is now a function of (r_0, r_1, θ, z, t) .

$$q(r, \theta, z, t) \rightarrow q(r_0, r_1, \theta, z, t)$$

An $O(1)$ variation in r_0 corresponds to an $O(1)$, or "fast" variation in r, whereas an $O(1)$ variation in r_1 corresponds to an $O(\epsilon^{-1})$, "slow", variation in r. In other words, r_0 characterizes the "small"

scale phenomena, which vary "quickly" on the scale of D, and r_1 charac-terizes the "large" scale phenomena, which vary "slowly" on the scale of D.

The steady basic state variables, which show no small-scale varia-tions, are then functions of r_1 and z only.

$$\bar{U}(r, z) \rightarrow \bar{U}(r_1, z)$$

and the perturbation quantities, which have small-scale phase variation and large-scale amplitude variation, depend on both r_0 and r_1.

$$u'(r, \theta, z, t) \rightarrow u'(r_0, r_1, \theta, z, t)$$

As a result of the scaling procedure, two non-dimensional numbers appear:

the Rossby number $Ro = \dfrac{U}{fL}$

and the Reynolds number $Re = \dfrac{U}{fD} = \dfrac{UD}{\nu} = \dfrac{U}{\sqrt{f\nu}}$ (2.2.11)

with $D = \sqrt{\dfrac{\nu}{f}}$

and they are related by the radial scaling parameter we have defined

$$Re = \epsilon^{-1} Ro \qquad (2.2.12)$$

2.3 THE NON-DIMENSIONAL BASIC STATE EQUATIONS

We assume that the mean hurricane is steady and axisymmetric. Then the non-dimensional basic state equations are:

$$Ro\left(\bar{u}\frac{\partial \bar{u}}{\partial r_1} + \bar{w}\frac{\partial \bar{u}}{\partial z} - \frac{\bar{v}^2}{r_1}\right) - \bar{v} = -Ro\frac{\partial}{\partial r_1}\left(\frac{\bar{p}}{\bar{\rho}}\right) + \frac{\partial^2 \bar{u}}{\partial z^2} \quad (2.3.1)$$

$$Ro\left(\bar{u}\frac{\partial \bar{v}}{\partial r_1} + \bar{w}\frac{\partial \bar{v}}{\partial z} + \frac{\bar{u}\bar{v}}{r_1}\right) + \bar{u} = \frac{\partial^2 \bar{v}}{\partial z^2} \quad (2.3.2)$$

$$0 = -\frac{1}{\bar{\rho}}\frac{\partial \bar{p}}{\partial z} - \frac{g D}{U^2} \quad (2.3.3)$$

$$\frac{1}{r_1}\frac{\partial r_1 \bar{u}}{\partial r_1} + \frac{1}{\bar{\rho}}\frac{\partial \bar{\rho}\bar{w}}{\partial z} = 0 \quad (2.3.4)$$

2.4 THE NON-DIMENSIONAL PERTURBATION EQUATIONS

The linearized equations governing the behavior of three-dimensional perturbations of the steady axisymmetric mean state are

$$Re\left[\frac{\partial u'}{\partial t} + R\bar{u}\frac{\partial}{\partial r_0}u' + \frac{\bar{v}}{r_0}\frac{\partial u'}{\partial \theta} + w'\frac{\partial \bar{u}}{\partial z} + R\frac{\partial}{\partial r_0}\left(\frac{p'}{\bar{\rho}}\right)\right]$$
$$- v' - \nabla^2 u' = -\epsilon Re\left[u'\frac{\partial \bar{u}}{\partial r_1} + \bar{u}\frac{\partial u'}{\partial r_1} + \bar{w}\frac{\partial u'}{\partial z}\right.$$
$$\left. - \frac{2\bar{v}}{r_1}v' + \frac{\partial}{\partial r_1}\left(\frac{p'}{\bar{\rho}}\right)\right] + \epsilon \mathcal{F}(u') \quad (2.4.1)$$

$$Re\left[\frac{\partial v'}{\partial t} + R\bar{u}\frac{\partial v'}{\partial r_0} + \frac{\bar{v}}{r_0}\frac{\partial v'}{\partial \theta} + w'\frac{\partial \bar{v}}{\partial z} + \frac{1}{r_0}\frac{\partial}{\partial \theta}\left(\frac{p'}{\bar{\rho}}\right)\right]$$
$$+ u' - \nabla^2 v' = -\epsilon Re\left[u'\frac{\partial \bar{v}}{\partial r_1} + \bar{u}\frac{\partial v'}{\partial r_1} + \bar{w}\frac{\partial v'}{\partial z}\right.$$
$$\left. + \frac{\bar{u}v'}{r_1} + \frac{\bar{v}u'}{r_1}\right] + \epsilon \mathcal{F}(v') \quad (2.4.2)$$

$$Re \left[\frac{\partial w'}{\partial t} + k \bar{u} \frac{\partial w'}{\partial r_0} + \frac{\bar{V}}{r_0} \frac{\partial w'}{\partial \theta} + \frac{\partial}{\partial z} \left(\frac{\rho'}{\bar{\rho}} \right) - b' \right]$$

$$- \nabla^2 w' = - \epsilon \, Re \left[\bar{U} \frac{\partial w'}{\partial r_1} + \bar{W} \frac{\partial w'}{\partial z} \right] + \epsilon \, \mathcal{F}(w') \qquad (2.4.3)$$

$$\frac{\partial b'}{\partial t} + k \bar{u} \frac{\partial b'}{\partial r_0} + \frac{\bar{V}}{r_0} \frac{\partial b'}{\partial \theta} + N^2 w'$$

$$= - \epsilon \left[\bar{U} \frac{\partial b'}{\partial r_1} + \bar{W} \frac{\partial b'}{\partial z} \right] \qquad (2.4.4)$$

$$k \frac{\partial u'}{\partial r_0} + \frac{1}{r_0} \frac{\partial v'}{\partial \theta} + \frac{1}{\bar{\rho}} \frac{\partial}{\partial z} (\bar{\rho} w')$$

$$= - \epsilon \left[\frac{u'}{r_1} + \frac{\partial u'}{\partial r_1} + \frac{\partial \bar{W}}{\partial z} \right] \qquad (2.4.5)$$

where $\quad \nabla^2 = k^2 \frac{\partial^2}{\partial r_0^2} + \frac{1}{r_0^2} \frac{\partial^2}{\partial \theta^2} + \frac{\partial^2}{\partial z^2}$

$$(2.4.6)$$

$$b' = \frac{\Theta'}{\bar{\Theta}} \frac{g D}{U^2}$$

$$N^2 = \frac{g D}{U^2} \frac{d \ln \bar{\Theta}}{\partial z}$$

$$\mathcal{F} = \frac{\partial k}{\partial r_1} \frac{\partial}{\partial r_0} + 2 k \frac{\partial^2}{\partial r_0 \partial r_1} + \frac{k}{r_0} \frac{\partial}{\partial r_0}$$

$$+ \epsilon \left(\frac{\partial^2}{\partial r_1^2} + \frac{1}{r_0} \frac{\partial}{\partial r_1} \right)$$

CHAPTER THREE - THE BASIC STATE

Because the forces which operate in the interior of the hurricane are different from those in the boundary layer, we shall consider the two regions separately.

3.1 THE INTERIOR BASIC STATE

Observational studies of the hurricane have concentrated on the interior of the hurricane where frictional effects are negligible. The hurricane circulation is predominantly a symmetric cyclonic vortex whose tangential wind speed $\overline{V}$ decreases with radius away from the eyewall. A simple representation of this radial distribution of $\overline{V}$ is $\overline{V} \sim r^{-\lambda}$, where $.5 < \lambda < 1$. The vertical shear of $\overline{V}$ is small as is evident from Figure 3.1 of Hurricane Hilda. Radial motion in the storm is confined to the inflow layer at the bottom of the storm, and the outflow layer at the top, and is negligible in the interior portion. (See Figure 3.2.) The hurricane clearly possesses vertical motions — as evident from the cloudy and clear regions. However, the maximum vertical velocity, which occurs at the base of the eyewall, is ~ 1 m/sec , and is small compared to the tangential wind ~ 30 m/sec .

Figure 3.3 shows a cross-section of the potential temperature in Hurricane Hilda. The bulk of the storm is stably stratified $\frac{\partial \overline{\theta}}{\partial z} > 0$, and, except for a region close to the eyewall, the horizontal temperature gradient is weak, which is consistent with the small $\frac{\partial \overline{V}}{\partial z}$.
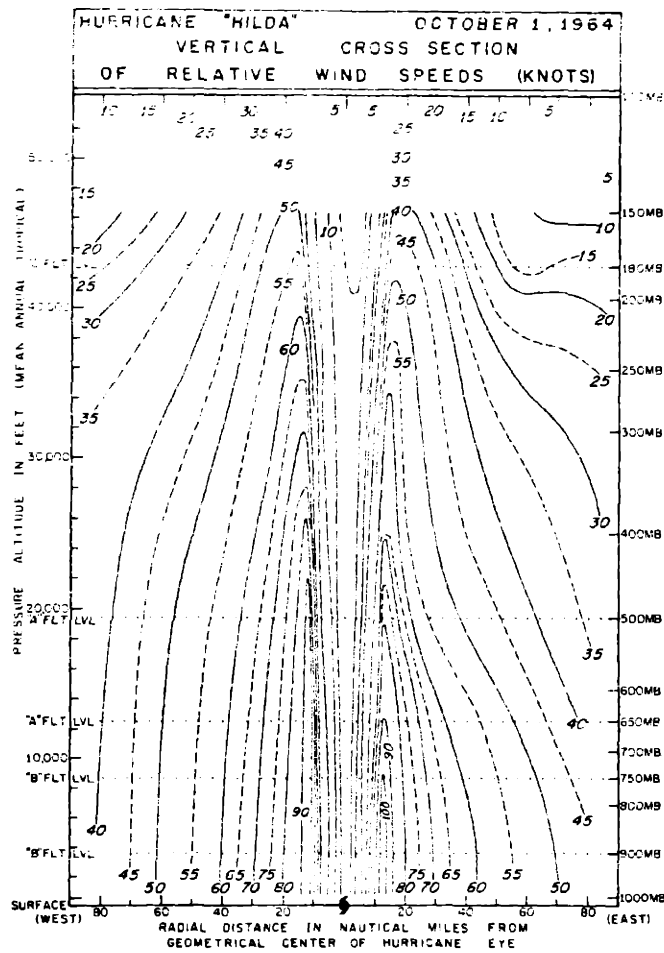
Fig. 3.1   Vertical cross-section of azimuthal winds
            (knots) in Hurricane Hilda (1964).   (From
            Hawkins et al., 1968).
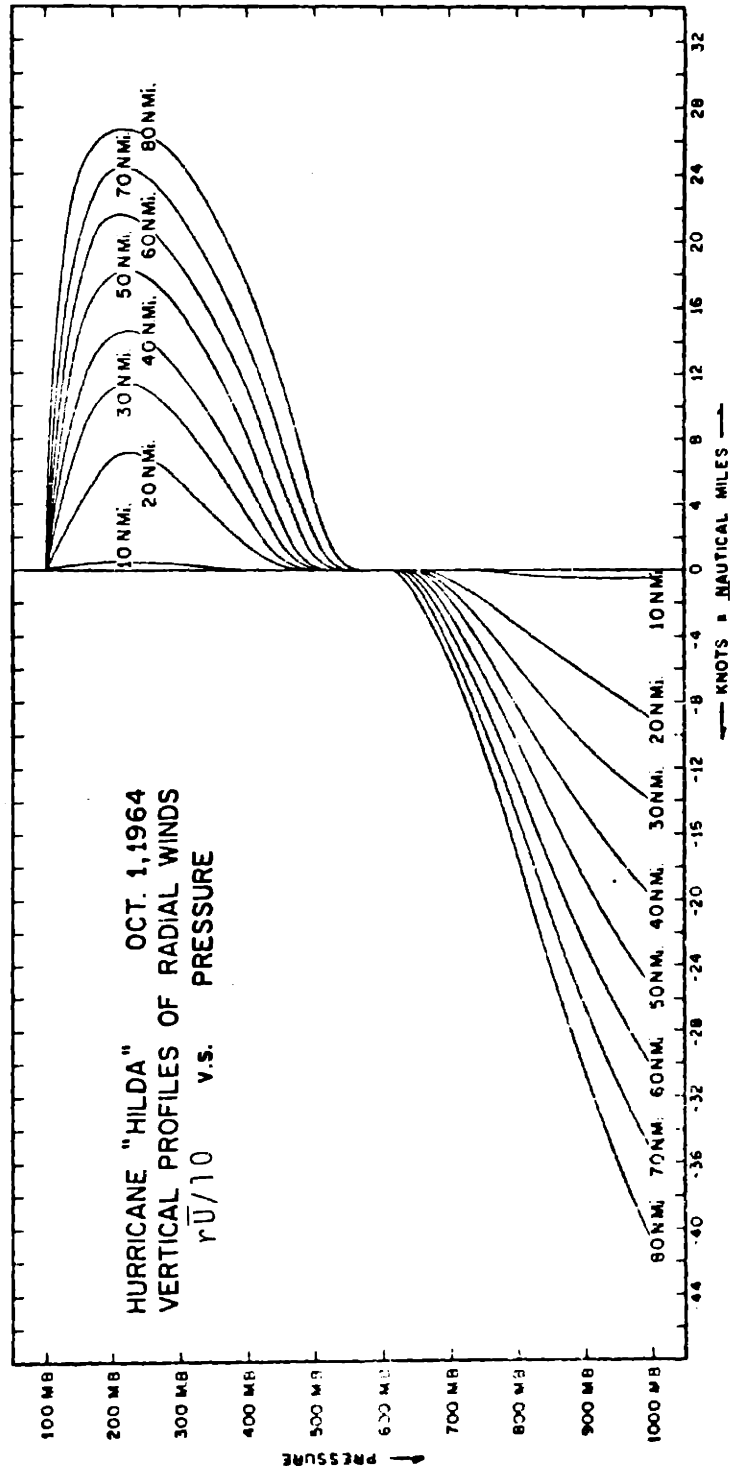
Fig. 3.2   Curves of $r\bar{U}/10$ (r in nautical miles, $\bar{U}$ in knots) against pressure for various radii in Hurricane Hilda (1964).   (From Hawkins et al.,1968) Maximum inflow velocity at each radius is about 5 knots.
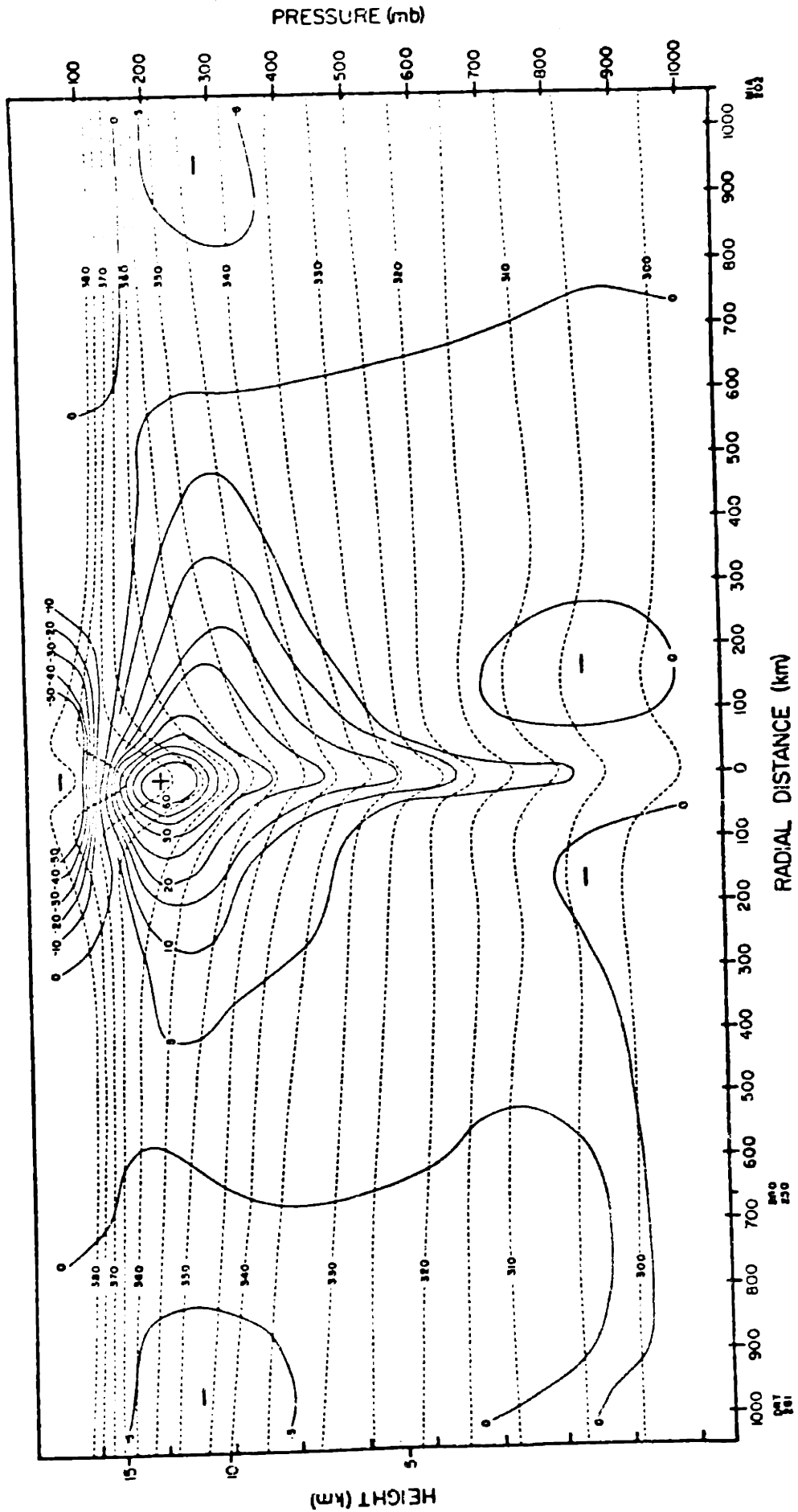
Fig. 3.3 Potential temperature (degrees kelvin, dashed lines) and mass-weighted efficiency factor (solid lines) cross-section through Hurricane Hilda (1964). (From Anthes, 1974).

We shall, therefore, make the following assumptions for the
interior of the mean hurricane:

1) Steady, axisymmetric   (3.1.1a)

2) Constant angular momentum: $\bar{V} \sim \frac{1}{r}$ (3.1.1b)

3) No vertical shear: $\frac{\partial \bar{V}}{\partial z} = 0$ (3.1.1c)

4) No mean radial motion: $\bar{U} \equiv 0$ (3.1.1d)

5) $\bar{\rho} = e^{-(z - H_2)/\eta_\perp}$ (3.1.1e)

where $\eta_\perp$ is the density scale height, H_2 is the height of the
top of the boundary layer, and $N^2 = g \frac{\partial \ln \bar{\theta}}{\partial z} = \text{constant} > 0$.
We shall call $\bar{V}$ in the interior $\bar{V}_\infty$. This reduces the interior basic
state equation to:

$$ - R_0 \frac{\bar{V}_\infty^2}{r_1} - \bar{V}_\infty = - R_0 \frac{1}{\bar{\rho}} \frac{\partial \bar{\rho}}{\partial r_1} \tag{3.1.2} $$

$$ 0 = - \frac{1}{\bar{\rho}} \frac{\partial \bar{\rho}}{\partial z} - g \frac{D}{U^2} \tag{3.1.3} $$

with $\bar{\rho} = e^{-(z - H_2)/\eta_\perp}$, and

$$ \bar{V}_\infty = \frac{c}{r_1} \tag{3.1.4} $$

where c = circulation of the hurricane. A plot of $\bar{V}_\infty$ is shown in
Figure 3.4.
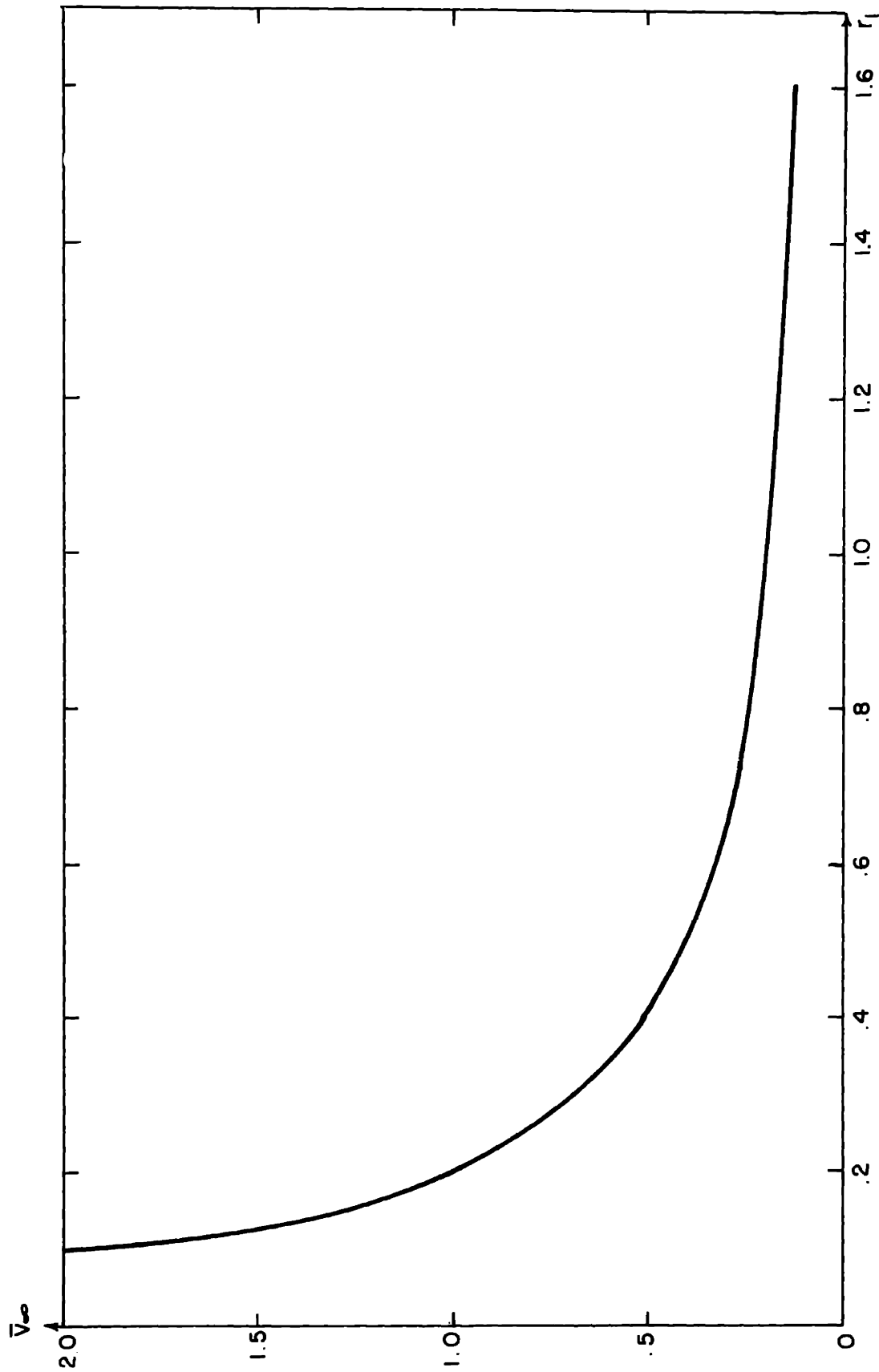
Fig. 3.4 Curve of azimuthal wind $\overline{V}_\infty(r)$ in the hurricane interior used in the model

3.2 THE BOUNDARY LAYER BASIC STATE

Because of the strong winds in the boundary layer, and the lack of observation stations in the ocean, especially during a hurricane, there is little information about the structure in the lowest 1 to 2 km where friction plays an important role. Low-level flights (~3000 feet) reveal that most of the inflow into the hurricane occurs in this layer [Hawkins and Rubsam (1968)]. Because of the conservation of angular momentum and the finite amount of energy possessed by the inflow air, this inflow cannot penetrate into the center of the storm, and erupts upwards at the eyewall. The maximum vertical velocity attained in this region is ~ 1 m/sec at the base of the eyewall and is very small compared to the tangential wind there (~ 50 m/sec).

The hurricane owes its origins to, and spends most of its life over the warm tropical ocean where the strong evaporation at the surface provides upwards fluxes of heat into its boundary layer.

The question then arises as to whether it is convection or friction that plays the dominant role in the boundary layer. A convectively driven boundary layer, usually called the "mixed layer", is characterized by nearly uniform potential temperature and wind profile; whereas the frictionally driven layer has uniform potential temperature but a variable Ekman-like, veering velocity profile.

Instead of estimating fluxes of heat and momentum under hurricane conditions to determine the relative importance of these mechanisms, we turn to wind profiles observed at land stations under the influence of a mature (not-yet-decaying) hurricane. Figure 3.5 shows the hodograph of the wind observed at Miami at various distances from the center of

10 m sec⁻¹
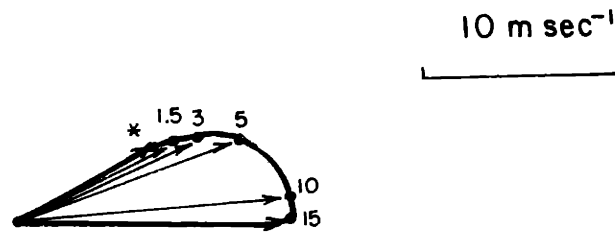
Miami   Sept. 8   1960   1900EST ,   ~ 340 mi. from   storm   center
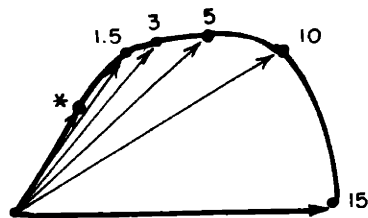
Miami   Sept. 9   1960   100 EST ,   ~ 260 mi. from   storm   center
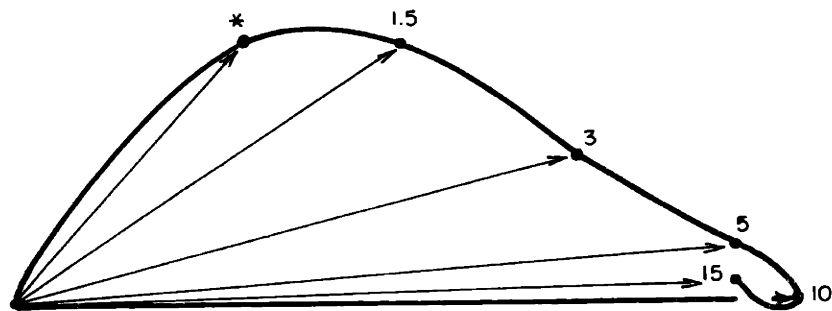
Miami   Sept. 10   1960   100EST ,   ~ 75 mi. from   storm   center

Fig. 3.5   Hodograph of boundary layer winds under Hurricane Donna. Numbers indicate height in units of 100 m. * indicates anemometer level.

Hurricane Donna (September 8-10, 1960). The diagrams are plotted from the Northern Hemisphere Data Tabulations Daily Bulletin. They indeed show an Ekman-type spiral structure.

It is not surprising that the hurricane boundary layer is frictionally driven. The buoyancy effects from the warm ocean, which would have generated an unstable mixed layer under ordinary quiescent conditions, are inadequate to compete with the turbulent momentum fluxes which are produced under the stronger hurricane winds.

In view of the discussion above, we make the following assumptions about the mean hurricane boundary layer:

1) Steady, axisymmetric

2) $\bar{\rho} = 1$, $N^2 = 0$

3) ν , the eddy coefficient of friction, is constant. This assumption may not be realistic, but it provides a qualitatively correct first attempt at the solution of the problem.

The boundary layer basic state equations are then:

$$R_0 \left(\bar{U} \frac{\partial \bar{U}}{\partial r_1} + \bar{W} \frac{\partial \bar{U}}{\partial \zeta} - \frac{\bar{V}^2}{r_1} \right) - \bar{V} = - R_0 \frac{\partial \bar{P}}{\partial r_1} + \frac{\partial^2 \bar{U}}{\partial \zeta^2} \qquad (3.2.1)$$

$$R_0 \left[\bar{U} \left(\frac{\partial \bar{V}}{\partial r_1} + \frac{\bar{V}}{r_1} \right) + \bar{W} \frac{\partial \bar{V}}{\partial \zeta} \right] + \bar{U} = \frac{\partial^2 \bar{V}}{\partial \zeta^2} \qquad (3.2.2)$$

$$0 = - \frac{\partial \bar{P}}{\partial \zeta} - \frac{g D}{U^2} \qquad (3.2.3)$$

$$\frac{\partial r_1 \bar{U}}{\partial r_1} + \frac{\partial r_1 \bar{W}}{\partial \zeta} = 0 \qquad (3.2.4)$$

We shall solve Equations (3.2.1) – (3.2.4) subject to the following boundary conditions:

$$\overline{U} = \overline{V} = \overline{W} = 0 \qquad \text{at} \quad z = o$$

$$\overline{U} = 0 , \quad \overline{V} = \overline{V}_\infty \qquad \text{as} \quad z \to \infty$$

Replacing the pressure gradient in (3.2.1) by that in the interior, we have:

$$R_o\left(\overline{U} \frac{\partial \overline{U}}{\partial r_1} + \overline{W} \frac{\partial \overline{U}}{\partial \zeta} + \frac{\overline{V}_\infty^2 - \overline{V}^2}{r_1} \right) + \left(\overline{V}_\infty - \overline{V} \right) = \frac{\partial^2 \overline{U}}{\partial \zeta^2} \qquad (3.2.5)$$

$$R_o\left[\overline{U} \left(\frac{\partial \overline{V}}{\partial r_1} + \frac{\overline{V}}{r_1} \right) + \overline{W} \frac{\partial \overline{V}}{\partial \zeta} \right] + \overline{U} = \frac{\partial^2 \overline{V}}{\partial \zeta^2} \qquad (3.2.6)$$

$$\frac{\partial r_1 \overline{U}}{\partial r_1} + \frac{\partial r_1 \overline{W}}{\partial \zeta} = 0 \qquad (3.2.7)$$

Equations (3.2.5) to (3.2.7) are not easy to solve because of their non-linearity and the radial dependence of $\overline{V}_\infty$. They are not separable in r_1 and z except in special cases [like pure solid rotation, solved by Bödewadt (1940)].

The momentum-integral method due to Th. von Karman (see Schlichting, 1955, page 144, for a detailed discussion) is an approximate method which finds depth-averaged solutions to the boundary layer equations rather than solutions at every point in the flow. It has been used by Smith (1968) and Kuo (1971), and is dependent on the similarity property of the flow for convergence. (In the presence of rotation, similarity is not possible.)

Carrier et al. (1971) obtained solutions to the non-linear boundary layer equations by representing the dependent variables by

series expansions. The Galerkin technique yielded ordinary differential equations governing the coefficients of the series expansions. These equations were integrated radially inwards from an Ekman flow at large radii.

In this thesis, we shall find solutions to the steady state boundary layer equations by solving the "pseudo-time-dependent" equations by an ingeniously simple scheme by Rivas (1975).

3.2.1 The Rivas Scheme (1975)

In order to solve a system of equations

$$F(u) = 0 \qquad\qquad (3.2.8)$$

where F is a non-linear, in general complex, matrix operator, and u is the vector of dependent variables, we look for the steady state solution to

$$\frac{\partial u}{\partial t} = F(u) \qquad\qquad (3.2.9)$$

We iterate (3.2.9) in the following manner from the νth "time step" to the $\nu + 1^{th}$ "time step":

$$\tilde{u} = u^\nu + \Delta t \left[F_S^*(u^\nu) - F_A^*(u^\nu) \right] \qquad (3.2.10)$$

$$\tilde{\tilde{u}} = u^\nu + \Delta t \left[F_S(u^\nu) + F_A(u^\nu) \right] \qquad (3.2.11)$$

$$u^{\nu+1} = \tilde{u} - \Delta t \left[F_S^*(\tilde{\tilde{u}}) - F_A^*(\tilde{\tilde{u}}) \right] \qquad (3.2.12)$$

where the * denotes complex conjugates, and F_S and F_A are the symmetric

and anti-symmetric matrices of F.

$$F_S + (F + F^T)/2 \ , \qquad F_A + (F - F^T)/2 \ .$$

The superscript T denotes transpose.

3.2.2 Test of the Rivas Scheme with Carrier's Model (1971)

Carrier et al. (1971) solved the following equations:

$$\frac{\partial}{\partial r}(ru) + \frac{\partial}{\partial z}(rw) = 0 \tag{3.2.16}$$

$$u\frac{\partial u}{\partial r} + w\frac{\partial u}{\partial z} - 2\Omega v - \frac{v^2}{r} + \frac{\partial p}{\partial r} = \nu\frac{\partial^2 u}{\partial z^2} \tag{3.2.17}$$

$$u\frac{\partial}{\partial r}(rv) + w\frac{\partial}{\partial z}(rv) + 2\Omega rv = \nu\frac{\partial^2 rv}{\partial z^2} \tag{3.2.18}$$

$$0 = \frac{\partial p}{\partial z} + g \tag{3.2.19}$$

subject to the boundary conditions:

at z = 0 $\quad u = v = w = 0$

at z → ∞ $\quad u = 0, \ v(r,\infty) = V(r)$ (specified) (3.2.20)

They applied a series expansion method in combination with the Galerkin technique to solve the equations. They were primarily interested in predicting the vertical velocity at the top of the boundary layer — an extremely small but physically important quantity. They specified the interior flow $\overline{V}(r)$:

$$\overline{V}(r) = \begin{cases} c_1/r & 0 < r \leq \tfrac{1}{2}r_0 \\ c_2(r_0-r) & \tfrac{1}{2}r_0 < r < r_0 \end{cases} \tag{3.2.21}$$
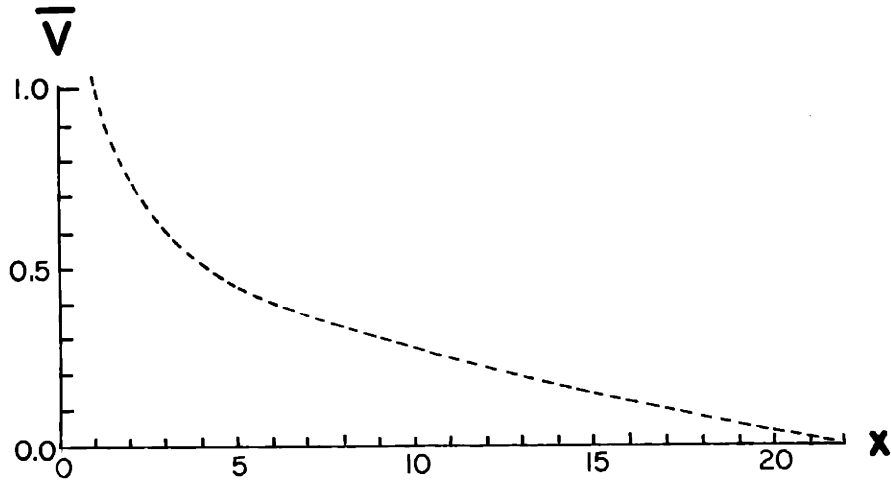
Fig. 3.6   Curve of azimuthal wind in the hurricane
            interior used in Carrier et al.'s (1971)
            model. $(x \sim r^2)$.

with $c_2 = \dfrac{4c_1}{r_o^2}$. This is illustrated in Figure 3.6. They chose:

$$\nu = 10^5 \ cm^2/sec.$$
$$V_{max} = 150 \ mi/hr \quad at \quad r_1 = 20 \ miles$$
$$\Omega = \tfrac{3}{2} \ radians/day$$

(3.2.22)

We solved Carrier's system of Equations (3.2.16) to (3.2.21) by Rivas' Scheme. The results are shown in Figure 3.7. We see that the agreement between our solution and Carrier's solution is very good. (We note that Carrier's solution near the center is an "artifact of the methodology".)

The discrepancy between our solution and Carrier's solution at large z could be due to several factors. First, we obtained u and v directly from the momentum equations in r-z coordinates, and interpolated our result to x-z coordinates ($x \sim r^2$) for comparison with Carrier's results. Carrier et al. obtained convergent solutions for the expansion coefficients, and their solutions u, v, w were still dependent on their choice of expansion function. Also, our choice of infinity in z coordinates was $z = 5$, whereas Carrier's was $z = 5.6$. Since w was computed from the continuity equation in both Carrier's and our solutions, any discrepancy in u between the two solutions become magnified in w.

3.2.3 The Boundary Layer Solution

We apply the Rivas Scheme to Equations (3.2.5) to (3.2.7) subject to the boundary conditions:
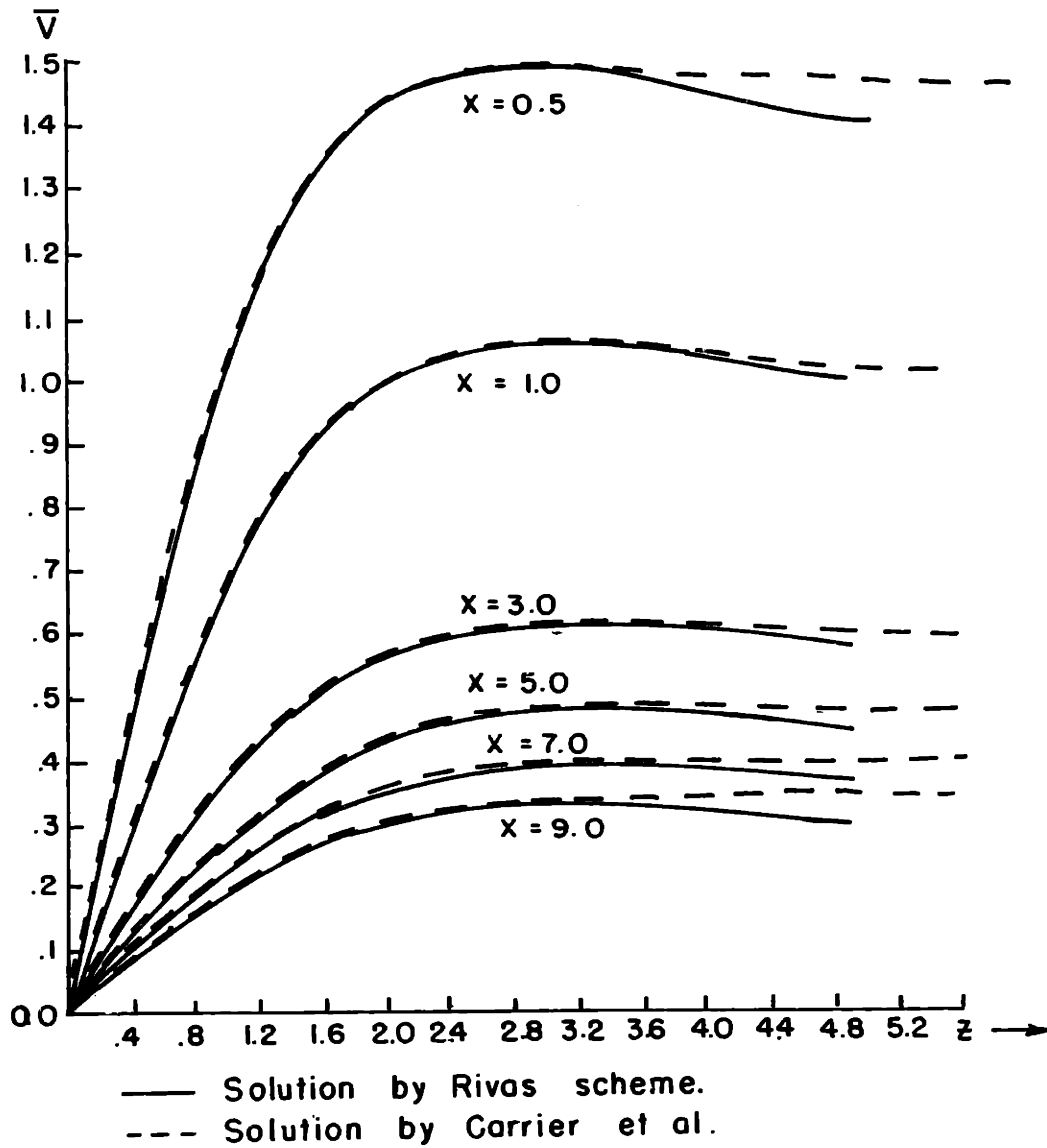
Fig. 3.7a   Comparison of profiles of boundary layer winds obtained by
using the Rivas Scheme and by Carrier et al. (1971) for the
interior wind shown in Fig. 3.6 (x ∿ r²). Profiles of V.
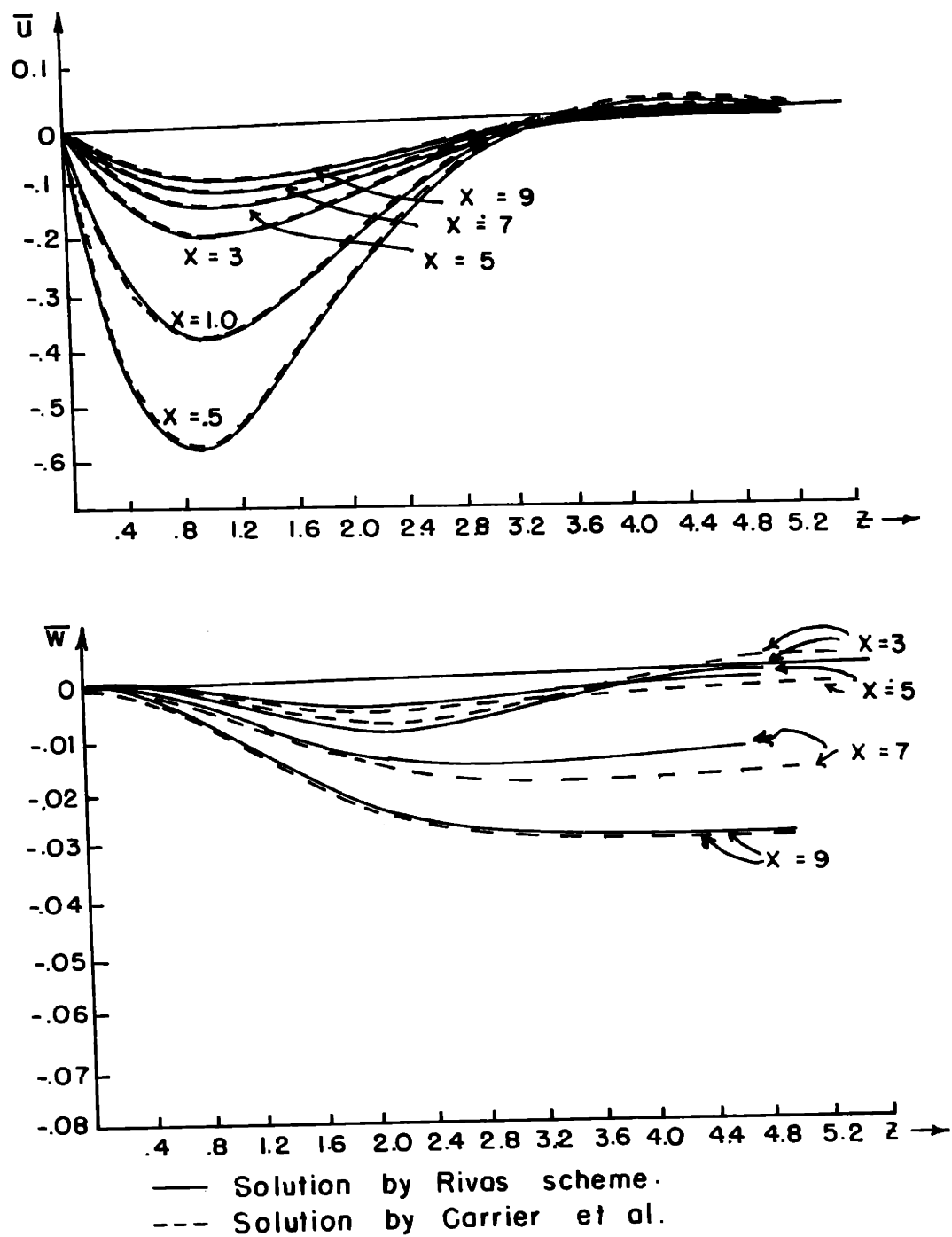
Figure 3.7b. Comparison of $\overline{U}$ and $\overline{W}$ obtained by using the Rivas Scheme and by Carrier et al. (1971) for the interior wind shown in Figure 3.6. ($x \sim r^2$).
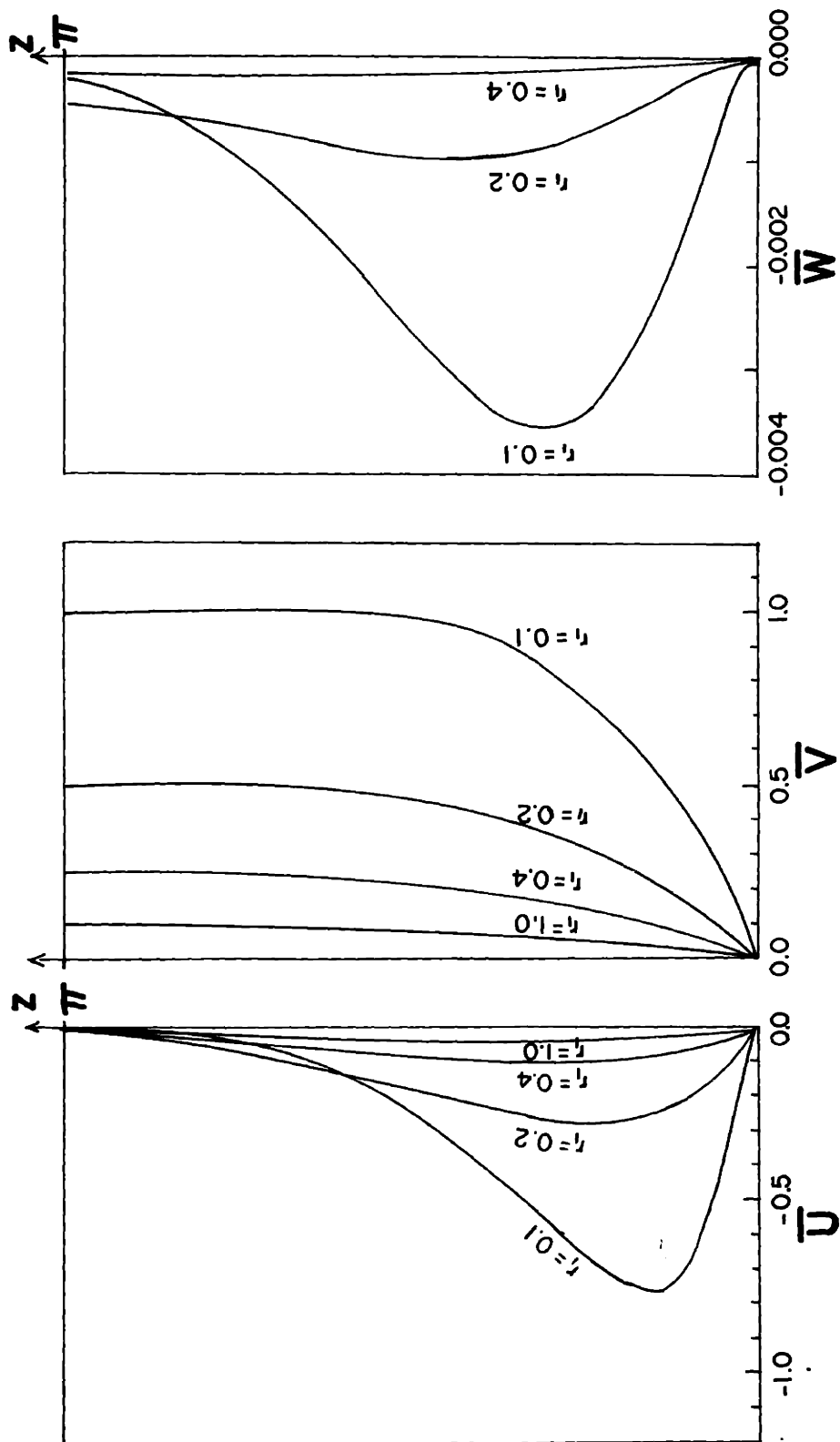
Figure 3.8. Profiles of boundary layer winds obtained by using the Rivas Scheme for the interior wind shown in Figure 3.4.

at $z = 0$ $\bar{U} = \bar{V} = \bar{W} = 0$

$$(3.2.23)$$

at $z \to \infty$ $\hat{U} = 0$, $\bar{V} = \bar{V}_\infty$

$$(3.2.24)$$

We specify $\bar{V}_\infty = 50$ m/sec at $r = 25$ km

so that $c = .1$

Pick

$$\nu = 5 \times 10^5 \text{ cm}^2/\text{sec}$$

$$f = 5 \times 10^{-5}/\text{sec}$$

$$(3.2.25)$$

$$U = 25 \text{ m/sec}$$

$$L = 500 \text{ km}$$

so that

$$R_o = \frac{U}{fL} = 1$$

$$(3.2.26)$$

$$D = \sqrt{\frac{\nu}{f}} = 1 \text{ km}.$$

The numerical scheme is shown in Appendix A. The solutions are shown in Figure 3.8.

3.3 BOUNDARY LAYER INSTABILITY

At each radius, the boundary layer profile obtained in Section 3.2 resembles that of the classical Ekman profile under a constant wind aloft.

53.
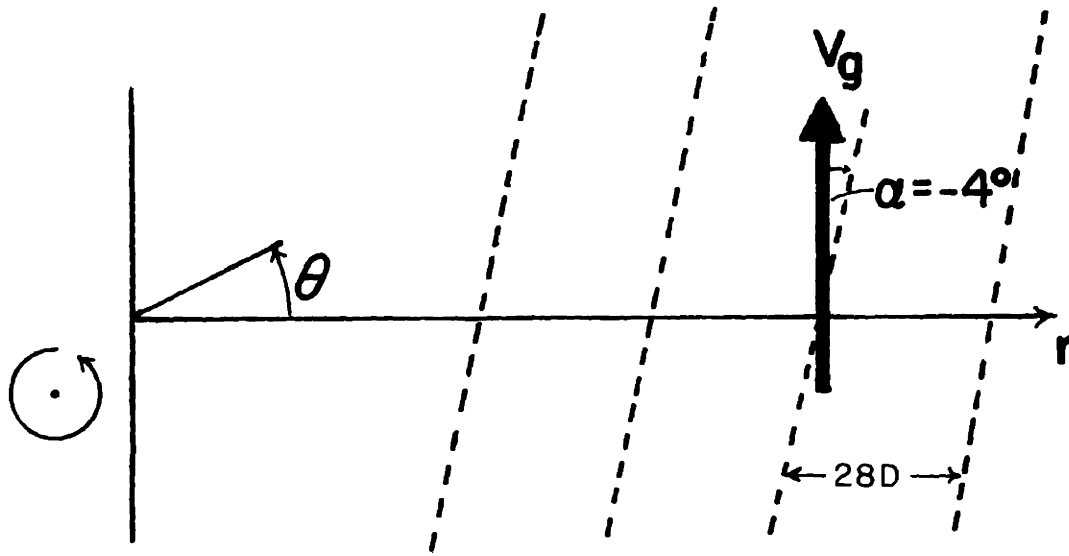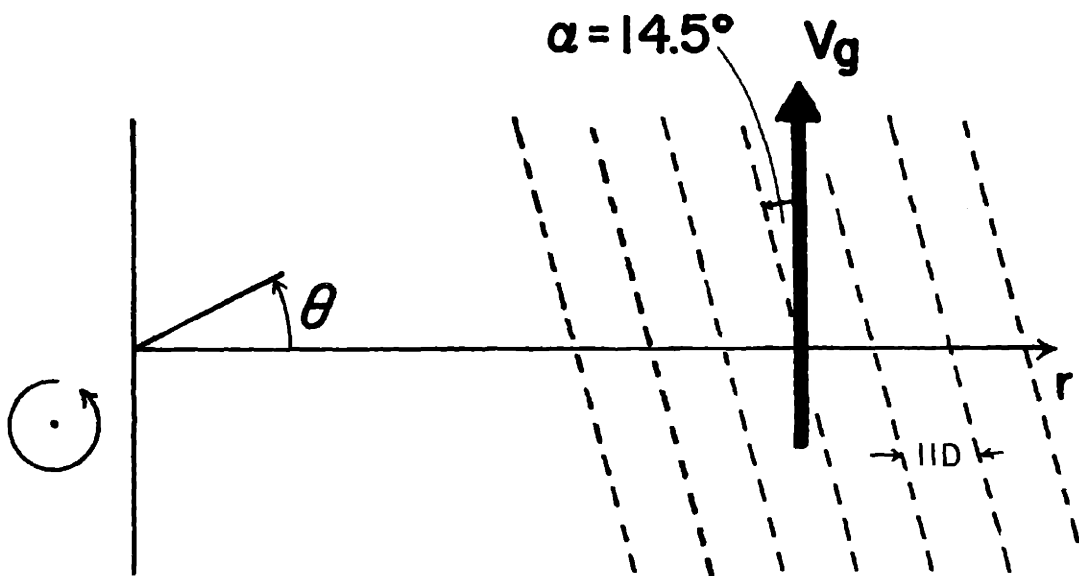
CLASS A WAVES

CLASS B WAVES

Figure 3.9. Schematic picture of Class A and Class B waves to
illustrate the measured wavelengths and wave front
orientations.

Instability of the classical Ekman layer in a neutrally stratified atmosphere has been investigated experimentally by Faller (1963), Tatro and Mollo-Christensen (1967), numerically by Faller and Kaylor (1966), and analytically by Lilly (1966).

Their results show that there are two different types of instability associated with this boundary layer; each forms a series of horizontal roll vortices whose spacing is related to the depth of the boundary layer. These are summarized in Figure 3.9. The first type, called class A waves, which occurs at $Re > 55$, but vanishes at Re larger than 110, is oriented at an angle $0°$ to $8°$ to the right of the geostrophic wind, and has wavelengths of about 28D. These waves derive their energy from the boundary layer wind component which is parallel to the roll axis, and are hence called "parallel instabilities".

The other type of instability, called class B waves, occurs at $Re \geq 110$. They are of shorter wavelengths, about 11D, and are oriented at an angle about $14°$ to the left of the geostrophic wind. They derive their energy from the shear of the boundary layer wind components perpendicular to the roll axis. Their existence depends crucially on the existence of an inflection point in the wind profile, i.e. a maximum of vorticity somewhere in the flow, and are referred to as "inflection point instabilities". Since this class of instabilities was first discovered by Rayleigh (1887), it is also referred to as "Rayleigh Instability".

In the hurricane, the Reynolds number is of the order of 500, much greater than the critical 110 for instability, and so we expect to find, and do indeed find, that the presence of an inflection point in the radial wind profile is the cause of the incipient unstable waves.

3.4 THREE-LAYER APPROXIMATION OF THE BASIC STATE

In order to obtain an analytic solution for the linear perturbations, we shall replace, at each radius, the continuous velocity profile in z by three layers of constant shear, the velocities being continuous across each interface. The uppermost layer then corresponds to the stably stratified interior flow of no vertical shear. The lower two layers approximate the boundary layer solution obtained in Section 3.2. The top of the lowest layer is chosen to be the height H_1 at which the radial velocity exhibits its minimum value. The top of the middle layer is chosen to be the height H_2 at which the boundary layer winds are equal to the interior winds. Results from Section 3.2 show that both H_1 and H_2 are nearly constant with radius.

With this "broken-line" approximation, the vorticity is constant within each layer, but discontinuous across each interface. The flow no longer possesses an inflection point, but is still unstable if the criteria Rayleigh developed in 1887 in the original derivation of Rayleigh instability are satisfied.

Rayleigh used three layers of constant shear, the velocities being continuous across the interface. The criterion for the flow to be unstable is that the vorticity jumps across the two interfaces be of different signs. This indeed is satisfied by our "broken-line" profiles.

3.4.1 Test of the "Broken-Line" Approximation

In order to show that the broken-line approximation of the basic state does represent fairly accurately the character of the most

unstable wave, and to check the validity of the large Reynolds number assumption which we shall employ in Chapter 4, we work out the large Re stability analysis of the classical neutral Ekman flow, approximated by a three-layer system, as shown in Figure 3.10.

The results will be compared with those of Lilly (1966) who found the eigenvalue solution to the "complete set of linear perturbation equations" (which includes the effects of the Coriolis force and friction) and the "Orr-Sommerfeld equations" (which include only the effects of friction on the perturbations).

We shall express the linear perturbation equation in Cartesian coordinates and neglect curvature terms. The constant geostrophic wind is in the x-direction. Since we are looking for banded disturbances, we assume that the derivatives of all perturbation quantities vanish along the bands. We then rotate the horizontal coordinate axis through an angle α such that the new x' axis is aligned with the band axis, and $\frac{\partial}{\partial x'} = 0$. Now we approximate the basic Ekman flow $\overline{U}, \overline{V}$ by three layers as in Figure 3.10 so that within each layer:

$$\overline{U_j}' = \overline{U_j} \cos\alpha + \overline{V_j} \sin\alpha \tag{3.4.1}$$

$$\overline{V_j}' = -\overline{U_j} \sin\alpha + \overline{V_j} \cos\alpha \tag{3.4.2}$$

$\overline{W_j} \equiv 0$ for the classical Ekman solution under constant geostrophic wind. The perturbation equations within each layer then are:

$$Re\left(\frac{\partial u_j'}{\partial t} + \overline{V_j}'\frac{\partial u_j'}{\partial y'} + w_j'\frac{\partial \overline{u_j}}{\partial z}\right) - \nu' = \frac{\partial^2 u_j'}{\partial y'^2} + \frac{\partial^2 u_j'}{\partial z^2} \tag{3.4.3}$$
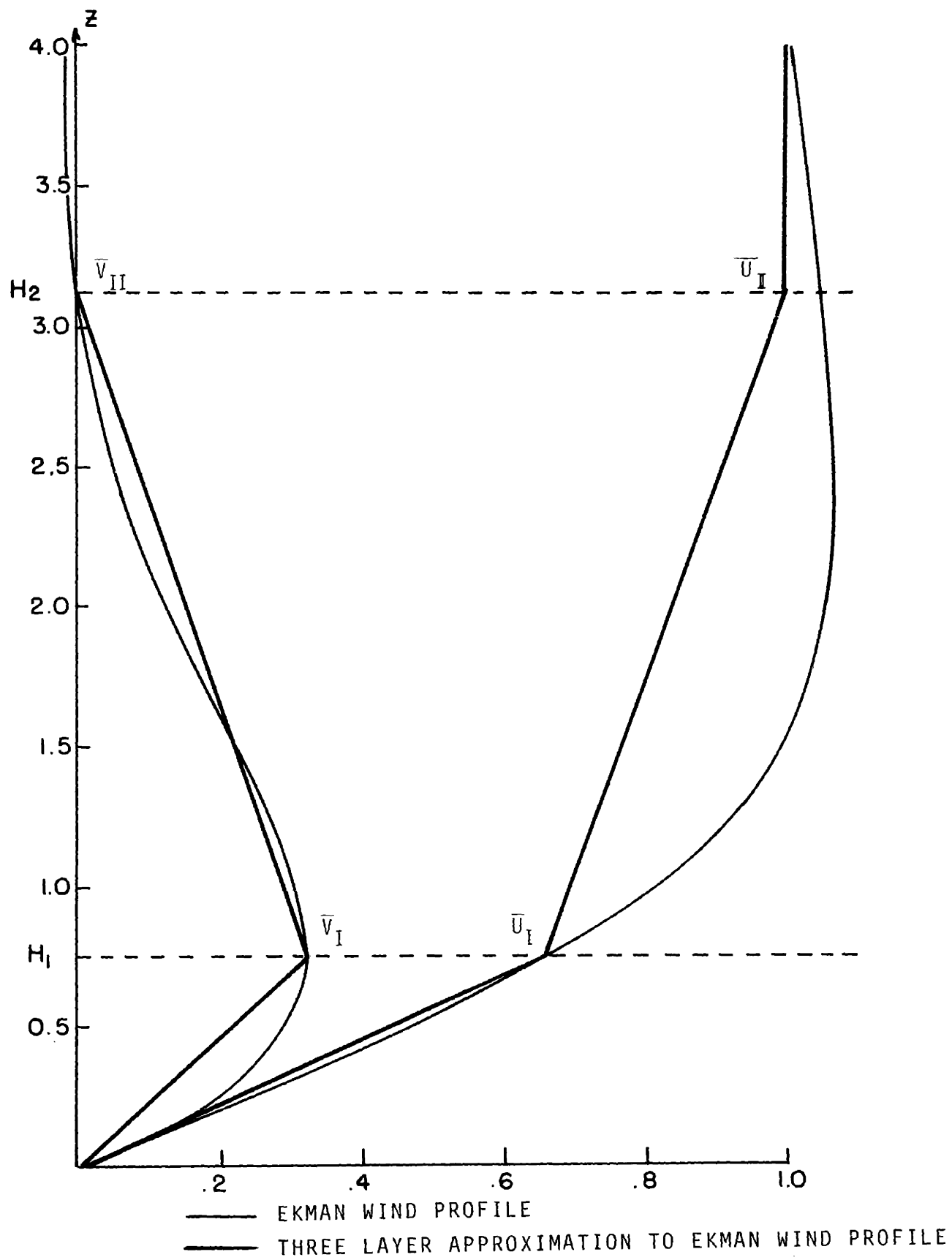
Figure 3.10. Three layer approximation to the classical Ekman profile.

$$Re \left(\frac{\partial w_j'}{\partial t} + \bar{V}_j' \frac{\partial w_j'}{\partial y'} + w_j' \frac{\partial \bar{V}_j}{\partial z} \right) + u' = - Re \frac{\partial p_j'}{\partial y'}$$
$$+ \frac{\partial^2 w_j'}{\partial y'^2} + \frac{\partial^2 w_j'}{\partial z^2} \qquad (3.4.4)$$

$$Re \left(\frac{\partial w_j'}{\partial t} + \bar{V}_j' \frac{\partial w_j'}{\partial y'} \right) = - Re \frac{\partial p_j'}{\partial z} + \frac{\partial^2 w_j'}{\partial y'^2} + \frac{\partial^2 w_j'}{\partial z^2} \qquad (3.4.5)$$

$$\frac{\partial v_j'}{\partial y'} + \frac{\partial w_j'}{\partial z'} = 0 \qquad (3.4.6)$$

We shall solve these equations subject to the boundary conditions

$$u_1' = v_1' = w_1' = 0 \qquad at \quad z = 0$$

$$w_1' = w_2' \; ; \qquad p_1 = p_2' \qquad at \quad z = H_1$$

$$w_2' = w_3' \; ; \qquad p_2' = p_3' \qquad at \quad z = H_2$$

$$w_3' = 0 \qquad \qquad as \quad z \to \infty$$

$$(3.4.7)$$

Introducing a stream function ψ_j' such that

$$v_j' = - \frac{\partial \psi_j'}{\partial z}$$

$$(3.4.8)$$

$$w_j' = \frac{\partial \psi_j'}{\partial y'}$$

Assuming solutions of the form

$$\psi_j' = \varphi_j(z) e^{i\kappa(y' - \omega t)}$$

$$u_j' = u_j(z) e^{i\kappa(y' - \omega t)} \qquad (3.4.9)$$

$$p_j' = P_j(z) e^{i\kappa(y' - \omega t)}$$

we reduce Equations (3.4.3) to (3.4.6) to two equations

$$\left(\frac{d^2 \varphi_j}{dz^2} - \kappa^2 \varphi_j \right)^2 - i \, Re \left[(\kappa \bar{V}_j - \omega) \left(\frac{d^2 \varphi_j}{dz^2} - \kappa^2 \varphi_j \right) - \kappa \frac{d^2 \bar{V}_j}{dz^2} \varphi_j \right]$$

$$+ \frac{d \mathcal{U}_j}{dz} = 0 \qquad\qquad (3.4.10)$$

$$\frac{d^2 \mathcal{U}_j}{dz^2} - \kappa^2 \mathcal{U}_j - i \, Re \left[(\kappa \bar{V}_j - \omega) \mathcal{U}_j + \frac{d \bar{\mathcal{U}}_j}{dz} \varphi_j \right]$$

$$- \frac{d \varphi_j}{dz} = 0 \qquad\qquad (3.4.11)$$

where $\dfrac{d^2 \bar{V}_j}{dz^2} = 0$ for each layer because of the constant shear approximation.

When the Reynolds number is large, we neglect, to the lowest order,

terms of order $\dfrac{1}{Re}$. Hence we get:

$$\frac{d^2 \mathcal{U}_j}{dz^2} - \kappa^2 \mathcal{U}_j = 0 \qquad\qquad (3.4.12)$$

The B.C. for (3.4.12) are:

$$\varphi_1 = 0 \qquad\qquad at \quad z = 0$$

$$\varphi_1 = \varphi_2, \quad P_1 = P_2 \qquad at \quad z = H_1 \qquad\qquad (3.4.13)$$

$$\varphi_2 = \varphi_3, \quad P_2 = P_3 \qquad at \quad z = H_2$$

$$\varphi_3 = 0 \qquad\qquad as \quad z \to \infty$$

A non-trivial solution to the system of equations (3.4.12) subject to the

conditions (3.4.13) exists only if:

$$
\det \begin{vmatrix} (S_2 - S_1)\,\sinh \kappa H_1 & -\sigma_{II}\,\kappa \\ \sigma_{II}\kappa(\sinh \kappa H_2 + \cosh \kappa H_2) & \sigma_{II}\,\kappa(\sinh \kappa D_2 + \cosh \kappa D_2 \\ \quad - S_2\,\sinh \kappa H_2 & \quad - S_2\,\sinh \kappa D_2 \end{vmatrix} \tag{3.4.14}
$$

$$
= 0
$$

where

$$
S_j = \kappa \frac{d\bar{V_j}}{d\gamma} \qquad\qquad j = 1,\,2
$$

$$
D_2 = H_2 - H_1
$$

$$
\sigma_J = \kappa\,\bar{V_J} - \omega \qquad J = I,\,II
$$

(3.4.14) is the dispersion relationship. It is a quadratic equation in ω, from which ω can be solved explicitly. We search through the $\kappa - \alpha$ plane numerically to look for the ω with the largest ω_I.

In order to investigate the dependence of the properties of the most unstable wave on the choice of H_1, U_I, and V_I, we studied three cases indicated in Table 1. We kept the parameters H_2, U_{II}, V_{II} fixed.

Results regarding the most unstable wave are compared with those from the eigenvalue study of Lilly (1966), the numerical study of Faller and Kaylor (1966), and the experimental study of Tatro and Mollo-Christensen (1971). These are summarized in Table 2.

We see that the results compare very well. In the continuous model, the growth rate is governed by the magnitude of the shear across the inflection point in the velocity component perpendicular to the wave-front $U_\perp$. The most unstable wave is thus oriented at such an angle to the geostrophic wind aloft so that $U_\perp$ possesses maximum shear across the inflection point. Since the source of the eddy kinetic energy is at the inflection point of $U_\perp$, we expect that the most unstable wave would be

stationary relative to the inflection point for most efficient extraction

of the mean kinetic energy.

All of these results are fairly well demonstrated in the layered

models, as can be seen in Table 2.

TABLE 1

	Case 1	Case 2	Case 3
H_1	$\pi/3$	$\pi/4$	$\pi/3$
H_2	π	π	π
V_I	.304	.322	.3
U_I	.826	.678	.8
V_{II}	0	0	0
U_{II}	1	1	1

Three Three-Layer Approximations to the Ekman flow.

TABLE 2

	Case 1 Re → ∞	Case 2 Re → ∞	Case 3 Re → ∞	Lilly (1966) OSE Re = 500	Lilly (1966) Complete Re = 500	Faller & Kaylor (1966) Re = 300	Tatro & Mollo-Christensen (1967)
$\lambda = 2\pi/\kappa$	14	15.8	12.6	12.6	12.3	16.5	11.8
α (to left of U_{II})	12°	14°	10°	18.7°	19°	14°	14.6°
ω_R	-.0236	-.0220	-.016	–	–	–	–
ω_I	.0250	.0220	.0250	.0251	.0243	–	–
$C_{ph} = \omega_R/\kappa$	-.0515	-.055	-.032	-.051	-.046	.026	-.034
$U\|$ at $z = \dfrac{H_1 + H_2}{2}$	-.041	-.047	-.009				
$\dfrac{1}{\kappa}\dfrac{\partial U\|}{\partial z}$	-.0714	-.066	-.078				

Comparison of the Properties of the Most Unstable Wave Solution between the Three-Layer Models and Previous Studies of Ekman Instability.

CHAPTER FOUR – THE LINEAR PERTURBATIONS

4.1 THE LINEAR PERTURBATION PROBLEM

The linear perturbation equations in cylindrical coordinates for a viscous, rotating and stratified quasi-Boussinesq fluid are: (refer to Section 2.4)

$$\frac{\partial u'}{\partial t} + k\bar{u}\frac{\partial u'}{\partial r_0} + \frac{\bar{V}}{r_0}\frac{\partial u'}{\partial \theta} + w'\frac{\partial \bar{U}}{\partial \zeta} + k\frac{\partial}{\partial r_0}\left(\frac{p'}{\bar{\rho}}\right) = -\epsilon\left[\bar{u}\frac{\partial u'}{\partial r_1}\right.$$
$$\left. + \bar{w}\frac{\partial u'}{\partial \zeta} - \frac{2\bar{V}v'}{r_1} + u'\frac{\partial \bar{u}}{\partial r_1} + \frac{\partial}{\partial r_1}\left(\frac{p'}{\bar{\rho}}\right)\right] + \frac{1}{Re}\left[v' + \nabla^2 u'\right]$$

(4.1.1)

$$\frac{\partial v'}{\partial t} + k\bar{u}\frac{\partial v'}{\partial r_0} + \frac{\bar{V}}{r_0}\frac{\partial v'}{\partial \theta} + w'\frac{\partial \bar{V}}{\partial \zeta} + \frac{1}{r_0}\frac{\partial}{\partial \theta}\left(\frac{p'}{\bar{\rho}}\right) = -\epsilon\left[\bar{u}\frac{\partial v'}{\partial r_1}\right.$$
$$\left. + \bar{w}\frac{\partial v'}{\partial \zeta} + u'\left(\frac{\partial \bar{v}}{\partial r_1} + \frac{\bar{v}}{r_1}\right) + \frac{\bar{u}v'}{r_1}\right] + \frac{1}{Re}\left[-u' + \nabla^2 v'\right]$$

(4.1.2)

$$\frac{\partial w'}{\partial t} + k\bar{u}\frac{\partial w'}{\partial r_0} + \frac{\bar{V}}{r_0}\frac{\partial w'}{\partial \theta} + \frac{\partial}{\partial \zeta}\left(\frac{p'}{\bar{\rho}}\right) + b'$$
$$= -\epsilon\left[\bar{u}\frac{\partial w'}{\partial r_1} + \bar{w}\frac{\partial w'}{\partial \zeta}\right] + \frac{1}{Re}\left[\nabla^2 w'\right]$$

(4.1.3)

$$\frac{\partial}{\partial t}(b') + k\bar{u}\frac{\partial b'}{\partial r_0} + \frac{\bar{V}}{r_0}\frac{\partial b'}{\partial \theta} + N^2 w'$$
$$= -\epsilon\left[\bar{u}\frac{\partial b'}{\partial r_1} + \bar{w}\frac{\partial b'}{\partial \zeta}\right]$$

(4.1.4)

$$k\frac{\partial u'}{\partial r_0} + \frac{1}{r_0}\frac{\partial v'}{\partial \theta} + \frac{1}{\bar{\rho}}\frac{\partial}{\partial \zeta}(\bar{\rho}w') = -\epsilon\left[\frac{u'}{r_1} + \frac{\partial u'}{\partial r_1}\right.$$
$$\left. + \frac{\partial \bar{w}}{\partial \zeta}\right]$$

(4.1.5)

4.1.1 Boundary Conditions in the Vertical

Equations (4.1.1) to (4.1.5) relate the perturbation quantities within each layer. In order to establish the eigenvalue problem, we shall need interfacial matching conditions as well as conditions at the sea surface and at the top of the atmosphere.

At the sea surface, we demand that

$$w' = 0 \quad \text{at} \quad z = 0 \qquad (4.1.6)$$

In the lowest order solution, the fluid is inviscid because of the large Reynolds number approximation. Thus u' and v' may be non-zero at $z = 0$.

At the top of the atmosphere, $z \to \infty$, we shall demand that the eigen wave mode be trapped, i.e., that the amplitude approach zero, or else that the energy radiated be upward,

$$\iiint \bar{\rho} \; \mathcal{R}_e(p') \; \mathcal{R}_e(w') \; r \, dr \, d\theta \, dt \; > \; 0 \qquad (4.1.7)$$

It turns out that these waves are indeed trapped, as predicted by Charney and Pedlosky (1963) for vibrations in a fluid which is unstable below and stable above.

At the interfaces $z = H_1$ and $z = H_2$, we require that the pressure p' and vertical velocity w' be continuous. $\qquad$ (4.1.8)

4.1.2 Radial Boundary Conditions

The generation of perturbation kinetic energy (EKE) is mainly in the region of the boundary layer close to the eyewall where the vertical shear of the radial velocity is strongest. This EKE may be propagated

away from or towards the eyewall, depending on the group velocity of the
waves. Since the eyewall is a practically impenetrable region of intense
updraft, most of the energy incident on the eyewall will be reflected.
There may still be residual energy flux across the eyewall into the eye
region. However, this energy will be reflected outwards at $r = 0$ since
there can be no energy build-up at the center of the hurricane. We shall
therefore assume that all the energy reflection takes place at the eye-
wall, and that there is no energy flux across $r_1 = Ro$, i.e.,

$$\iiint \bar{\rho} \; Re(p') \; Re(u') \; r_1 \, d\theta \, dz \, dt = 0 \qquad at \quad r_1 = Ro \tag{4.1.9}$$

(4.1.9) is satisfied if

$$u' = 0 \quad at \quad r_1 = Ro \tag{4.1.10}$$

At large distances from the center of the storm, we shall demand
that the energy density be bounded, i.e.,

$$\frac{1}{2} \iiint \bar{\rho} (u'^2 + v'^2 + w'^2) \, r \, d\theta \, dz \, dt \quad is \; bounded \tag{4.1.11}$$

4.2 OUTLINE OF PROCEDURE TO SOLVE THE LINEAR PERTURBATION EQUATIONS

Let us stop briefly to review the purpose of our investigation so
as to give some direction to the lengthy algebra which is to follow.
Equations (4.1.1) to (4.1.5) govern the behavior of the small-amplitude,

short-wavelength perturbations on the equilibrium state obtained in Section 3.2. We are looking for the most unstable wave contained therein, on the assumption that the wave that draws energy fastest from the basic state is the one that is observed.

Suppose we can combine (4.1.1) to (4.1.5) into one equation in w:

$$\mathcal{L}(w) = \epsilon \, \mathcal{M}(w) \qquad (4.2.1)$$

where both $\mathcal{L}$ and $\mathcal{M}$ are operators of order 1, and $\epsilon = D/L \ll 1$ is the ratio between the radial scales of the perturbations and the large-scale flow. Because the mean quantities are functions of r_1 and z only, and because we have made the multiple scales assumption, $\mathcal{L}$ contains derivatives with respect to r_0 , θ , z and t but not w.r.t. r_1 .

In $\mathcal{L}$, the coefficients of the derivatives of w are the basic state quantities which are functions of r_1 and z only. This allows us to write

$$w(r_0, r_1, \theta, z, t) = \left[w^{(0)}(r_1, z) + \epsilon \, w^{(1)}(r_1, z) + \epsilon^2 w^{(2)}(r_1, z) + \cdots \right]$$
$$\times \, e^{i(r_0 + m\theta - \omega t)} \qquad (4.2.2)$$

Substituting (4.2.2) into (4.2.1), and equating powers in ϵ, we get:

$$\mathcal{L}'(w^{(0)}) = 0 \qquad (4.2.3a)$$

$$\mathcal{L}'(w^{(1)}) = \mathcal{M}'(w^{(0)}) \qquad (4.2.3b)$$

$$\vdots$$

where $\mathcal{L}'$ and $\mathcal{M}'$ are $\mathcal{L}$ and $\mathcal{M}$, respectively, with $\frac{\partial}{\partial r_0}$ replaced by i, $\frac{\partial}{\partial \theta}$ by im and $\frac{\partial}{\partial t}$ by $-i\omega$. $\mathcal{L}'$ contains only z derivatives:

r_1 enters only parametrically. $\mathcal{M}'$ contains both z derivatives and first order derivatives in r_1 .

4.2.1 The Lowest Order Equation: The Local Dispersion Relationship

Equation (4.2.3a) allows solutions of the form

$$w^{(0)} \sim A(r_1)\, \psi(\mathfrak{z};\ r_1,\, \omega,\, m,\, k) \tag{4.2.4}$$

where $\mathcal{L}(\psi) = 0$ and $A(r_1)$ is the yet-undetermined amplitude of the solution.

Applying the boundary conditions in z (4.1.6) to (4.1.8) gives us the local dispersion relationship between the wave number k, m and the frequency ω at every r_1 . We write the local dispersion relationship as

$$\mathcal{D}(\omega,\, k,\, m;\, r_1) = 0 \tag{4.2.5}$$

Since $\mathcal{L}$ depends only on forces acting at r_1 , the dispersion relationship (4.2.5) is local in r_1 . However, by demanding that it be uniformly valid in the entire domain in r_1, we make it apply globally. This is done by a normal mode analysis.

4.2.2 Normal Mode Analysis

For a given azimuthal wavenumber m(=integer), we consider the frequency ω as a (complex) constant over the whole domain, and then solve for the radial wavenumbers $k(r_1)$ from the local dispersion relationship (4.2.5). There are as many solutions $k(r_1)$ for each ω as the order of $\frac{\partial}{\partial r_0}$ in $\mathcal{L}$. The $k(r_1)$'s are, in general, complex, since they depend on ω, which is complex for unstable waves. This procedure does not, however, lead to the unique determination of the most unstable eigenwave mode, since (4.2.5) gives complex solutions $k(r_1)$ for _any_ complex ω assumed. We need

to apply the radial boundary conditions to find the most unstable wave
mode which allows the radial boundary condition to be satisfied.

It is difficult to apply the radial boundary conditions to
Equation (4.2.3a) which has vertical as well as radial dependences. The
$k(r_1)$'s , however, have no vertical dependence, and an ordinary differen-
tial equation may be constructed whose wave-like solutions have the same
wavenumbers $k(r_1)$ as would have been obtained by using (4.2.3a). The
radial boundary conditions can then be applied to the new ordinary dif-
ferential equations, giving a condition on the wavenumbers k, and hence
a unique determination of ω.

It turns out that (4.2.3a) is a fourth order in $\frac{\partial}{\partial r_0}$, so that
$\mathcal{D}(k;\omega) = 0$ has four k solutions. If ω were real, then the coefficients
of k in $\mathcal{D}$ would be real, and the k solutions would be complex conjugate
pairs. (Since the flow is unstable, $\mathcal{D}(k;\omega) = 0$ does not permit real k
together with real ω as solutions.) When ω becomes slightly complex, as
is the case for unstable waves, the pairs of $k(r_1)$ solutions can still
be identified. We shall consider such a complex conjugate pair solution.

$$k(r_1) = a(r_1) \pm i\, b(r_1) \tag{4.2.6}$$

The lowest order representation

$$w(r_0, r_1, \theta, z, t) = w^{(0)}(r_1, z)\, e^{i(r_0 + m\theta - \omega t)}$$

with $\qquad r_0 = \lambda \int_{R_0}^{r_1} k\, dr \quad ; \qquad \lambda = \frac{1}{\epsilon}$

may be rewritten

$$w(r_1, \theta, z, t) = w^{(0)}(r_1, z)\, \chi(r_1)\, e^{i(m\theta - \omega t)} \tag{4.2.7}$$

so that
$$\chi(r_1) \sim e^{i\lambda \int_{R_o}^{r_1} \text{tr} \, dr}$$

We shall construct an equation for $\chi(r_1)$. Since we expect that $\chi(r_1)$ would have two wave solutions with wavenumbers given by (4.2.6), the governing equation is second order in r_1 , and is (see Section 4.5 for details):

$$\frac{d^2 \chi}{dr_1^2} - 2\lambda a i \frac{d\chi}{dr_1} - \lambda^2 (a^2 + b^2) \chi = 0 \qquad (4.2.8)$$

Removing the common wave-factor $e^{i\lambda \int adr}$ from χ

$$\chi = \tilde{\chi} \, e^{i\lambda \int_{R_o}^{r_1} a \, dr} \qquad (4.2.9)$$

we can transform (4.2.8), and after dropping terms small compared to λ^2 , obtain:

$$\frac{d^2 \tilde{\chi}}{dr_1^2} - \lambda^2 b^2 \tilde{\chi} = 0 \qquad (4.2.10)$$

It turns out that $b^2(r_1)$ has the schematic form shown in Figure 4.1, and can be represented by

$$b^2(r_1) = f(r_1)(r_1 - r_c)^2 + q_2 \qquad (4.2.11)$$

where $f(r_1) > 0$ and $q_2 \sim O(\lambda^{-1})$ and $q_2 > 0$.
$b^2(r_1)$ has a double zero (of order 1) at $r_1 = r_c$.

We can transform (4.2.10) into a standard equation (in this case, the Weber's Equation) whose solution (the parabolic cylinder functions)

$$\tilde{\chi} = a_1 \chi_{s_1} + a_2 \chi_{s_2} \qquad (4.2.12)$$

where a_1 and a_2 are constants
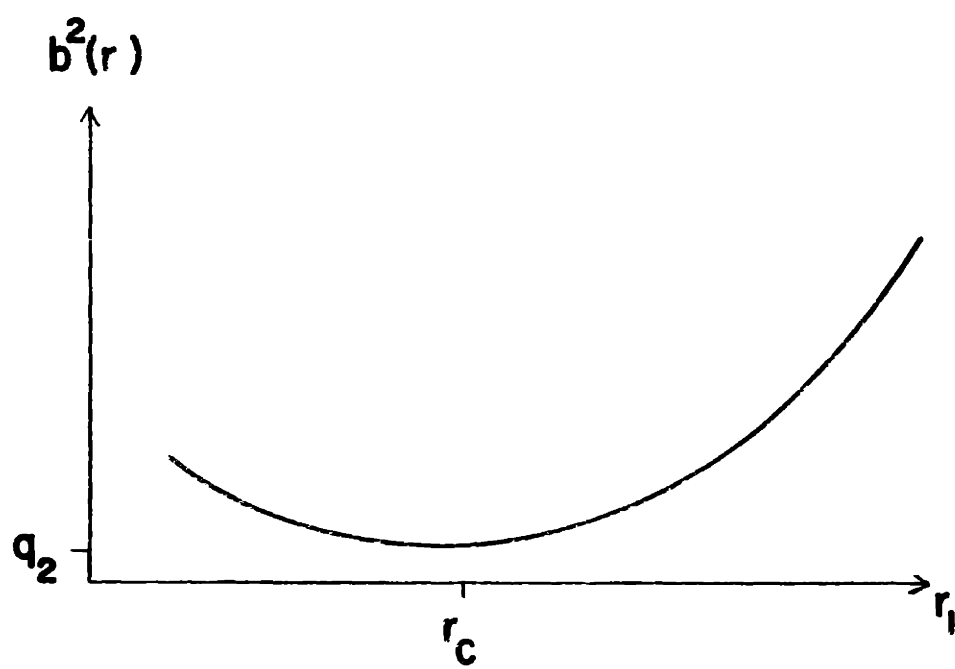
Fig. 4.1 Schematic plot of $b^2(r_1)$.

is valid in the entire domain $R_o \leq r_1 < \infty$, including the turning point $r_1 = r_c$.

The asymptotic form of $\overset{\sim}{\chi}$ at large $r_1 > r_c$ has to satisfy the boundary condition at $r_1 = \infty$ (4.1.11). This allows only the component of χ (we shall designate χ_{s1}) which decays for $r_1 > r_c$. This determines $a_2 \equiv 0$.

For $R_o \leq r_1 < r_c$, and r_1 far away from r_c , $\overset{\sim}{\chi} = a_1 \chi_{s1}$ (which decays for $r_1 > r_c$) has a standard asymptotic form which includes both a decaying and an amplifying component. (Refer to Appendix D for asymptotic formulae of parabolic cylinder functions).

$$\overset{\sim}{\chi} \sim C(r_1) \left[e^{\lambda \int_{r_c}^{r_1} \theta \, dr} + \Lambda e^{-\lambda \int_{r_c}^{r_1} \theta \, dr} \right] \qquad 4.2.13)$$

where Λ is given explicitly by the standard asymptotic formula of χ_{s1} in the domain $R_o \leq r_1 < r_c$.

$\overset{\sim}{\chi}$ given by (4.2.13) has to satisfy the boundary condition (4.1.10) at $r_1 = R_o$. However, this involves tedious algebraic manipulations which can be avoided.

The WKB solution to (4.2.10) is given by

$$\overset{\sim}{\chi} = A(r_1) e^{\lambda \int_{R_o}^{r_1} \theta \, dr} + B(r_1) e^{-\lambda \int_{R_o}^{r_1} \theta \, dr} \qquad (4.2.14)$$

This is valid in the domain $R_o \leq r_1 < r_c$ (but not at $r_1 = r_c$).

The boundary condition at $r_1 = R_o$ can be transformed into a condition on χ (see Section 4.5 for details).

$$\frac{d\chi}{dr_1} = 0 \qquad \text{at} \qquad r_1 = R_o \qquad (4.2.15)$$

By demanding that $\overset{\sim}{\chi}$ given by (4.2.14) satisfy (4.2.15), we obtain the relationship between $A(r_1)$ and $B(r_1)$:

$$B(r_1) = A(r_1) \, \Delta \tag{4.2.16}$$

with

$$\Delta = - \tan^{-1} \left[\frac{b(R_0)}{a(R_0)} \right]$$

(4.2.14) thus becomes

$$\overset{\sim}{\chi} = A(r_1) \left[e^{\lambda \int_{R_0}^{r_1} b \, dr} + \Delta \, e^{-\lambda \int_{R_0}^{r_1} b \, dr} \right] \tag{4.2.17}$$

Since (4.2.13) and (4.2.17) are two expressions for $\overset{\sim}{\chi}(r_1)$ for $R_0 \leq r_1 < r_c$, they must be identical, $\underline{i.e.}$ we must demand that

$$\frac{A \, e^{\lambda \int_{R_0}^{r_c} b \, dr}}{C} = \frac{A \, \Delta \, e^{-\lambda \int_{R_0}^{r_c} b \, dr}}{C \, \Lambda}$$

or

$$e^{2\lambda \int_{R_0}^{r_c} b \, dr} = \frac{\Delta}{\Lambda} \tag{4.2.18}$$

We shall write (4.2.18) as

$$\mathcal{D}(\omega; \, k, \, m, \, r_1) = 0$$

Since the initial guess of ω determines $k(r_1)$, and subsequently $b(r_1)$ (4.2.9), r_c (4.2.11), Λ (4.2.13) and Δ (4.2.16), (4.2.18) is a condition on ω which is imposed by the radial boundary conditions. $\mathcal{D} = 0$ is hence the <u>global dispersion relationship</u> which yields discrete values of the normal mode frequency ω.

The most unstable wave is, in the usual sense, the one with the maximum $\text{Im}(\omega)$. The fact that the normal mode approach involves radial boundary conditions at $r_1 = R_0$ and $r_1 = \infty$ in order to determine ω and $k(r_1)$ of the disturbance points out that the eigenvalue ω is the frequency

at which the <u>overall system</u> has to oscillate in order to constitute a single mode. The associated eigenfunctions, then, are global solutions.

We note that with the local dispersion relationship (4.2.5), we could also determine the local behavior of prescribed disturbances. We fix m, $k(r_1)$ and solve for $\omega(r_1)$. $k(r_1)$ is assumed real, and $\omega(r_1)$ may be complex. The $\omega(r_1)$ thus obtained is the frequency with which the given disturbance at any part of the vortex is able to oscillate due to the physical balance of forces at r_1 . This is the approach adopted by Kurihara (1976). At each of the two reference radii he chose, Kurihara solved an eigenvalue problem for perturbations of spiral shape. At $R = 150$ km and $R = 400$ km , he assumed the basic state variables $\overline{U}(R,p)$, $\overline{V}(R,p)$, $\overline{\Theta}(R,p)$ as well as $\frac{\partial \overline{U}}{\partial r}(R,p)$, $\frac{\partial \overline{V}}{\partial r}(R,p)$ and $\frac{\partial \overline{\Theta}}{\partial r}(R,p)$. The perturbations were assumed to be Archimedes spirals with m arms and a constant radial wavelength D. These spirals were allowed to extend to the center of the storm. The vertical structure was approximated by a $5\frac{1}{2}$ level model (thus giving extraneous roots as eigenvalues). Kurihara found that unstable waves existed only at $R = 150$ km where both the vertical and horizontal shears of the basic state were strong. At $R = 400$ km , the flow was stable. Of the family of spiral perturbations Kurihara assumed, the spiral with $m = 2$ and $D = 200$ km was the most unstable and it propagated outwards. (Bands which propagated inwards were attributed to artificial layering in the vertical.) From his study we can conclude that a wave perturbation with fixed radial and azimuthal wavenumbers may grow in the inner, strong-shear region of the storm, and become neutral as it propagates outwards. Left unanswered are the questions: 1) what actually determines the observed configuration of the spiral rainbands, 2) what is the mechanism that continuously generates these bands and 3) what is the nature of the bands with D of the order of 20-60 km?

4.2.3 The First-order Equation: The Amplitude Equation

The first-order equation is

$$\mathcal{L}'(w^{(1)}) = \mathcal{m}'(w^{(0)}).$$ (4.2.3b)

If $\tilde{\mathcal{L}}'$ is the adjoint operator of $\mathcal{L}'$, and $\tilde{w}^{(0)}$ is the solution of

$$\tilde{\mathcal{L}}'(\tilde{w}^{(0)}) = 0$$ (4.2.18)

then the condition for solvability of (4.2.3b) is (see Morse and Feshbach (1953), pages 874–877):

$$\int_0^\infty \tilde{w}^{(0)} \mathcal{m}'(w^{(0)}) \, d\zeta = 0$$ (4.2.19)

provided that $\tilde{w}^{(0)} = 0$ at $z = 0$ and ∞.

In our problem, it turns out that $\mathcal{L}'$ is self-adjoint, so that $\mathcal{L}' = \tilde{\mathcal{L}}'$, and $\tilde{w}^{(0)} = w^{(0)}$. Equation (4.2.19) is reduced to

$$\int_0^\infty w^{(0)} \mathcal{m}'(w^{(0)}) \, d\zeta = 0$$ (4.2.20)

Substituting (4.2.4) into (4.2.20), we get

$$\int_0^\infty \varphi \, \mathcal{m}'(A \varphi) \, d\zeta = 0$$ (4.2.21)

Since the highest order of the r_1 derivative in $\mathcal{m}'$ is one, (4.2.21) is a first-order ordinary differential equation in $A(r_1)$ which can easily be solved subject to a radial boundary condition on the amplitude.

The analysis outlined in equations (4.2.1) to (4.2.21) solves for the lowest order w solution.

4.3. A SIMPLE EXAMPLE: WAVES IN A BAROTROPIC VORTEX

To illustrate the procedure outlined in Section 4.2 and to investigate the gravity waves in the interior of a hurricane vortex, we solve Equations (4.1.1) to (4.1.5) when the basic flow is a Boussinesq, frictionless axisymmetric vortex $\overline{V}(r)$ with no vertical shear. In order to impose a modal structure in the vertical, we confine the vortex between rigid walls at $z = 0$ and $z = H_3$.

Equations (4.1.1) to (4.1.5) can be combined to form one equation in w:

$$\frac{D^2}{Dt^2}\left(\frac{\partial^2 w'}{\partial z^2} + k^2 \frac{\partial^2 w'}{\partial r_0^2} + \frac{1}{r_0^2}\frac{\partial^2 w'}{\partial \theta^2} \right) \tag{4.3.1}$$

$$+ N^2 \left(k^2 \frac{\partial^2 w'}{\partial r_0^2} + \frac{1}{r_0^2}\frac{\partial^2 w'}{\partial \theta^2} \right) = Z$$

where $\dfrac{D}{Dt} = \dfrac{\partial}{\partial t} + \dfrac{\overline{V}}{r_0}\dfrac{\partial}{\partial \theta}$

$$Z = \left(k^2 \frac{\partial^2}{\partial r_0^2} + \frac{1}{r_0^2}\frac{\partial^2}{\partial \theta^2} \right)\left(\frac{D Y_3}{Dt} + Y_4 \right)$$
$$+ \frac{D}{Dt}\frac{\partial}{\partial z}\left(\frac{D Y_5}{Dt} - k\frac{\partial Y_1}{\partial r_0} - \frac{1}{r_0}\frac{\partial Y_2}{\partial \theta} \right) \tag{4.3.2}$$

$$Y_1 = -\epsilon\left[-\frac{2\overline{V}}{r_1}v' - v' + \frac{\partial}{\partial r_1}\left(\frac{\rho'}{\rho} \right) \right] \tag{4.3.3}$$

$$Y_2 = -\epsilon\left[\left(\frac{\partial \overline{V}}{\partial r_1} + \frac{\overline{V}}{r_1} + 1 \right)u' \right] \tag{4.3.4}$$

$$Y_3 = -\epsilon\left[\overline{u}\frac{\partial w'}{\partial r_1} + \overline{w}\frac{\partial w'}{\partial z} \right] = 0 \tag{4.3.5}$$

$$Y_4 = -\epsilon\left[\overline{u}\frac{\partial \theta'}{\partial r_1} + \overline{w}\frac{\partial \theta'}{\partial z} \right] = 0 \tag{4.3.6}$$

$$Y_5 = -\epsilon\left[\frac{u'}{r_1} + \frac{\partial u'}{\partial r_1} \right] \tag{4.3.7}$$

We shall solve Equation (4.3.1) subject to the boundary conditions:

1) $w = 0$ at $z = 0$ and at $z = H_3$

and 2) the wave energy flux be directed outwards as $r_1 \to \infty$

Assuming

$$w' = \left[w^{(0)} + \epsilon w^{(1)} + \epsilon^2 w^{(2)} + \cdots \right] e^{i(r_0 + m\theta - \omega t)} \tag{4.3.8}$$

we get the lowest order equation

$$-\left(\frac{m\bar{V}}{r_0} - \omega\right)^2 \left(\frac{\partial^2 w^{(0)}}{\partial z^2} - \left(k^2 + \frac{m^2}{r_0^2}\right) w^{(0)}\right) -$$

$$N^2 \left(k^2 + \frac{m^2}{r_0^2}\right) w^{(0)} = 0 \tag{4.3.9}$$

and the first-order equation

$$-\left(\frac{m\bar{V}}{r_0} - \omega\right)^2 \left(\frac{\partial^2 w^{(1)}}{\partial z^2} - \left(k^2 + \frac{m^2}{r_0^2}\right) w^{(1)}\right) -$$

$$N^2 \left(k^2 + \frac{m^2}{r_0^2}\right) w^{(1)} = Z_1 \tag{4.3.10}$$

where $\sigma = \dfrac{m\bar{V}}{r_D} - \omega$ \tag{4.3.11}

$$Z_1 = -\left(k^2 + \frac{m^2}{r_0^2}\right) \left(i\sigma Y_3 + Y_4\right)$$

$$+ i\sigma \frac{\partial}{\partial z}\left(i\sigma Y_5 - ik Y_1 - \frac{im}{r_1} Y_2\right) \tag{4.3.12}$$

(4.3.9) has solution

$$w^{(0)} = A e^{-i\gamma z} + B e^{i\gamma z} \tag{4.3.13}$$

where

$$\gamma^2 = -\left(k^2 + \frac{m^2}{r_0^2}\right) \frac{\sigma^2 - N^2}{\sigma^2} \tag{4.3.14}$$

and $\text{Re}(\gamma) > 0$

The boundary conditions of zero vertical velocity at $z = 0$ and at $z = H_3$ give us

$$w^{(0)} = A(r_1) \sin \gamma z \qquad (4.3.15)$$

and

$$\gamma H_3 = n\pi, \qquad n = \pm 1, \pm 2, \pm 3, \cdots \qquad (4.3.16)$$

Choosing the lowest mode $n = 1$, we have $\gamma^2 = \dfrac{\pi^2}{H_3^2}$ and

$$k^2(r_1) = \frac{\pi^2}{H_3^2} \frac{\sigma^2}{N^2 - \sigma^2} - \frac{m^2}{r_0^2} \qquad (4.3.17)$$

Equation (4.3.17) is the dispersion relationship relating the local horizontal wave numbers $k(r_1)$ and m to the frequency ω. Since ω is real for all real $k(r_1)$, the short waves that we have assumed are locally neutral in the basic flow. Hence, in the absence of a selection mechanism for the waves, the waves defined by (4.3.17) are all possible. In the following analysis, we shall assume m and ω and study the radial behavior of these internal gravity waves.

For the case where $\omega > 0$ and $k > 0$, the lowest order w' has the solution

$$w = A(r_1) \sin\left(\frac{\pi}{H_3} z\right)\left[C e^{i\int_{R_0}^{r_1} k dr} + D e^{-i\int_{R_0}^{r_1} k dr} \right] e^{i(m\theta - \omega t)} \qquad (4.3.18)$$

The first wave component $Ce^{(i\int k dr - i\omega t)}$ represents an outward propagating internal gravity wave. Its group velocity is also outwards. The second component $De^{(-i\int k dr - i\omega t)}$ represents an inward propagating wave carrying energy inwards towards the center of the storm. The radial boundary

condition of outward energy flux at $r \to \infty$ demands $D \equiv 0$. Therefore,

we can assume $C = 1$ without loss of generality, and

$$w' = A(r_1) \sin \frac{\pi}{H_3} z \, e^{i\left(\frac{1}{\epsilon}\int_{R_0}^{r_1} k \, dr + m\theta - \omega t\right)} \tag{4.3.19}$$

The first-order equation is

$$\left(\frac{m\bar{v}}{r_0} - \omega\right)^2 \frac{\partial^2 w^{(1)}}{\partial z^2} + \left(k^2 + \frac{m^2}{r_0^2}\right)\left(N^2 - \left(\frac{m\bar{v}}{r_0} - \omega\right)^2\right) w^{(1)} \tag{4.3.20}$$

$$= Z_1$$

where

$$Z_1 = C_1(r_1) \frac{\partial^2 w^{(0)}}{\partial z^2} + C_2(r_1) \frac{\partial}{\partial r_1} \frac{\partial^2 w^{(0)}}{\partial z^2}$$

$$C_1(r_1) = \sigma^2 \frac{1}{r_1} \frac{\partial}{\partial r_1}\left(\frac{i k r_1}{k^2}\right) + \sigma k \left[\left(\frac{2\bar{v}}{r_1} + 1\right)\frac{i m}{r_0 k^2}\right. \tag{4.3.21}$$

$$\left. + \frac{\partial}{\partial r_1}\left(\frac{i \sigma}{k^2}\right)\right] - \sigma \frac{m}{r_0} \frac{i k}{k^2}\left(\frac{\partial \bar{v}}{\partial r_1} + \frac{\bar{v}}{r_1} + 1\right)$$

$$C_2(r_1) = \frac{2 i \sigma^2 k}{k^2}$$

The condition for solvability of $w^{(1)}$ is

$$\int_0^\infty w^{(0)} Z_1 \, dz = 0 \tag{4.3.22}$$

or

$$\int_0^\infty \left[C_1(r_1) \, w^{(0)} \frac{\partial^2 w^{(0)}}{\partial z^2} + C_2(r_1) w^{(0)} \frac{\partial}{\partial r_1} \frac{\partial^2 w^{(0)}}{\partial z^2} \right] dz \tag{4.3.23}$$

$$= 0$$

This can be simplified to

$$C_1(r_1) A(r_1) + C_2(r_1) \frac{dA}{dr_1} = 0 \qquad (4.3.24)$$

with the solution

$$A(r_1) = A(R_0) e^{-\int_{R_0}^{r_1} (C_1/C_2)\, dr} \qquad (4.3.25)$$

Equation (4.3.24) could have been obtained more easily from Equation (4.3.20) in the usual fashion by perturbation analysis. Since

$$Z_1 = C_1(r_1) \frac{\partial^2 w^{(0)}}{\partial z^2} + C_2(r_1) \frac{\partial}{\partial r_1} \frac{\partial^2 w^{(0)}}{\partial z^2}$$

when we substitute $w^{(0)}$ into (4.3.19) into Z_1, we obtain

$$Z_1 = -\frac{\pi^2}{H_3} \left[C_1(r_1) A(r_1) + C_2(r_1) \frac{dA}{dr_1} \right] \times$$
$$e^{i\left(\frac{1}{\varepsilon}\int k\, dr + m\theta - \omega t\right)}$$

In order to eliminate secular terms in $w^{(1)}$, the expression in the square brackets must be zero, i.e.,

$$C_1(r_1) A(r_1) + C_2(r_1) \frac{dA}{dr_1} = 0$$

This is exactly Equation (4.3.24).

The amplitude and phase variation for the gravity waves in a vortex are illustrated for three cases:

1) when the mean vortex is a potential vortex: $\overline{V} = 1/r$;

2) when the vortex has constant tangential velocity: $\overline{V} = 1$; and

3) when the vortex has constant angular velocity: $\overline{V} = r$.

The results are illustrated in Figures 4.2a-c. We have chosen $N^2 = .1$, $m = 2$, and $\omega = 0$.
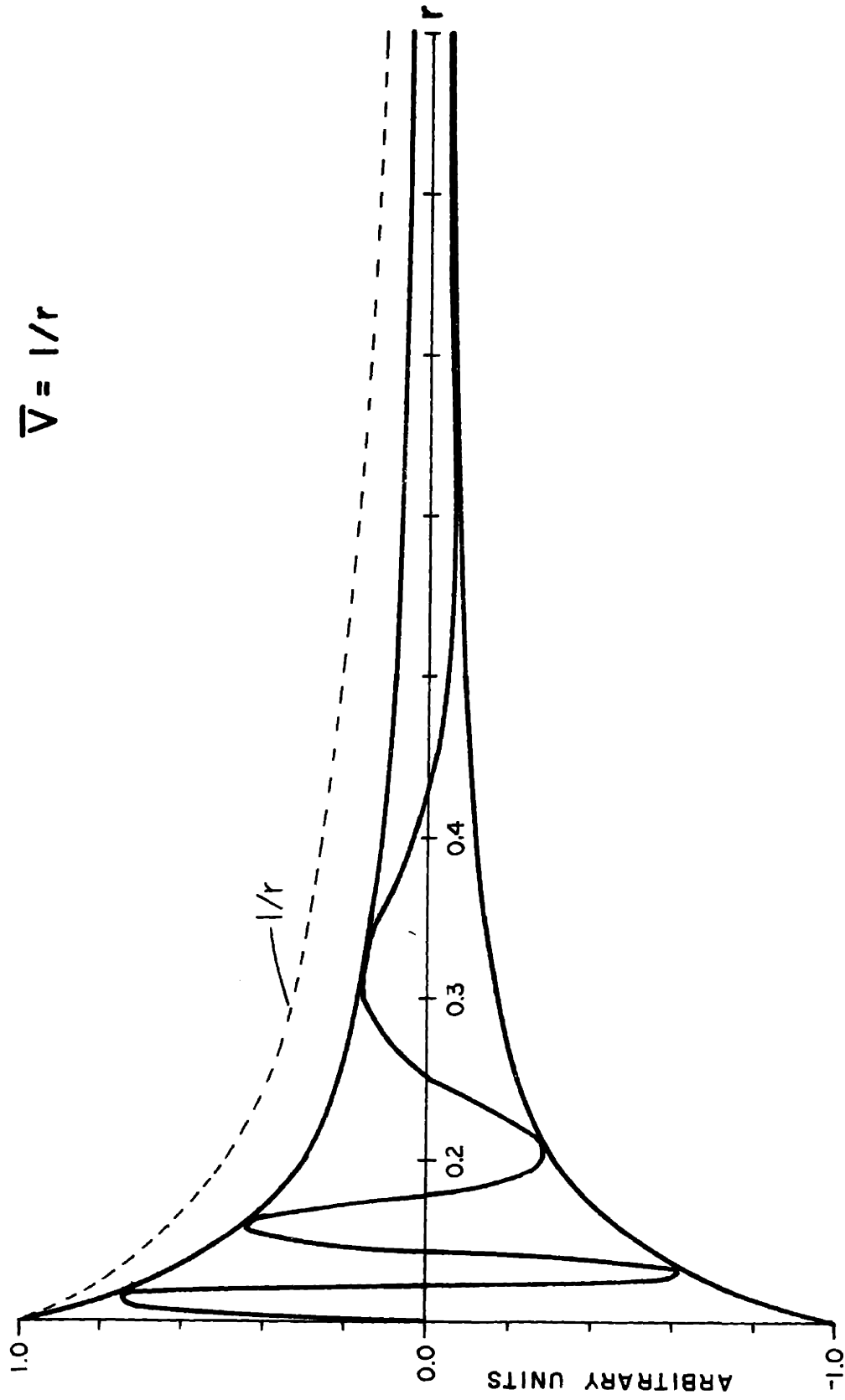
Figure 4.2a. Graph of amplitude and phase variations of internal gravity waves in a differentially rotating vortex. $\bar{V}(r) = 1/r$.

$\overline{V} = 1.$

1/r

r

ARBITRARY UNITS

0.0

0.2

0.4

0.5

0.6

0.7

1.0

-1.0
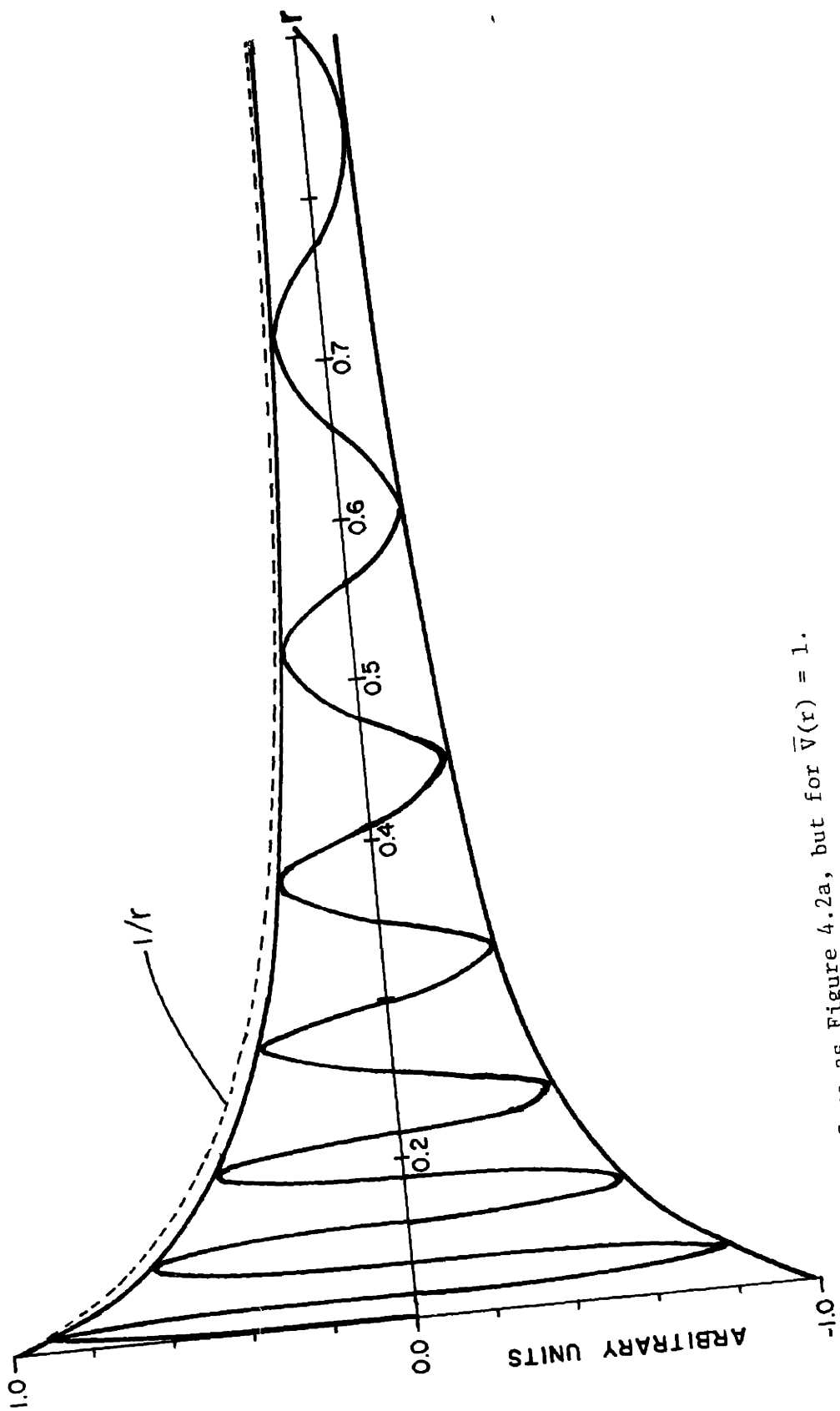
Figure 4.2b. Same as Figure 4.2a, but for $\overline{V}(r) = 1.$

$$\overline{V} = r$$
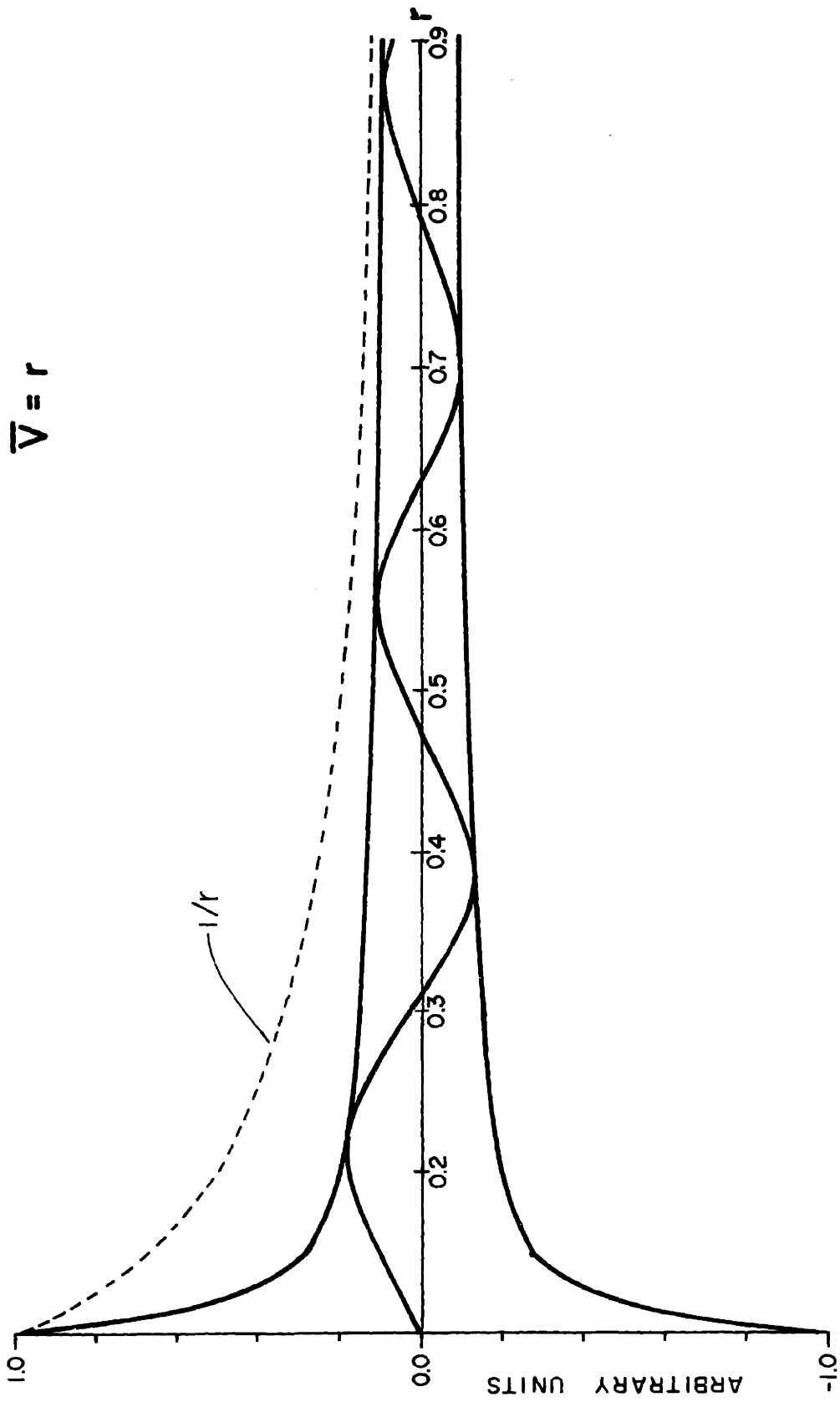
Figure 4.2c. Same as Figure 4.2a, but for $\overline{V}(r) = r$.

From Figure 4.2, we note that the wavelength is related to the strength of the flow relative to the propagating wave. The greater $(\frac{m\bar{V}}{r_p} - \omega)$, the shorter the wavelength. Also, both the amplitude and the energy density decrease outwards with r_1 , which is consistent with the radiation condition at large r.

This exercise suggests that in the stably stratified region of the hurricane, the spiral bands could indeed possess the properties of internal gravity waves. However, in the absence of some forcing or selection mechanism in the flow, we would have no way of picking a particular mode from the continuous spectrum of these gravity waves.

We note that we arrive at the above conclusion after we impose only one radial boundary condition, i.e., radiation condition at $r_1 = \infty$. However, if we had put in, in addition, a wall at $r_1 = Ro$ and had demanded that $u' = 0$ at $r_1 = Ro$ (the wall condition), we would have had no eigen-solutions unless we had included extra physics in the problem. This is because we need two wave components ($e^{i\int kdr}$, $e^{-i\int kdr}$) to form a standing wave $(\sin\int kdr)$ so that $u' = 0$ at $r = Ro$, whereas the radiation condition allows one wave solution ($e^{i\int kdr}$). However, if we have some turning point $r = r_c$ in the flow which separates a two-wave inner region from a one-wave outer region, both the radiation condition and the wall condition can be satisfied, and we can have discrete eigen-frequencies. This problem has been studied by Lau et al. (1976). Their point $r = r_c$ turns out to be the critical level or "co-rotation circle" in the flow where $\frac{m\bar{V}}{r_p} = \omega$. The inclusion of a turning point essentially reduces a semi-infinite string problem (which has no modal solutions) into a finite string problem where modal solutions are allowed.

4.4 THE LOCAL DISPERSION RELATIONSHIP

We now return to the flow under consideration where the basic state is the three-layer representation of the hurricane equilibrium state defined in Section 3. Equations (4.1.1) to (4.1.5) represent the linear perturbations within each layer. We shall use Arabic numeral subscripts (1, 2, 3) to denote values within each layer, and Roman numeral subscripts (I, II) to denote values at the interfaces $z = H_1$ and $z = H_2$.

We assume the following basic density distribution

$$\bar{\rho}_j = \begin{cases} 1 & 0 \leq z \leq H_2; \quad j = 1, 2 \\ e^{-z/\lambda} & H_2 \leq z; \quad j = 3 \end{cases} \tag{4.4.1}$$

where λ is the density scale height of the atmosphere, so that

$$\frac{1}{\mathcal{H}_j} = \begin{cases} 0 & 0 \leq z \leq H_2; \quad j = 1, 2 \\ \frac{1}{\lambda} & H_2 \leq z; \quad j = 3 \end{cases} \tag{4.4.2a}$$

and

$$N_j^2 = \begin{cases} 0 & 0 \leq z \leq H_2; \quad j = 1, 2 \\ N^2 & H_2 \leq z; \quad j = 3 \end{cases} \tag{4.4.2b}$$

Within each layer j, (4.1.1) to (4.1.5) can be combined to form one equation in w_j' :

$$\frac{D_j^2}{Dt^2} \left(k^2 \frac{\partial^2}{\partial r_0^2} + \frac{1}{r_0^2} \frac{\partial^2}{\partial \theta^2} + \frac{\partial^2}{\partial z^2} - \frac{1}{\mathcal{H}_j} \frac{\partial}{\partial z} \right) w_j'$$

$$+ N_j^2 \left(k^2 \frac{\partial^2}{\partial r_0^2} + \frac{1}{r_0^2} \frac{\partial^2}{\partial \theta^2} \right) w_j' - \left(\frac{\partial^2 \bar{U}_j}{\partial z^2} k \frac{\partial}{\partial r_0} + \frac{\partial \bar{V}_j}{\partial z} \frac{1}{r_0} \frac{\partial}{\partial \theta} \right) \frac{D_j w_j'}{Dt} \tag{4.4.3}$$

$$= m_j \qquad\qquad j = 1, 2, 3$$

where $\nabla^2 = k^2 \dfrac{\partial^2}{\partial r_0^2} + \dfrac{1}{r_0^2}\dfrac{\partial^2}{\partial \theta^2} + \dfrac{\partial^2}{\partial z^2}$

$\dfrac{D_j}{Dt} = \dfrac{\partial}{\partial t} + k\,\bar{u}_j \dfrac{\partial}{\partial r_0} + \dfrac{\bar{V}_j}{r_0}\dfrac{\partial}{\partial \theta}$

$$\eta_j = \epsilon\left\{\left(k^2\dfrac{\partial^2}{\partial r_0^2} + \dfrac{1}{r_0^2}\dfrac{\partial^2}{\partial \theta^2}\right)\left(\dfrac{D_j}{Dt}Q_{3j} + Q_{4j}\right)\right.$$

$$\left. - k\dfrac{\partial}{\partial r_0}\dfrac{D_j}{Dt}\dfrac{\partial Q_{1j}}{\partial z} - \dfrac{1}{r_0}\dfrac{\partial}{\partial \theta}\dfrac{D_j}{Dt}\dfrac{\partial Q_{2j}}{\partial z} + \dfrac{D_j^2}{Dt^2}\dfrac{\partial Q_{5j}}{\partial z}\right\}$$

$$Q_{1j} = -\left[\bar{u}_j\dfrac{\partial u_j'}{\partial r_1} + u_j'\dfrac{\partial \bar{u}_j}{\partial r_1} + \bar{W}_j\dfrac{\partial u_j'}{\partial z} - \dfrac{2\bar{V}_j v_j'}{r_1}\right.$$

$$\left. - \dfrac{\partial}{\partial r_1}\left(\dfrac{p_j'}{\bar{\rho}_j}\right) - v_j' - \nabla^2 u_j'\right]$$

$$(4.4.4)$$

$$Q_{2j} = -\left[\bar{u}_j\dfrac{\partial v_j'}{\partial r_1} + u_j'\dfrac{\partial \bar{V}_j}{\partial r_1} + \bar{W}_j\dfrac{\partial v_j'}{\partial z} + \dfrac{\bar{u}_j v_j'}{r_1}\right.$$

$$\left. + \dfrac{\bar{V}_j u_j'}{r_1} + u_j' - \nabla^2 v_j'\right]$$

$$Q_{3j} = -\left[\bar{u}_j\dfrac{\partial w_j'}{\partial r_1} + \bar{W}_j\dfrac{\partial w_j'}{\partial z} - \nabla^2 w_j'\right]$$

$$Q_{4j} = -\left[\bar{u}_j\dfrac{\partial b'}{\partial r_1} + \bar{W}_j\dfrac{\partial b'}{\partial z}\right]$$

$$Q_{5j} = -\left[\dfrac{u_j'}{r_1} + \dfrac{\partial u_j'}{\partial r_1} + \dfrac{\partial \bar{W}}{\partial z}\right]$$

We note that with the layered representation of the mean state,

$$\dfrac{\partial^2 \bar{u}_j}{\partial z^2} = \dfrac{\partial^2 \bar{V}_j}{\partial z^2} = 0$$

Assuming

$$w_j' = \left\{w_j^{(0)} + \epsilon w_j^{(1)} + \epsilon^2 w_j^{(2)} + \cdots\right\} e^{\frac{z}{2H_j}} e^{i(r_0 + m\theta - \omega t)} \qquad (4.4.5)$$

we have the lowest order equations within each layer:

$$- \sigma_1^2 \left[\frac{\partial^2 w_1^{(0)}}{\partial \zeta^2} - \kappa^2 w_1^{(0)} \right] = 0$$

$$- \sigma_2^2 \left[\frac{\partial^2 w_2^{(0)}}{\partial \zeta^2} - \kappa^2 w_2^{(0)} \right] = 0 \qquad (4.4.6)$$

$$- \sigma_3^2 \left[\frac{\partial^2 w_3^{(0)}}{\partial \zeta^2} - \kappa^2 \left(N^2 - \sigma_3^2 \right) - \frac{\sigma_3^2}{4 N^2} \right] w_3^{(0)} = 0$$

where

$$\sigma_j = \hbar \bar{u}_j + \frac{m}{r_0} \bar{V}_j - \omega \quad , \quad j = 1, 2, 3 \qquad (4.4.7)$$

$$\kappa^2 = \hbar^2 + \frac{m^2}{r_0^2}$$

Equation (4.4.6) together with the boundary conditions at $z = 0$ and at $z \to \infty$ have solutions:

$$w_1^{(0)} = A(r_1) \sinh \kappa \zeta$$

$$w_2^{(0)} = A(r_1) \sinh \kappa \zeta + B(r_1) \sinh \kappa (\zeta - H_1) \qquad (4.4.8)$$

$$w_3^{(0)} = C(r_1) e^{-\tilde{\gamma} \zeta} \quad ,$$

where

$$\tilde{\gamma}^2(r_1) = \kappa^2 \frac{\sigma_3^2 - N^2}{\sigma_3^2} + \frac{1}{4 N^2} \; ; \quad Re(\tilde{\gamma}) > 0 \qquad (4.4.9)$$

Matching pressure and vertical velocity at the interfaces H_1 and H_2 gives us the three equations in the three unknown amplitudes $A(r_1)$, $B(r_1)$ and $C(r_1)$. The condition for nontrivial solutions A, B, C gives the dispersion relationship: (next page)

$$\det \begin{vmatrix} (S_2-S_1)\sinh \kappa H_1 & -\sigma_{I\!I} \kappa \\[2mm] (\sigma_{I\!I}\hat{\imath}-S_2)\sinh \kappa H_2 & (\sigma_{I\!I}\hat{\imath}-S_2)\sinh \kappa D_2 \\ +\sigma_{I\!I} \kappa \cosh \kappa H_2 & +\sigma_{I\!I} \kappa \cosh \kappa D_2 \end{vmatrix} = O^{(4.4.10)}$$

where

$$S_j = k\frac{\partial \bar{u}_j}{\partial \xi} + \frac{m}{r_0}\frac{\partial \bar{v}_j}{\partial \xi} \quad , \quad j = 1, 2$$

$$\sigma_J = k\,\bar{u}_J + \frac{m}{r_0}\,\bar{v}_J - \omega \quad , \quad J = I, I\!I$$

$$\hat{\imath} = \sqrt{\kappa^2 \frac{\sigma_{I\!I}^2 - N^2}{\sigma_{I\!I}^2} + \frac{1}{4\eta J^2}} + \frac{1}{2\eta \nu}$$

$$D_2 = H_2 - H_1$$

4.4.1 Solution of the Dispersion Relationship

For given values of ω and m, $k(r_1)$ is found from the dispersion relationship by applying SUBROUTINE LSQNK2 from MIT IPC Mathlib AP-26 (See Appendix B). The subroutine finds up to four zeros of an analytic function Δ (k) within a contour in the complex k plane. If there are more than four zeros within the contour, the subroutine reports only the number of zeros, and a new smaller contour must then be found.

The domain of analyticity of the dispersion relationship (4.4.10) in the k-plane is established in Appendix C.

The number of zeros reported within a contour is checked independently by Hamming's "crude method" (see Hamming (1962), page 80). For every point in the complex k plane, Δ (k) is evaluated and the quadrant number (1, 2, 3, 4) in which Δ (k) lies is plotted. A point k_0 is a

zero of multiplicity n if a closed contour around k_0 traverses n cycles of quadrant numbers.

The solution $k(r_1)$ of (4.4.10) for $\omega = .001$, $m = 2$, and $N^2 = .1$ is shown in Figure 4.3. There are two branches of $k(r_1)$ in the right half plane. The branch in the upper half plane represents a trailing wave whose amplitude decays outwards, whereas the branch in the lower half plane represents a trailing wave whose amplitude increases outwards. We note that these two branches are complex conjugates of each other and we can write

$$k(r_1) = a(r_1) \pm i\, b(r_1) \qquad (4.4.11)$$

$b(r_1)$ has an extremum at $r_1 = r_c$.

Since $b(r_c) \sim .005 \ll b(r_1)$, $r_1 \neq r_c$, we can write

$$b^2(r_1) = q_1(r_1) + q_2 \qquad (4.4.12)$$

where $q_2 = b(r_c)^2 \sim 0(6)$ and $q_1(r_1)$ has a double zero at $r_1 = r_c$. Thus we can write

$$q_1(r_1) = f(r_1)(r_1 - r_c)^2 \quad , \quad f(r_1) > 0$$

and

$$b^2(r_1) = f(r_1)(r_1 - r_c)^2 + q_2 \qquad (4.4.13)$$

We also note from Figure 4.3 that in the region $Ro \leq r_1 < r_c$,

$$|b(r_1)| < |a(r_1)| \qquad \text{for } Re(k) > 0 \qquad (4.4.14)$$
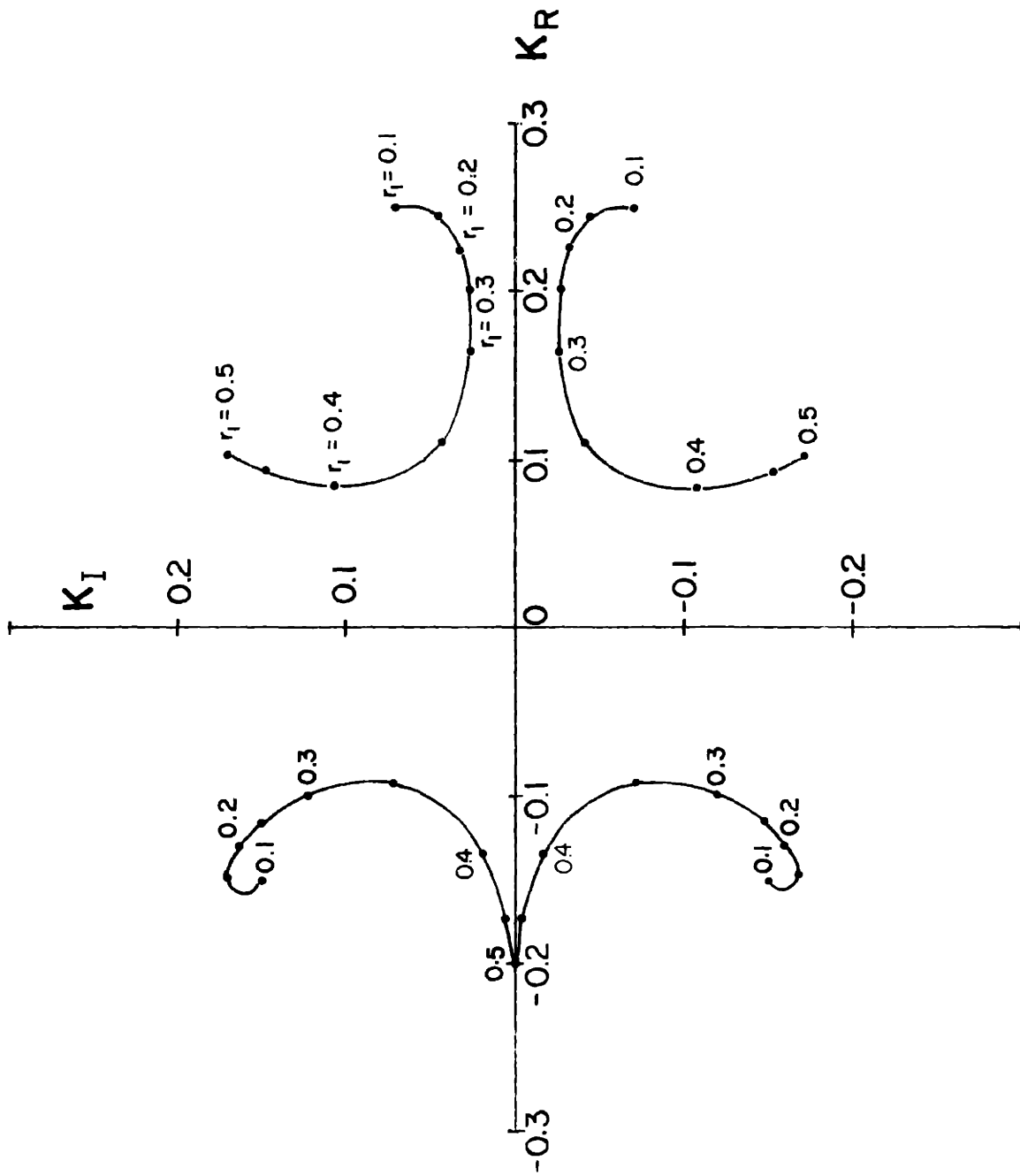
Figure 4.3. $k(r_1)$ solutions from $\mathcal{D}$ $(k; \omega, m, r_1) = 0$ for $\omega = .001$, $m = 2$.

4.5 THE GLOBAL EIGENVALUE PROBLEM

In this section, the local dispersion relationship (4.3.10) together with the radial boundary conditions (4.1.10) and (4.1.11) is used to obtain a global condition on ω. Since the linear perturbation equations (4.4.6) contain both a vertical and a radial dependence, it is difficult to apply the radial boundary conditions to them. However, the radial wavenumber $k(r_1)$ has no z dependence, and an <u>ordinary</u> differential equation may be constructed whose solutions have the same $k(r_1)$ as would have been obtained by using (4.4.6). We shall thus apply the radial boundary conditions to the new differential equation.

After we have obtained the new ordinary differential equation and its boundary conditions, we follow, to obtain the global dispersion relationship, the procedure in Lau <u>et al</u>. (1976) and Mark (1977) who studied unstable spiral modes in disk-shaped galaxies.

The representation (4.1.2)

$$w(r_0, r_1, \theta, z, t) = \left[w^{(0)}(r_1, z) + \cdots \right] e^{z/2u} \wedge$$
$$e^{i(r_0 + m\theta - \omega t)} \tag{4.5.1}$$

with

$$r_0 = \lambda \int_{R_0}^{r_1} k(r_1') \, dr_1' \quad , \qquad \lambda = \frac{1}{\epsilon}$$

may be written

$$w(r_1, \theta, z, t) = \left[w^{(0)}(r_1, z) + \cdots \right] e^{z/2u} \wedge$$
$$\chi(r_1) e^{i(m\theta - \omega t)} \tag{4.5.2}$$

We shall construct a differential equation for $\chi(r_1)$, governing the phase distribution in the radial direction. Since

$$\chi(r_1) \sim e^{i\lambda \int_{R_0}^{r_1} k \, dr}$$

(4.5.3)

and

$$\frac{d\chi}{dr_1} \sim i \lambda k \chi$$

for a pair of solutions

$$k(r_1) = a(r_1) \pm i b(r_1)$$

(4.5.4)

the governing equation for $\chi(r_1)$ is second-order:

$$\frac{d^2\chi}{dr_1^2} + \mu_1 \frac{d\chi}{dr_1} + \mu_2 \chi = 0$$

(4.5.5)

where μ_1 and μ_2 are to be determined. Substituting (4.5.3) into (4.5.5), we obtain a quadratic equation in k:

$$-\lambda^2 k^2 + i \lambda k \mu_1 + \mu_2 = 0$$

(4.5.6)

whose solutions are

$$k = \frac{i \mu_1}{2\lambda} \pm \sqrt{-\frac{\mu_1^2}{4\lambda^2} + \frac{\mu_2}{\lambda^2}}$$

(4.5.7)

Equating (4.5.7) with (4.5.4), we get

$$\frac{i \mu_1}{2\lambda} = a \quad \text{and} \quad \frac{\mu_1^2}{4\lambda^2} - \frac{\mu_2}{\lambda^2} = b^2$$

(4.5.8)

or
$$\mu_1 = -2\lambda a i$$

(4.5.9)

and
$$\mu_2 = -\lambda^2 (a^2 + b^2)$$

Substituting μ_1 and μ_2 into (4.5.5), we obtain the governing equation for $\chi(r_1)$:

$$\frac{d^2\chi}{dr_1^2} - 2\lambda a i \frac{d\chi}{dr_1} - \lambda^2(a^2 + b^2)\chi = 0 \qquad (4.5.10)$$

We shall now derive the boundary conditions for $\chi(r_1)$ from (4.1.10) and (4.1.11). From the linear perturbation equations (4.1.1) to (4.1.5), we can express u' in terms of w'. With the representation (4.5.1) for w', u' in the interior of the hurricane is

$$u'(r_0, r_1, \theta, \zeta, t) = \tilde{u}^{(0)}(r_1, \zeta) e^{\frac{3}{2}\mu} ik\, e^{i(\lambda \int_{R_0}^{r_1} k\,dr + m\theta - \omega t)}$$

with

$$\tilde{u}^{(0)}(r_1, \zeta) = -\left[+ \frac{1}{k^2} \frac{\partial^2 w^{(0)}}{\partial \zeta^2} + \frac{1}{i\sigma_{II} k^2 \mathcal{N}} w^{(0)} \right]$$

Thus if we write w' as (4.5.2), u' becomes

$$u'(r_0, \theta, \zeta, t) = \tilde{u}^{(0)}(r_1, \zeta) e^{\frac{3}{2}\mu} \epsilon \frac{d\chi}{dr_1} e^{i(m\theta - \omega t)} \qquad (4.5.11)$$

The wall condition $u' = 0$ at $r_1 = Ro$ becomes

$$\frac{d\chi}{dr_1} = 0 \qquad\qquad at \quad r_1 = R_0 \qquad (4.5.12)$$

The condition at $r_1 = \infty$ becomes

(4.5.13)

$$\chi \text{ remains bounded as } r_1 \to \infty .$$

We write

$$\chi = \tilde{\chi} \, e^{i\lambda \int_{R_0}^{r_1} a(r_1') \, dr_1'} \tag{4.5.14}$$

so that

$$\frac{d\chi}{dr_1} = \left(\frac{d\tilde{\chi}}{dr_1} + i\lambda a \tilde{\chi} \right) e^{i\lambda \int_{R_0}^{r_1} a(r_1') \, dr_1'}$$

and

$$\frac{d^2\chi}{dr_1^2} = \left[\frac{d^2\tilde{\chi}}{dr_1^2} + 2i\lambda a \frac{d\tilde{\chi}}{dr_1} + i\lambda \frac{da}{dr_1} \tilde{\chi} - \lambda^2 a^2 \tilde{\chi} \right] \cdot \tag{4.5.15}$$
$$e^{i\lambda \int_{R_0}^{r_1} a(r_1') \, dr_1'}$$

This transforms (4.5.10) into

$$\frac{d^2\tilde{\chi}}{dr_1^2} - \left(\lambda^2 b^2 - i\lambda \frac{da}{dr_1} \right) \tilde{\chi} = 0$$

Dropping $i\lambda \frac{da}{dr_1}$ which is small compared to $\lambda^2 b^2$, we have

$$\frac{d^2\tilde{\chi}}{dr_1^2} - \lambda^2 b^2(r_1) \tilde{\chi} = 0 \tag{4.5.16}$$

We note that $b^2(r_1) = q_1(r_1) + q_2$

with $q_1(r_1) = f(r_1)(r - r_c)^2$, $f(r_1) > 0$ and $q_2 \sim 0(\varepsilon)$ so that

Equation (4.5.16) has a double turning point at $r_1 = r_c$.

Away from $r_1 = r_c$, (4.5.16) has WKB solutions

$$\tilde{\chi}(r_1) \sim \frac{1}{\sqrt{q_1}} e^{\pm \lambda \int_{R_0}^{r_1} b(r_1') \, dr_1'} \tag{4.5.17}$$

This solution is not valid at $r_1 = r_c$ where $q_1 \simeq 0$. (See Nayfeh, 1973, Section 7.1.3.)

Instead of matching asymptotic solutions at $r_1 = r_c$, we shall find a solution for $\tilde{\chi}$ valid in the whole domain $R_0 \leq r_1 < \infty$,

including the turning point. The aysmptotic behavior of this solution at large $r_1 > r_c$ must satisfy the condition of boundedness at infinity. And its asymptotic behavior for large $r_1 < r_c$ must be identical to the WKB solution for $\overset{\sim}{\chi}$ for $Ro \leq r_1 < r_c$.

4.5.1 Solution Near the Turning Point $r_1 = r_c$

When $r_1 \simeq r_c$

$$\beta^2(r_1) \simeq f_0 (r_1 - r_c)^2 + q_2 \tag{4.5.18}$$

where $fo = f(r_c)$. We shall assume that r_1 is such that $r_1 \simeq r_c$, yet $fo(r_1 - r_c)^2 \gg 1$ and $(b^2)''''(r_1 - r_c)^3 \ll (b^2)''(r_1 - r_c)^2$ so that (4.5.18) is valid.

Now we introduce the Langer transformation (See Nayfeh, 1973, Section 7.3.2) of both the dependent and independent variables of (4.5.16):

$$\lambda \int_{r_c}^{r_1} f_0^{1/2} (r_1 - r_c) \, dr_1 = \frac{1}{4} \xi^2 \tag{4.5.19}$$

and

$$\overset{\sim}{\chi} = \left(\frac{d\xi}{dr_1} \right)^{-1/2} \phi$$

so that

$$\lambda \int_{r_c}^{r_1} b \, dr = \lambda \int_{r_c}^{r_1} \left(f_0 (r_1 - r_c)^2 + q_2 \right)^{1/2} dr$$

$$= \lambda \int_{r_c}^{r_1} f_0^{1/2} (r_1 - r_c) \, dr + \frac{\lambda q_2}{2 f_0^{1/2}} \int_{r_2}^{r_1} \frac{dr}{r - r_c} \tag{4.5.20}$$

$$= \frac{1}{4} \xi^2 + \frac{\lambda q_2}{2 f_0^{1/2}} \left[\ln(r_1 - r_c) - 1 \right]$$

$$= \frac{1}{4} \xi^2 + \frac{\lambda q_2}{2 f_0^{1/2}} \left[\ln \frac{\xi}{\sqrt{2\lambda f_0^{1/2}}} - 1 \right]$$

(4.5.19) transforms Equation (4.5.16) into

$$\frac{d^2\phi}{d\xi^2} - \left[\frac{\lambda^2 b^2}{\xi'^2} + \frac{3}{4}\frac{\xi''^2}{\xi'^4} - \frac{1}{2}\frac{\xi'''}{\xi'^3} \right]\phi = 0 \qquad (4.5.21)$$

Since the last two terms on the square bracket are of order 1 and are small compared to the first term which is of order λ^2, ϕ is given approximately by

$$\frac{d^2\phi}{d\xi^2} - \frac{\lambda^2 b^2}{\xi'^2}\phi = 0 \qquad (4.5.22)$$

Using (4.5.18) and (4.5.19), we obtain

$$\frac{d^2\phi}{d\xi^2} + \left[-\frac{1}{4}\xi^2 - p \right]\phi = 0 \qquad (4.5.23)$$

with $p = \lambda q_2 / 2fo^{1/2}$

This is Weber's Equation whose solutions are the parabolic cylinder functions of order $n = -p - 1/2$

$$\phi(\xi) = c_1 D_n(\xi) + c_2 D_{-n-1}(i\xi) \qquad (4.5.24)$$

c_1 and c_2 are arbitrary constants.

For convenience, we have summarized the asymptotic behavior of parabolic cylinder functions in Appendix D.

As $r_1 \to \infty$, or $\xi \to \infty$, we see (refer to Appendix D) that $D_n(\xi)$ decays while $D_{-n-1}(i\xi)$ grows exponentially. Thus the condition of boundedness at $r_1 = \infty$ demands that $c_2 \equiv 0$. c_1 is the arbitrary constant which remains undetermined in a linear problem, and we can set $c_1 = 1$ without loss of generality. Thus,

$$\phi(\xi) = D_n(\xi) \qquad (4.5.25)$$

The asymptotic expression for $\phi(\xi)$ when $r_1 < r_c$ or $\text{Arg}(\xi) = \pi$ is

$$\phi(\xi) \sim e^{-\frac{1}{4}\xi^2} \xi^m - \frac{\sqrt{2\pi}}{\Gamma(-m)} e^{m\pi i} e^{\frac{1}{4}\xi^2} \xi^{-m-1} \qquad (4.5.26)$$

Thus from (4.5.19) we get

$$\tilde{\chi}(r_1) \sim \left(\frac{d\xi}{dr_1}\right)^{-\frac{1}{2}} \xi^{-\frac{1}{2}} \left[e^{-\frac{1}{4}\xi^2} \xi^p - \frac{\sqrt{2\pi}}{\Gamma(p+\frac{1}{2})} e^{-(p+\frac{1}{2})\pi i} e^{\frac{1}{4}\xi^2} \xi^{-p} \right] \qquad (4.5.27)$$

4.5.2 Solution for $R_o \le r_1 < r_c$

WKB solution for Equation (4.5.16) is valid in the interval

$R_o \le r_1 < r_c$:

$$\tilde{\chi}(r_1) = a_1 e^{\lambda \int_{R_o}^{r_1} b \, dr} + a_2 e^{-\lambda \int_{R_o}^{r_1} b \, dr} \qquad (4.5.28)$$

where a_1 and a_2 are arbitrary constants. From (4.5.14) we have

$$\chi(r_1) = a_1 e^{\lambda \int_{R_o}^{r_1} (ia+b) \, dr} + a_2 e^{\lambda \int_{R_o}^{r_1} (ia-b) \, dr} \qquad (4.5.29)$$

The boundary condition $\dfrac{d\chi}{dr_1} = 0$ at $r_1 = R_o$ gives

$$a_2 = -a_1 e^{-2i\beta_o} \qquad (4.5.30)$$

where $\beta_o = \tan^{-1}\left[\dfrac{b(R_o)}{a(R_o)}\right]$

4.5.3 The Global Dispersion Relationship

Now we want to express (4.5.28) in a form similar to that of

(4.5.27). We can, again, take $a_1 = 1$ without loss of generality. We

note that

$$\tilde{\chi} = e^{\lambda \int_{R_0}^{r_1} b\,dr} - e^{-2i\beta_0} e^{-\lambda \int_{R_0}^{r_1} b\,dr}$$

$$= e^{\lambda \int_{R_0}^{r_c} b\,dr} e^{\lambda \int_{r_c}^{r_1} b\,dr} - e^{-2i\beta_0} e^{-\lambda \int_{R_0}^{r_c} b\,dr} e^{-\lambda \int_{r_c}^{r_1} b\,dr}$$

Using (4.5.20) we have

$$\tilde{\chi} = \left[e^{\lambda \int_{R_0}^{r_c} b\,dr} e^{-\rho} \left(2\lambda f_0^{1/2} \right)^{-\rho/2} \right] e^{\frac{1}{4}\xi^2} \xi^\rho$$

$$+ \left[-e^{-2i\beta_0} e^{-\lambda \int_{R_0}^{r_c} b\,dr} e^{\rho} \left(2\lambda f_0^{1/2} \right)^{\rho/2} \right] e^{-\frac{1}{4}\xi^2} \xi^{-\rho} \tag{4.5.31}$$

Since (4.5.27) and (4.5.31) are two expressions for $\tilde{\chi}(r_1)$ in the

domain $R_0 \le r_1 < r_c$, we must have

$$\frac{e^{\lambda \int_{R_0}^{r_c} b\,dr} e^{-\rho} \left(2\lambda f_0^{1/2} \right)^{-\rho/2}}{e^{-2i\beta_0} e^{-\lambda \int_{R_0}^{r_c} b\,dr} e^{\rho} \left(2\lambda f_0^{1/2} \right)^{\rho/2}} = \frac{\sqrt{2\pi}}{\Gamma(\rho+\frac{1}{2})} e^{-(\rho+\frac{1}{2})\pi i}$$

or

$$\lambda \int_{R_0}^{r_c} b\,dr = \rho - \frac{\rho}{2} \ln\left(2\lambda f_0^{1/2} \right) - \frac{1}{2}\ln\left(\frac{\sqrt{2\pi}}{\Gamma(\rho+\frac{1}{2})} \right)$$

$$- i\left[-\frac{(\rho+\frac{1}{2})\pi}{2} + \beta_0 + \pi(j) \right] = \mathcal{H} = 0 \tag{4.5.32}$$

$$j = 0, \pm 1, \pm 2, \dots$$

Since $k(r_1)$ is determined from the local dispersion relationship

for an assumed value of ω (and for m), ω is hidden in Equation (4.5.32)

in the parameters b , r_c , fo , p , and βo [cf. (4.4.4), (4.5.18),

(4.5.23) and (4.5.20)]. Equation (4.5.32) is the global dispersion relationship which yields discrete values for the eigenfrequency ω.

4.6. RESULTS

4.6.1. Solution of the Global Dispersion Relationship

To find the eigenvalue ω from the global dispersion relationship $\mathcal{G}$ (ω; m) = 0, we follow the procedure as outlined in Figure 4.4. The computation is long and tedious since we have to first assume an ω and find $k(r_1)$ from the local dispersion relationship $\mathcal{D}$ (k; ω, m, r_1) = 0 before we can obtain b, r_c, p, fo and β_o to substitute into $\mathcal{G}$. Then we have to evaluate $\mathcal{G}$ to see if both the real and imaginary parts of $\mathcal{G}$ are zero. It takes about half minute of cpu time to evaluate $\mathcal{G}$ for a given ω. If $|\mathcal{G}|$ = 0, then the ω assumed is an eigenvalue. We then have to vary m and repeat the procedure until we find a maximum of Im(ω) for various values of m.

From Figure 4.3, we see that the leading wave solutions (Real(k) < 0) has a k_I of the order of k_R ($k_I \sim .2$ near the eyewall) so that the amplitude of the wave ($e^{i\int k_r \, dr}$) would have an e-folding length of about the wavelength of the disturbance. This violiates our original assumption that the scale of the amplitude variation is much greater than the scale of the phase variation. Hence, we shall use only the right-half k-plane in the solution of $\mathcal{D}$ (k) = 0. We are looking for trailing waves only.

Because of the lengthy computations involved, we set j = 0 in Equation (4.5.32) and stop the search for ω when we have located a local maximum in ω_I.
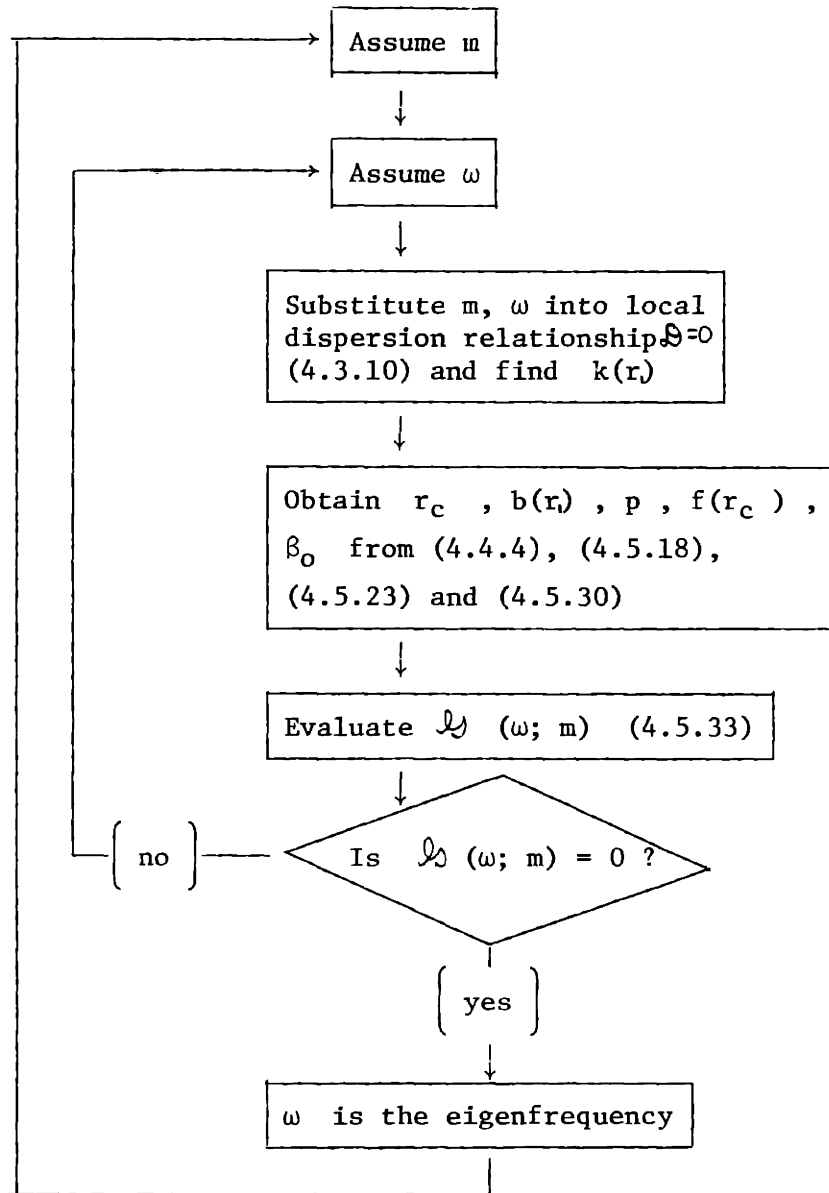
Figure 4.4 Flow chart for the solution of the
global dispersion relationship.

4.6.2. The Most Unstable Wave Mode

Figure 4.5 shows the graph of the eigenvalue ω for three values of m. The local maximum of ω_I corresponds to a wave where m = 4, and ω = (.295x10^{-2}, .295x10^{-3}). The turning circle is at r_c = .23. In the inner region between the eyewall and the turning circle, the wave mode consists of two wave components, one with an exponentially growing and the other with an exponentially decaying amplitude. We shall denote their wave numbers by k_1 and k_2.

Since Re(k_1) $\simeq$ Re(k_2), we can describe the properties of the most unstable wave mode with the average wave number

$$\bar{k} = \frac{1}{2} \left[Re(k_1) + Re(k_2) \right] \qquad (4.6.1)$$

$\bar{k}$ ranges from $\bar{k}$ = .33 at r_1 = .1 to $\bar{k}$ = .12 at r_1 = .6 , giving wavelengths λ of λ = 19 at r_1 = .1 to λ = 52 at r_1 = .6 .

The lines of constant phase given by

$$\frac{1}{\epsilon} \int_{R_o}^{r_1} k \, dr + m\theta = constant \qquad (4.6.2)$$

are shown in Figure 4.6. Comparison of Figure 4.6 with the radar picture of Hurricane Caroline (Figure 1.1) shows an amazing agreement between the predicted and observed phenomena. The crossing angle $\alpha = \tan^{-1}\left(\frac{m/r}{\bar{k}}\right)$ for the predicted wave ranges from α = 13.6° at r_1 = .1 to α = .6° at r_1 = .6 .

The phase speed $c_{ph} = \frac{\omega_R}{\bar{k}}$ then ranges from c_{ph} = .009 at r_1 = .1 to c_{ph} = .025 at r_1 = .6. The predicted rainband pattern is thus nearly stationary relative to the storm center.

The eigenfunctions associated with the most unstable wave mode are shown in Figures 4.7 a-c. The perturbation kinetic energy
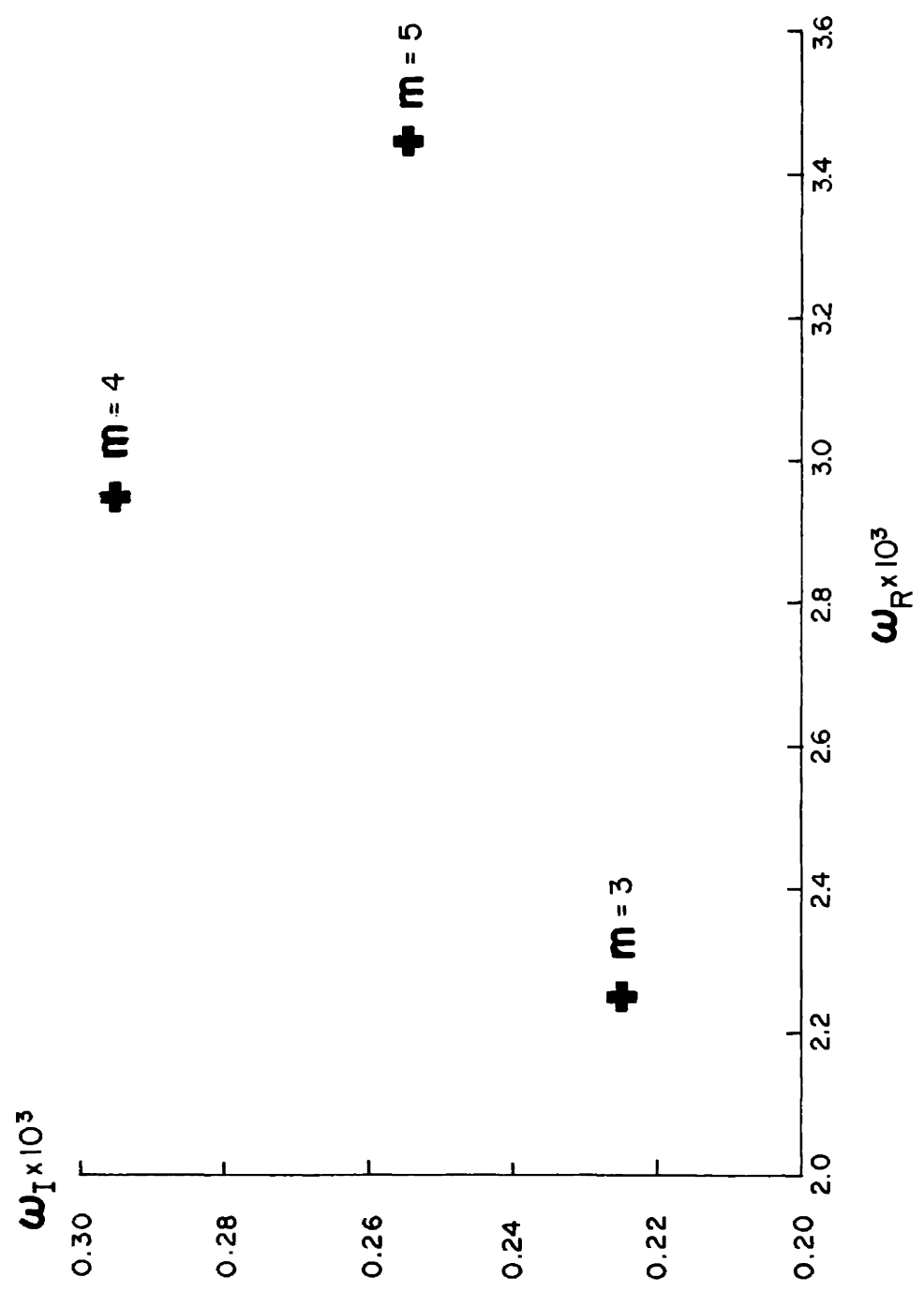
Figure 4.5. Graph of the global eigenvalue ω versus m.

Fig. 4.6   Lines of constant phase: m=4 , ω =$(2.95 \times 10^{-3}, 0.295 \times 10^{-3})$
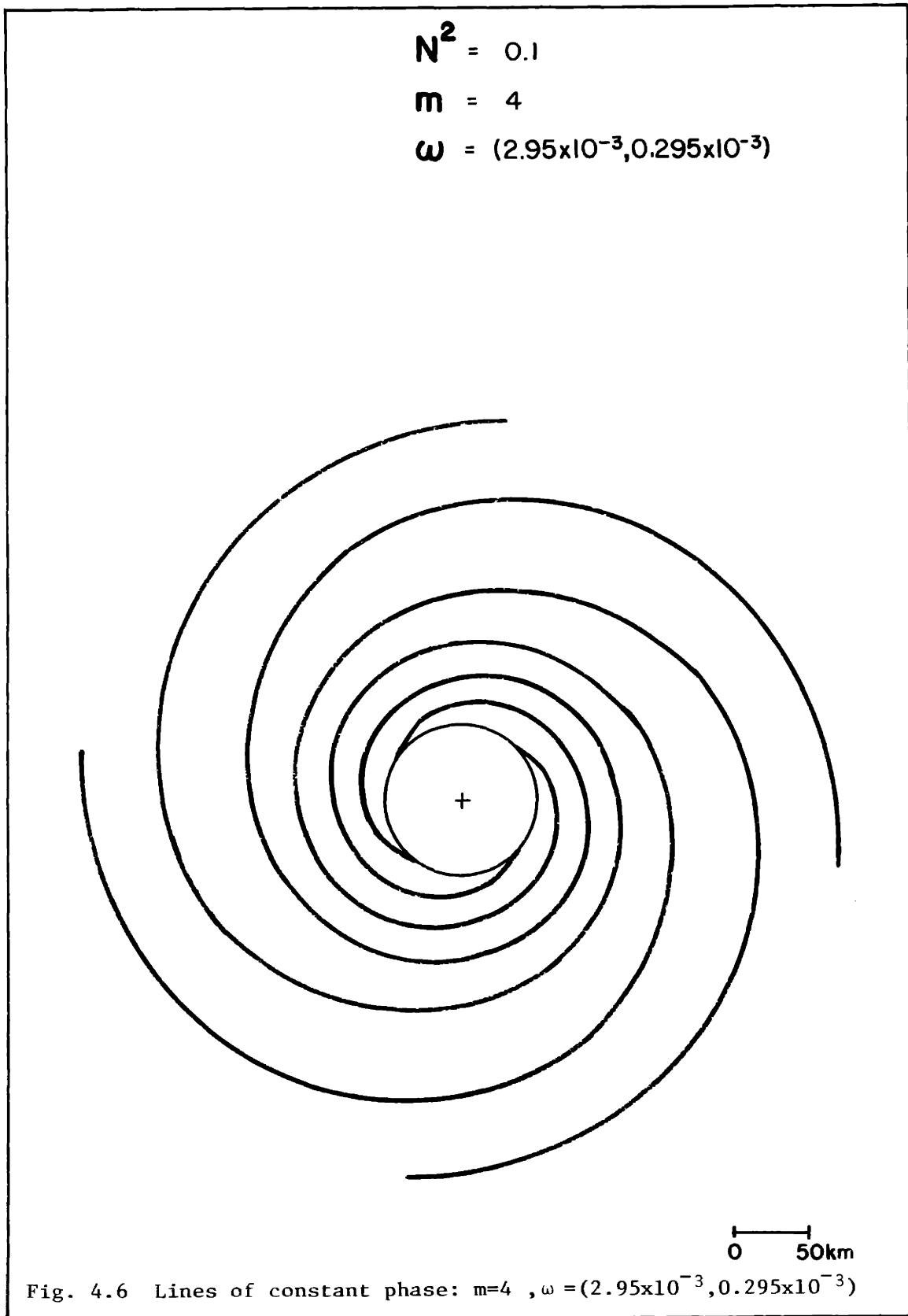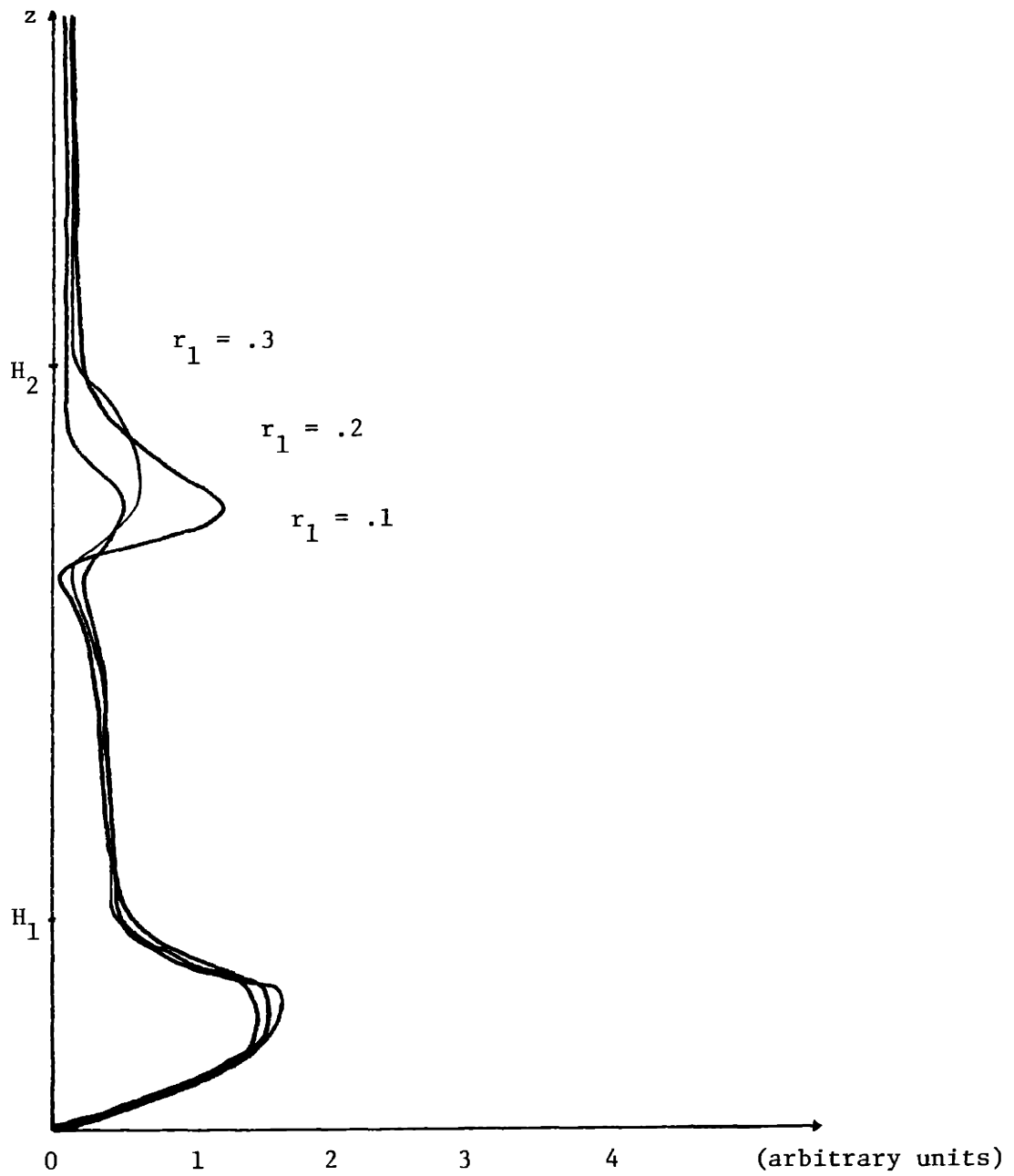
Figure 4.7a. Graph of $|u^{(o)}(r_1,z)|$ at $r_1 = .1$, .2, and .3 , associated with the wave mode $m = 4$ and $\omega = (.295 \times 10^{-2} , .295 \times 10^{-3})$.
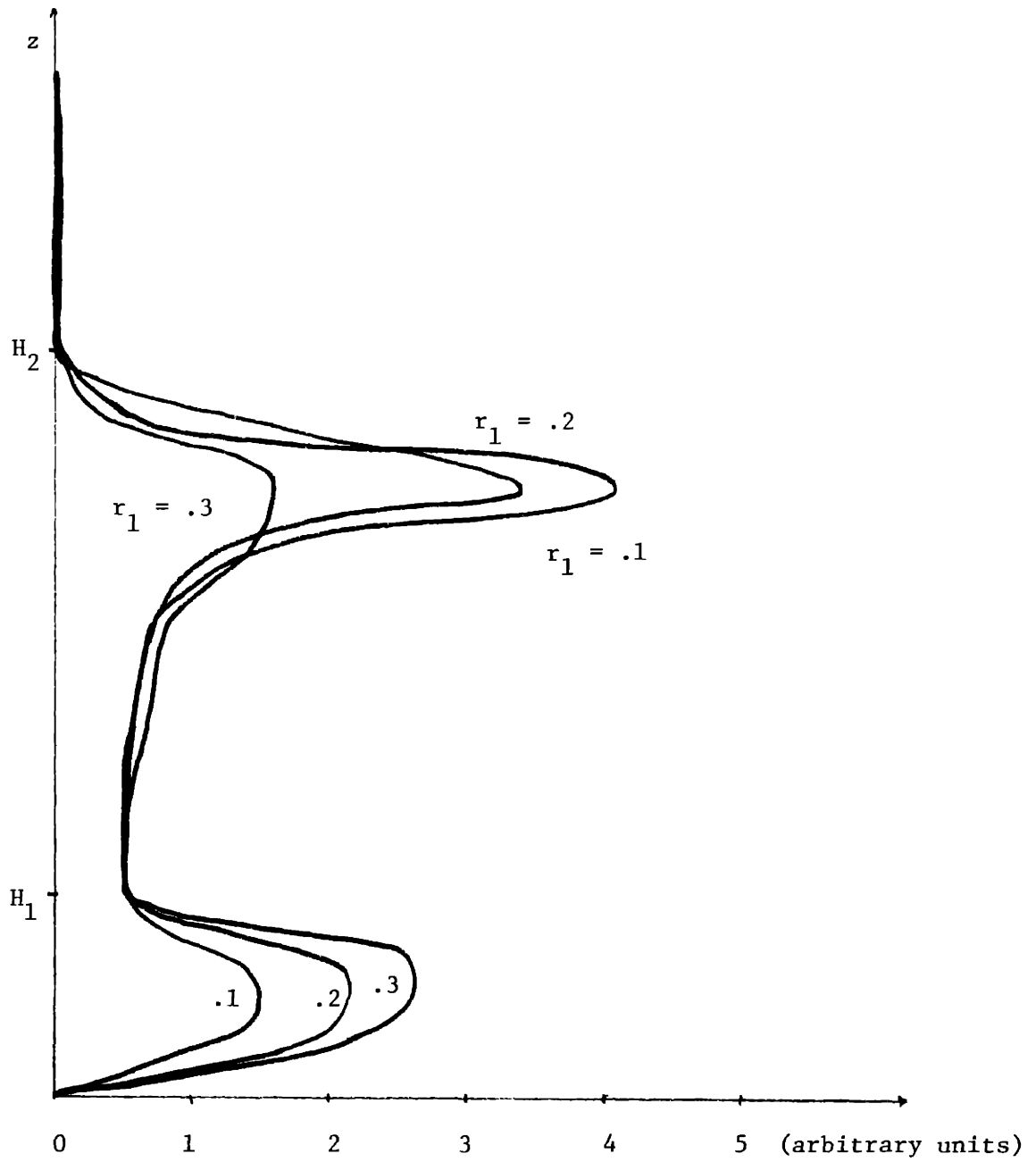
Figure 4.7b. Graph of $\left|v^{(o)}(r_1,z)\right|$ at $r_1 = .1$, $.2$ and $.3$, associated with the wave mode $m = 4$ and $\omega = (.295\times10^{-2}$, $.295\times10^{-3}$).
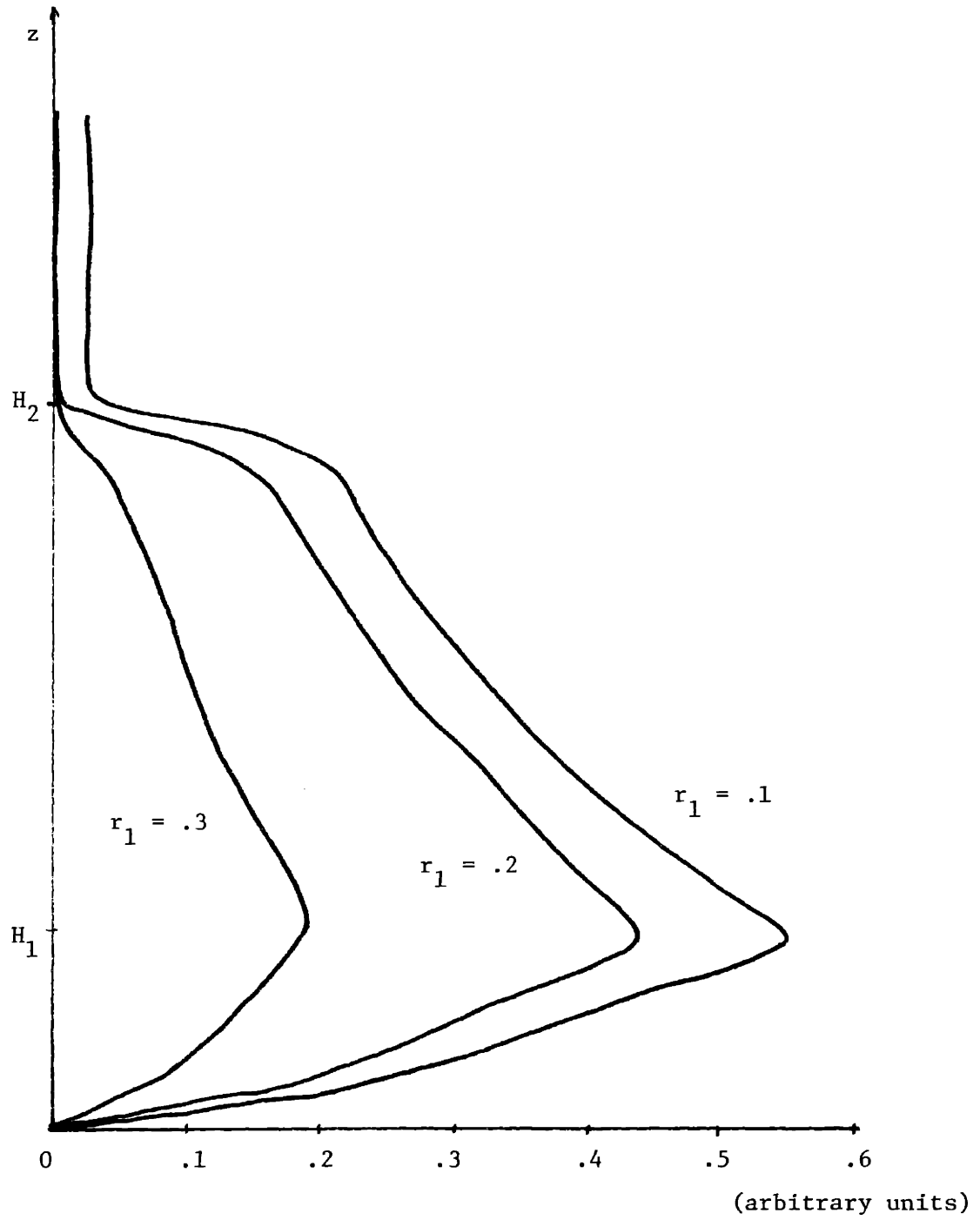
Figure 4.7c. Graph of $\left|w^{(o)}(r_1,z)\right|$ at r_1 = .1, .2 and .3.
associated with the wave mode m = 4 and
ω = (.295x10^{-2} , .295x10^{-3}).

(EKE) at each radius

$$EKE(r_1, \zeta) = \frac{1}{2} \bar{\rho} \left[|u^{(0)}|^2 + |v^{(0)}|^2 + |w^{(0)}|^2 \right] \qquad (4.6.3)$$

is shown in Figure 4.8. As is expected, EKE is maximum at a height

somewhere between H_1 and H_2, i.e. where the inflection point of

the velocity component perpendicular to the wavefront would be.

The slowly varying amplitude $A(r_1)$ of the lower order

solution w' is solved from

$$\int_0^\infty w^{(0)} \, \mathfrak{M}(w^{(0)}) \, d\zeta = 0 \qquad (4.6.4)$$

where $\mathfrak{M}$ is defined in Equation (4.4.4) and $w^{(0)}$ is given by (4.4.8).

Since

$$w' = A(r_1) \, \psi(r_1, \zeta) \, \chi(r_1) \, e^{i(m\theta - \omega t)}$$

the radial envelope of w' is given by

$$\mathcal{E}(r_1) = |A(r_1)| \, |\chi(r_1)| \qquad (4.6.5)$$

In Figure 4.9, we have plotted $\mathcal{E}$ for the most unstable wave mode.

$\mathcal{E}$ shows a peak near the eyewall and another peak at $r_1 = r_{co}$,

beyond which it decays exponentially outwards. The condition of

finite energy density at $r_1 = \infty$ is thus satisfied. We note that

this predicted behacior of the envelope of the most unstable wave

mode, i.e. a local maximum at $r_1 = r_{co}$ and exponential decay beyond,

is also very well exhibited in the actual hurricane. Hurricane Caroline

has an unbroken segment of rainband in the northwest quadrant at

$r \simeq 125$ km $(r_1 \simeq .25)$. Beyond that radius, no echoes are observed

despite the proximity to the radar.
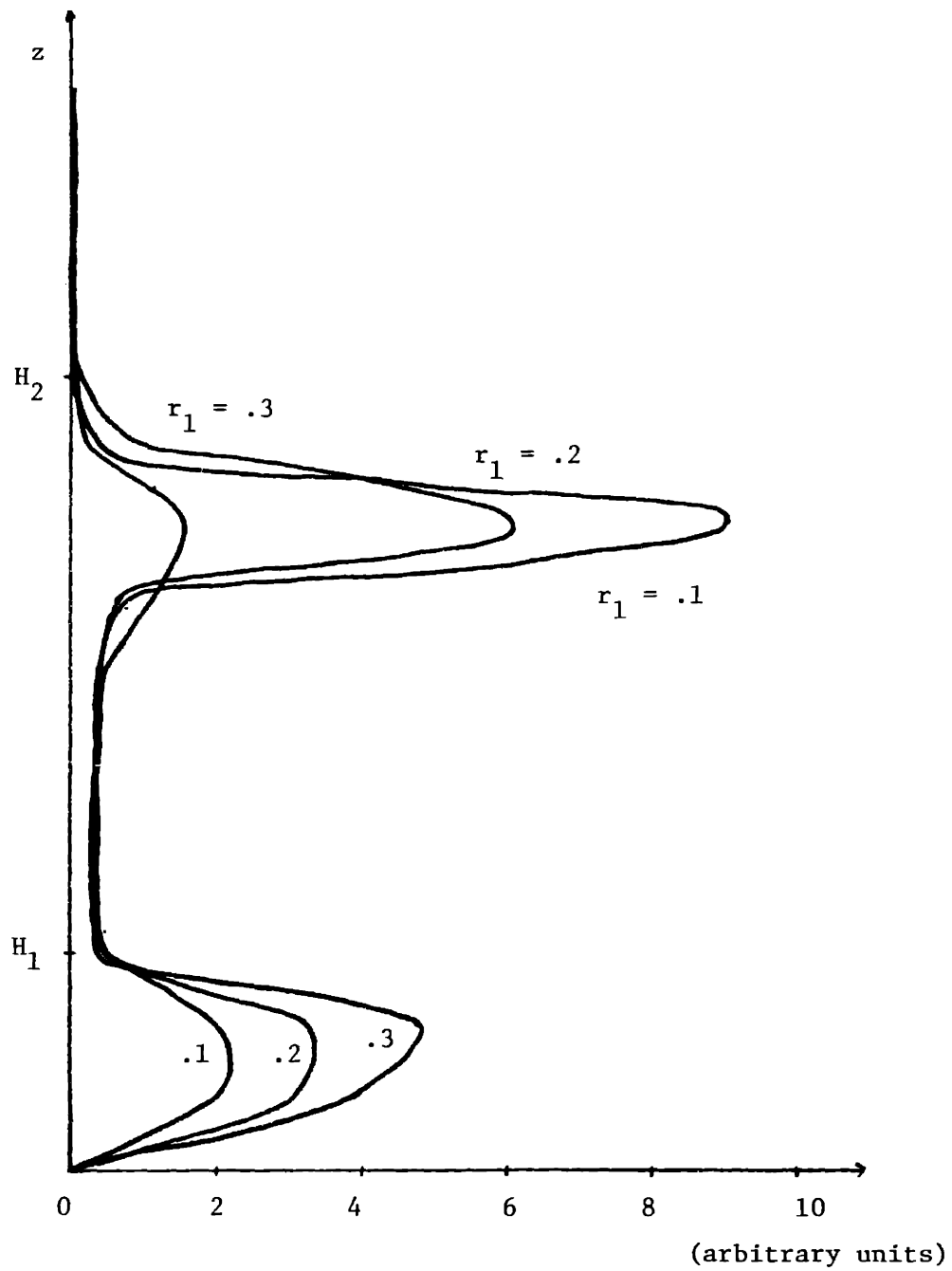
Figure 4.8. Graph of $EKE(r_1,z)$ at $r_1 = .1$, .2 and .3 , associated with the wave mode $m = 4$ and $\omega = (.295 \times 10^{-2}$, $.295 \times 10^{-3}$).
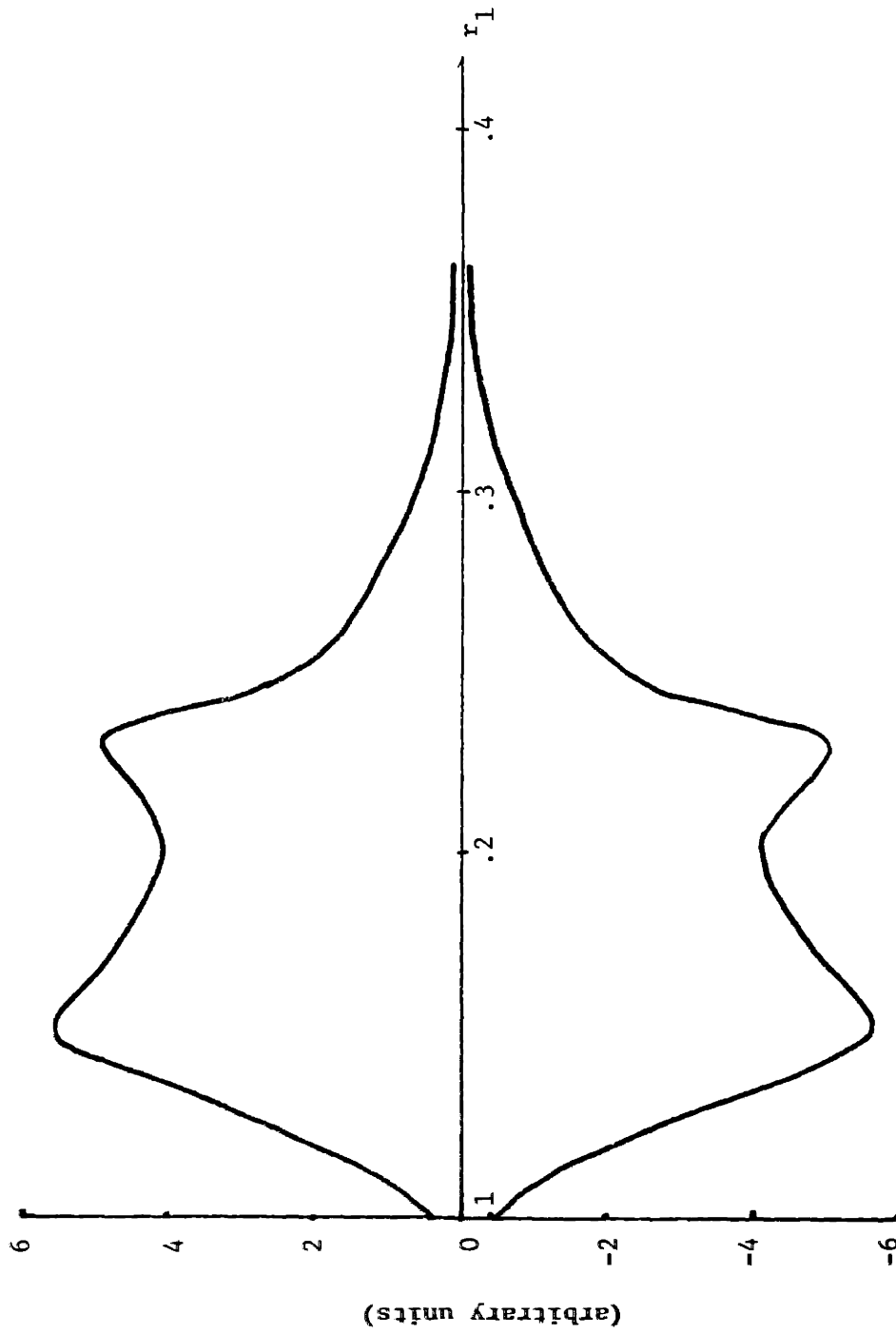
Figure 4.9. Graph of the envelope $\mathcal{E}$ associated with the wave mode $m = 4$ and $\omega = (.295\text{x}10^{-2}, .295\text{x}10^{-3})$.

  —

CHAPTER FIVE – SUMMARY AND CONCLUSIONS

Spiral rainbands are a characteristic feature of mature hurricanes. They have typical radial wavelengths of 20 to 60 km and are nearly stationary relative to the storm center. This thesis has investigated the hypothesis that the rainbands are organized by Rayleigh instability of the boundary layer.

A model of the hurricane is set up, where the interior is a stably-stratified, quasi-Boussinesq fluid whose mean flow is given by an axisymmetric potential vortex on an f-plane. The dynamics of the boundary layer is governed by frictional rather than convective processes, as is established by a crude analysis of observed boundary layer winds under Hurricane Donna; the winds have an Ekman-like profile with the velocities veering with height. The nonlinear nonseparable equations governing the neutral frictional boundary layer are solved by a numerical scheme devised by Rivas. The inflow velocity thus computed possesses an inflection point in the vertical, and this produces an instability in the boundary layer flow.

A global stability analysis of the steady-state axisymmetric hurricane for small-amplitude perturbations is performed. In order to make the nonseparable linear perturbation equations separable and tractable, a series of approximations are employed. First, the continuous velocity profiles in the vertical are represented by three layers of constant shear. Then, because the radial scale of the rainbands is small compared to the scale of the hurricane, a multiple scale approximation

is employed. With this approximation, the effects of friction and Coriolis forces on the local behavior of the perturbations is neglected, even though these forces are of primary importance in the maintenance of the mean boundary layer structure. With the separation of variables, the problem is reduced, at each position in r, to a familiar stability problem where the mean wind varies only in height. A local dispersion relationship is thus derived. This relationship describes how perturbations imposed on the mean hurricane flow would oscillate due to the local balance of forces. However, it does not describe how the entire hurricane as a whole oscillates. Finally, by employing an asymptotic analysis over the whole domain of the hurricane and by demanding that the radial boundary conditions be satisfied, we derive the global dispersion relationship from which discrete values of the eigenfrequency and the growth rate are obtained. These eigenfrequencies are the frequencies at which the entire hurricane would oscillate.

The results of the global stability analysis are compared with observations. The eigenwave mode with the largest growth rate (which corresponds to an e-folding time of 1.3 days) has four arms and has radial wavelengths of about 20 km near the eyewall and about 50 km at r = 300 km. The lines of constant phase agree remarkably well with the spiral rainband pattern of Hurricane Caroline. The mode is nearly stationary — the phase speed is about .25 m/sec near the eyewall, and even less farther out. The observed spiral structure is also nearly stationary! The eigen mode thus obtained consists of both an amplifying and a decaying wave in the inner region of the storm between the eyewall and about r = 115 km, and only a decaying wave in the region

beyond. For comparison, we see that the rainbands in the northwest quadrant of Hurricane Caroline are confined within a radius of about 125 km; no radar echoes are observed beyond this radius despite the proximity to the radar.

The linear asymptotic theory of Rayleigh instability in the hurricane boundary layer is, of course, limited by the approximations and assumptions made. However, the theory shows that Rayleigh instability is a mechanism which organises moist air into ascending and descending spiral regions, forming a spiral rainband pattern which resembles very closely the observed phenomenon. The implication of this theory goes beyond an explanation for hurricane rainbands. The global instability theory predicts where bands of clouds would form and how they would propagate even if the basic state were not an axisymmetric vortical flow, providing that the underlying moist boundary layer were frictionally controlled.

APPENDIX A

Rivas Scheme to Solve Equations (3.2.5) - (3.2.7)

Equations (3.2.5) - (3.2.7) are

$$R_0 \left[\bar{u} \frac{\partial \bar{u}}{\partial r_1} + \bar{w} \frac{\partial \bar{u}}{\partial z} + \frac{\bar{V}_\infty^2 - \bar{V}^2}{r_1} \right] + \left(\bar{V}_\infty - \bar{V} \right) = \frac{\partial^2 \bar{u}}{\partial z^2} \qquad (A.1)$$

$$R_0 \left[\bar{u} \frac{\partial \bar{v}}{\partial r_1} + \bar{w} \frac{\partial \bar{v}}{\partial z} + \frac{\bar{U} \bar{V}}{r_1} \right] + \bar{u} = \frac{\partial^2 \bar{v}}{\partial z^2} \qquad (A.2)$$

$$\frac{\partial r_1 \bar{u}}{\partial r_1} + \frac{\partial r_1 \bar{w}}{\partial z} = 0 \qquad (A.3)$$

The following notation will be used: For a variable q ($= \bar{u}$, $\bar{v}$, $\bar{w}$),
q_{jk}^ν denotes the value of q at the $(j,k)^{th}$ grid-point in the $(r_1 - z)$
plane and at the νth "time-step".
We write

$$\frac{\partial \bar{u}}{\partial t} = A + B \qquad (A.4)$$

$$\frac{\partial \bar{v}}{\partial t} = C + D \qquad (A.5)$$

$$\frac{\partial \bar{w}}{\partial z} = - \frac{1}{r_1} \frac{\partial r_1 \bar{u}}{\partial r_1} \qquad (A.6)$$

with

$$A = - R_0 \left[\bar{u} \, \frac{\partial \bar{u}}{\partial r_1} + \bar{w} \, \frac{\partial \bar{u}}{\partial \zeta} \right] \qquad (A.7)$$

$$B = - R_0 \left[\frac{\bar{V}_\infty^2 - \bar{V}^2}{r_1} \right] - \left[\bar{V}_\infty^2 - \bar{V}^2 \right] + \frac{\partial^2 \bar{u}}{\partial \zeta^2} \qquad (A.8)$$

$$C = - R_0 \left[\frac{\bar{u}}{r_1} \, \frac{\partial r_1 \bar{V}}{\partial r_1} + \bar{w} \, \frac{\partial \bar{V}}{\partial \zeta} \right] \qquad (A.9)$$

$$D = - \bar{u} + \frac{\partial^2 \bar{V}}{\partial \zeta^2} \qquad (A.10)$$

Since $\bar{u}$, $\bar{v}$, $\bar{w}$ are all real, $\bar{u}^* = \bar{u}$, $\bar{v}^* = \bar{v}$ and $\bar{w}^* = \bar{w}$.

The Rivas Scheme will be applied to (A.4) and (A.5), and $\bar{w}$ will be found from the continuity Equation (A.6). To go from the νth "time-step" to the $\nu+1^{th}$ "time-step" involves two forward steps and one backward step. At each step ^{s} , $\bar{w}$, A , B , C and D are evaluated from (A.6) - (A.10).

$$w^s_{jk} = w^s_{jk-2} - \frac{2\Delta z}{\Delta r} \left[\frac{(j+1) \, u^s_{j+1,k-1} - j \, u^s_{j,k-1}}{j + \frac{1}{2}} \right]$$
$$\qquad (A.11)$$

$$A^s_{jk} = - R_0 \left[\frac{(u^s_{j+1,k})^2 - (u^s_{jk})^2}{2.\,\Delta r} + w^s_{jk} \, \frac{u^s_{jk+1} - u^s_{jk-1}}{2\Delta z} \right]$$
$$\qquad (A.12)$$

$$B_{jk}^{s} = -R_o \left[\frac{\bar{V}_{\infty j}^{2} - v_{jk}^{2}}{j \Delta r} \right] - \left(\bar{V}_{\infty j} - v_{jk}^{s} \right) \tag{A.13}$$

$$+ \frac{u_{jk+2}^{s} - 2u_{jk}^{s} + u_{jk-2}^{s}}{\Delta z^{2}}$$

$$C_{jk}^{s} = -R_o \left[u_{jk}^{s} \frac{(j+1) u_{j+1, k}^{s} - j v_{jk}^{s}}{(j + \frac{1}{2}) \Delta r} + w_{jk}^{s} \frac{v_{jk+1}^{s} - v_{jk-1}^{s}}{2 \Delta z} \right] \tag{A.14}$$

$$D_{jk}^{s} = -u_{jk}^{s} + \frac{v_{jk+2}^{s} - 2v_{jk}^{s} + v_{jk-2}^{s}}{\Delta z^{2}} \tag{A.15}$$

The first forward step is:

$$\tilde{u}_{jk} = u_{jk}^{\smile} + \Delta T \left(-A_{jk}^{\smile} + B_{jk}^{\smile} \right) \tag{A.16}$$

$$\tilde{v}_{jk} = v_{jk}^{\smile} + \Delta T \left(-C_{jk}^{\smile} + D_{jk}^{\smile} \right) \tag{A.17}$$

The second forward step is:

$$\tilde{\tilde{u}}_{jk} = u_{jk}^{\smile} + \Delta T \left(A_{jk}^{\smile} + B_{jk}^{\smile} \right) \tag{A.18}$$

$$\hat{\tilde{v}}_{jk} = v_{jk}^{\smile} + \Delta T \left(C_{jk}^{\smile} + D_{jk}^{\smile} \right) \tag{A.19}$$

The backward step is:

$$u_{jk}^{\mu+1} = \hat{U}_{jk} - \Delta T \left(-\overset{a}{\hat{A}}_{jk} + \overset{\approx}{B}_{jk} \right) \qquad \text{(A.20)}$$

$$\mathcal{N}_{jk}^{\mu+1} = \tilde{\mathcal{V}}_{jk} - \Delta T \left(-\overset{\approx}{\hat{C}}_{jk} + \overset{\sim}{\hat{D}}_{jk} \right) \qquad \text{(A.21)}$$

In the computations, we chose

$$Ro = 1$$

$$\Delta r = .05$$

$$\Delta z = \pi/20$$

$$\Delta t = .01$$

$$J = 40$$

$$K = 20$$

$$\overline{V}_{\infty j} = c/j\Delta r \quad , \quad c = .1$$

The scheme converged within 1000 "time-steps".

APPENDIX B

Attached is the literature on SUBROUTINE LSQNK2 from the MIT Information

Processing Center.

Applications Program Series
AP-26

MASSACHUSETTS INSTITUTE OF TECHNOLOGY
INFORMATION PROCESSING CENTER

March 28, 1973

NAMES:

LSQNK1 and LSQNK2, to find the zeros of an analytic function.

DESCRIPTION:

LSQNK1 and LSQNK2 are FORTRAN IV subroutines which find all the zeros of an analytic function $f(z)$ within a contour in the z plane. The program LSQNK1 requires a single arbitrary closed curve described in parametric form. LSQNK2 requires a polygonal curve described in terms of the vertices of the polygon. Each program is limited to finding at most four zeros within a given contour. If there are more than four zeros within the contour, the programs will report only the actual number of zeros, and a new smaller contour must be chosen.

The method used is based on the theory of complex variables. Specifically, if $f(z)$ is an analytic function (has no poles or branch points) of z within and on C, where C is a closed curve in the complex plane not passing through a zero of $f(z)$, then

$$S_N = \frac{1}{2\pi i} \oint_C z^N \frac{f'(z)}{f(z)} \, dz = \sum_{i=1}^{v} z_i^N$$

where z_i (i = 1,2,...,v) are all the zeros of $f(z)$ which lie inside C. (A multiple zero is counted according to its multiplicity in this formula). The program computes a sequence of values S_N (N=0,1,...,m), m≤4 by numerically approximating the contour integrals. Using Newton's Identities, these approximations to S_N are used to form a polynomial $p(z)$ of degree less than or equal to 4 whose zeros coincide with the zeros of $f(z)$ inside C. The restriction to polynomials which are at most quartics (and thus to finding at most 4 zeros in a single call) is due to the fact that quartics can be solved analytically. LSQNK1 and LSQNK2 make use of a very accurate quartic solving program called ROOT4.

In order to numerically approximate the contour
integrals, an integration by parts is performed
on the above integrals to rid them of the
derivative f'(z). This yields:

$$\frac{1}{2\pi i} \oint_C z^N \frac{f'(z)}{f(z)} \, dz =$$

$$\frac{1}{2\pi i} z^N \ln(f(z)) \Big|_{z_a}^{z_b} - N \int_C z^{N-1} \ln(f(z)) \, dz =$$

$$J z_a^N - N \oint_C z^{N-1} \ln(f(z)) \, dz$$

where z_a and z_b are the initial and terminal points
of the curve C and J is the number of the complex
sheet above the initial sheet (J=0) of the Riemann
Surface for $\ln(f(z))$ at the termination of the
integration when $z = z_b$.

The contour integrals

$$N \oint_C z^{N-1} \ln(f(z)) \, dz$$

are evaluated using the equivalent real integral
of a complex function:

$$N \int_a^b z^{N-1} \ln(f(z)) \, g'(t) \, dt$$

where $z = g(t)$ is the parametric equation of the
contour C (describing the complex variable z in
terms of some real parameter t). A Simpson's Rule
adaptive contour integration program LSQNK is
used, which properly handles the branch cut of the
logarithm function and computes all the contour
integrals needed simultaneously. LSQNK is a
modification of SQUANK (refer to AP-31), an adap-
tive real integration program, and subsequently
CSQNK (refer to AP-70), an adaptive contour in-
tegration program which integrates any complex
function along an arbitrary contour.

AP-26

USAGE: LSQNK1

The calling statement for LSQNK1 is:

        CALL LSQNK1(A, B, ERROR, M, NPRINT, ANSW, RETERR,
                NO, CURVE, FUN)

Where:

REAL*4	A, B
COMPLEX*8	ERROR, ANSW(4), RETERR, CURVE, FUN
INTEGER*4	M, NPRINT, NO
EXTERNAL	CURVE, FUN

Input:

A and B
: are the values of the real parameter t at the initial point and terminal point of the closed curve C.

ERROR
: is the desired complex tolerance (absolute error) to be used in the computation of the contour integrals. This error tolerance affects only the contour integral calculation, not the formation and solution of the approximating polynomial. To avoid excessive subdivision of the interval and the possible resulting round-off error, it is suggested that a tolerance no smaller than about $10^{-3} + 10^{-3}i$ be specified. The answer is usually considerably more accurate than this.

M
: is the number of zeros of f(z) expected inside the contour. M must be a positive integer less than or equal to 4. The value of M is used to compute the number of contour integrals to perform so that if there are actually more than M zeros, the number of zeros will be returned and the program must be called again with a larger value for M. It is recommended that M=4 be used since most computer time is used in computing $\ln(f(z))$ which is done only once for each point z.

NPRINT   is an indicator specifying whether
                  or not to print intermediate re-
                  sults and error messages.

                  NPRINT = 0   results in no printing.

                  NPRINT ≥ 1   results in printing of
                                 information associated
                                 with each set of 5 points
                                 used in the Simpson's Rule
                                 calculation.

                  NPRINT = 2   results in printing of the
                                 values $(z, f(z))$ used in
                                 the integration.

                  The information printed is illustrated
                  and described in the section "Optional
                  Printouts."

Output:

ANSW   contains the answers, up to four zeros
                  of $f(z)$.

RETERR   is the claimed resulting error in the
                  computation of the contour integrals.

NO   is the number of function evaluations
                  $f(z)$ required.

External Routines:

CURVE   is a complex function subprogram
                  describing the parametric equation of
                  the contour $z = g(t)$ and its derivative
                  $\frac{dz}{dt} = g'(t)$.

```
   COMPLEX FUNCTION CURVE(T,DZDT)
   REAL*4 T
   COMPLEX*8 DZDT
C PROGRAM WHICH DEFINES CURVE AND DZDT
```

FUN   is a complex function subprogram describ-
                  ing the function $f(z)$.

```
   COMPLEX FUNCTION FUN(Z)
   COMPLEX*8 Z
C PROGRAM WHICH DEFINES FUN
```

AP-26

<u>LSQNK2</u>

The calling statement for LSQNK2 is

CALL LSQNK2(Z, N, ERROR, M, NPRINT, ANSW, RETERR,
NO, FUN)

Where:

COMPLEX*8   Z(N), ERROR, ANSW(4), RETERR, FUN
INTEGER*4   N, M, NPRINT, NO
EXTERNAL   FUN

Input:

Z   is a complex array describing the
            coordinates of the vertices of the
            polygonal contour. The vertices must
            be given in counterclockwise order.

N   is the number of vertices.

ERROR ⎫
M   ⎬   same as for LSQNK1
NPRINT ⎭

Output and External Routine:

ANSW   ⎫
RETERR ⎬   same as for LSQNK1
NO   ⎪
FUN   ⎭

Notice that no external CURVE function is neces-
sary in this case because the parametric equations
of the straight lines joining the given vertices
are built into LSQNK2.

Both LSQNK1 and LSQNK2 print the number of zeros
(minus the number of poles), the values of the
contour integrals (moments), the zeros (ANSW),
and the value of the function f at the zeros. A
sample printout is shown below.

```
NUMBER OF ZEROS MINUS NUMBER OF POLES =    4

            MOMENTS
   0.7500792E+00   -0.2664404E+00
   0.9132504E-01    0.6334190E+00
   0.3375626E+00    0.3164530E+00
  -0.3089142E-01   -0.8593953E-01

         ROOT  Z                            F(Z)
   0.7867154E-04    0.4830920E-04   -0.1204023E-04    0.1371213E-04
   0.5000539E+00    0.2119824E-04    0.3132679E-04   -0.4514447E-05
   0.4999380E+00    0.3334612E+00    0.1213434E-04   -0.3139525E-04
  -0.2499919E+00   -0.5999722E+00    0.1363856E-04    0.1674492E-04
```

AP-26

PERFORMANCE: The examples on page 8 illustrate the performance
of LSQNK1 and LSQNK2. In the first example, LSQNK1
finds, using various tolerances, the zeros of a
quartic which lie within the unit circle. Note that
specifying a smaller tolerance increases the number
of function evaluations greatly with very little,
if any, increase in accuracy. Also, the actual pre-
cision of the answers is much better than the preci-
sion returned in RETERR. The precision returned is
that of the most imprecise of the four contour
integrals computed in this case. This example
reinforces the warning that tolerances of less than
$10^{-2} + 10^{-2}i$ or $10^{-3} + 10^{-3}i$ should be avoided.

This same function was later examined by using LSQNK1
four times with small circles of radius 1/10 sur-
rounding the zeros found above. When tolerances of
$10^{-2} + 10^{-2}i$ were specified, each zero was determined
to between 5 and 6 significant figures, using between
33 and 53 function evaluations. Greater accuracy is
attained due to the smaller contours and to the fact
that they encircle just one zero each; the approxi-
mating polynomial is then linear and solved without
noticeable loss of precision. Thus using a large
contour first to estimate the zeros and then shrink-
ing it is the best strategy.

The accuracy of the routine is also affected by the
closeness of the zeros to the contour. The routine
is most accurate when the zeros are near the center
of the region surrounded by the contour since $\ln(f(z))$
becomes singular at the zeros. Sometimes LSQNK1 or
LSQNK2 is used just to estimate the zeros and then
a more localized method such as Newton's Method or
Muller's Method may be used to increase the precision.

When a quintic was used for the function $f(z)$, using
the unit circle as contour with four of the zeros
within it, specifying a tolerance of $10^{-2} + 10^{-2}i$
produced zeros with between 2 and 3 significant
digits in 145 function evaluations. This is not
as good as the accuracy for the quartic example.
In general the more the function $f(z)$ varies on the
contour, the more function evaluations are necessary
to obtain a given accuracy.

In the second example, the zeros of the same function are found using a square as contour. Although the calling program requires only one call to LSQNK2, internally the contour integration program is called separately for each of the four sides. Notice that the number of function evaluations is much less than for corresponding runs using LSQNK1, even though the square contour used is larger than the unit circle.

AP-26

EXAMPLE 1

Function: f(z)=z*(z-(.5,0.))*(z+(.25,.6))*(z-(.5,.3333333))

Contour curve: unit circle   x=cos2πt
                                  y=sin2πt   0≤t≤1

LSQNK1 results:

ERROR	ANSW (zeros)	f(z)	NO	RETERR
1.E-2 + 1.E-2 i	-.163903E-4 - .834595E-6 i	.7747E-6 - .3110E-5 i	137	1.E-2 + 1.E-2 i
	.500030 - .548350E-5 i	.2283E-5 - .4259E-5 i		
	-.249997 - .600002 i	.1301E-5 - .2429E-5 i		
	.499992 + .333342 i	.1657E-5 - .2186E-5 i		
1.E-3 + 1.E-3 i	-.115627E-4 - .190730E-5 i	.7992E-6 - .2145E-5 i	241	1.E-3 + 1.E-3 i
	.500026 - .202661E-5 i	.2376E-5 - .3489E-5 i		
	.249995 - .600001 i	.2809E-5 - .2289E-5 i		
	.499992 + .333340 i	.1832E-5 - .1670E-5 i		
1.E-5 + 1.E-5 i	-.181784E-4 + .154940E-5 i	.3848E-6 - .3542E-5 i	861	.3061E-4 + .3240E-4 i
	.500029 - .619857E-5 i	.2134E-5 - .4256E-5 i		
	-.249996 - .600004 i	.1750E-5 - .3777E-5 i		
	.499993 + .333342 i	.1464E-5 - .2255E-5 i		

EXAMPLE 2

Function : f(z) = z*(z-(.5,0.))*(z+(.25,.6))*(z-(.5,.3333333))

Contour polygon: square with vertices at (1,1),(-1,1),(-1,-1), and (1,-1)

LSQNK2 results:

ERROR	ANSW (zeros)	f(z)	NO	RETERR
1.E-1 + 1.E-1 i	.786716E-4 + .498207E-4 i	-.1249E-4 + .1321E-4 i	48	1.E-1 + 1.E-1 i
	.500054 + .211982E-4 i	.8040E-5 - .4614E-5 i		
	-.249992 - .599972 i	.1364E-4 + .1674E-4 i		
	.499938 + .333461 i	.1211E-4 - .3189E-4 i		
1.E-3 + 1.E-3 i	-.780886E-5 + .162124E-4 i	-.2815E-5 - .2105E-5 i	68	1.E-3 + 1.E-3 i
	.499994 - .174343-4 i	-.2758E-5 - .1021E-5 i		
	-.249999 - .599994 i	.2082E-5 + .3813E-5 i		
	.500022 + .333344 i	-.5361E-5 - .2177E-5 i		
1.E-5 + 1.E-5 i	-.953696E-5 + .548342E-5 i	-.6934E-6 - .2034E-5 i	240	1.E-5 + 1.E-5 i
	.499996 - .127552E-4 i	-.1976E-5 - .7986E-6 i		
	-.249999 - .600002 i	-.4091E-7 - .1491E-5 1		
	.500016 + .333350 i	-.4239E-5 - .3756E-5 i		

AP-26

OPTIONAL PRINTOUTS: When the NPRINT parameter is nonzero, two optional printouts may be produced. These allow the user to watch the progress of his contour integration. A sample of the optional printouts is given on page 10.

When NPRINT ≥ 1 the following information is printed for each five points involved in a Simpson's Rule calculation of the contour integrals:

PJUMP =
$$\begin{cases} T & \text{The angle between the } \ln(f(z)) \text{ values at any two adjacent points of the five is greater than } \pi/4. \text{ In this case, nonconvergence is assumed and the program proceeds to a finer level of subdivision of the integration interval.} \\ \\ F & \text{The angles described above are all } \leq \pi/4. \end{cases}$$

Z(1)   The initial point of the five used in the Simpson's Rule calculation.

ADIFF and ADIFFI   The real and imaginary parts, respectively, of the difference between the Simpson's Rule calculation for the wider mesh (3 points) and the finer mesh (5 points), using the calculation for that contour integral (of possibly four) which produces the greatest difference (error). This quantity is used to determine convergence or nonconvergence based on the specified tolerance, ERROR.

NJUMP   The number of the Riemann Surface or sheet above or below the initial sheet (numbered zero) for the ln(f(z)) value at the fifth point of the five used in the Simpson's Rule calculation.

LEVEL   The level of subdivision of the integration interval that these five points represent. The initial level is zero.

When NPRINT = 2 the following information is printed for each point of the five.

Z   The point itself.

F(Z)   The value of the function f at that point.

AP-26

OPTIONAL PRINTOUT FOR NPRINT = 2

```
Z =     0.1000E+01   C.1000E+01  F(Z) =    -0.2229E+01 -0.1479E+01
Z =     0.5000E+00   0.1000E+01  F(Z) =     0.8167E+00 -0.1033E+01
Z =     0.0          0.1000E+01  F(Z) =     0.8750E+00  0.1229E+01
Z =    -0.5000E+00   0.1000E+01  F(Z) =    -0.2242E+01  0.2108E+01
Z =    -0.1000E+01   C.1000E+01  F(Z) =    -0.7221E+01 -0.1596E+01
PJUMP = T    Z(1) =   0.1000E+01  0.1000E+01     ADIFF = 0.2905E+00    ADIFFI = 0.1086E+02    NJUMP = 1    LEVEL = 0
Z =     0.1000E+01   C.1000E+01  F(Z) =    -0.2229E+01 -0.1479E+01
Z =     0.7500E+00   0.1000E+01  F(Z) =    -0.4031E+00 -0.1683E+01
Z =     0.5000E+00   0.1000E+01  F(Z) =     0.8750E+00  0.1229E+01
Z =     0.2500E+00   C.1000E+01  F(Z) =     0.1266E+01  0.7083E-01
Z =     0.0          0.1000E+01  F(Z) =    -0.7221E+01 -0.1596E+01
PJUMP = T    Z(1) =   0.1000E+01  0.1000E+01     ADIFF = 0.2596E+00    ADIFFI = 0.6512E+00    NJUMP = 0    LEVEL = 1
Z =     0.1000E+01   C.1000E+01  F(Z) =    -0.2229E+01 -0.1479E+01
Z =     0.875CE+00   0.1000E+01  F(Z) =    -0.1254E+01 -0.1713E+01
Z =     0.7500E+00   0.1000E+01  F(Z) =     0.8750E+00  0.1229E+01
Z =     0.6250E+CC   C.1000E+01  F(Z) =     0.2950E+00 -0.1440E+01
Z =     0.5000E+00   C.1000E+01  F(Z) =    -0.7221E+01 -0.1596E+01
PJUMP = F    Z(1) =   0.1000E+01  0.1000E+01     ADIFF = 0.2578E-01    ADIFFI = 0.3159E-01    NJUMP = 0    LEVEL = 2
Z =     0.5000E+00   0.1000E+01  F(Z) =    -0.2229E+01 -0.1479E+01
Z =     0.3750E+00   C.1000E+01  F(Z) =     0.1144E+01 -0.5130E+00
Z =     0.2500E+00   C.1000E+01  F(Z) =     0.8750E+00  0.1229E+01
Z =     0.1250E+00   C.1000E+01  F(Z) =     0.1176E+01  0.6682E+00
Z =     0.0          0.1000E+01  F(Z) =    -0.7221E+01 -0.1596E+01
PJUMP = F    Z(1) =   0.5000E+00  0.1000E+01     ADIFF = 0.6378E-02    ADIFFI = 0.4155E-01    NJUMP = 0    LEVEL = 2
Z =     0.0          0.1000E+01  F(Z) =    -0.2229E+01 -0.1479E+01
Z =    -0.2500E+00   0.1000E+01  F(Z) =    -0.3333E+00  0.2042E+01
Z =    -0.5000E+00   0.1000E+01  F(Z) =     0.8750E+00  0.1229E+01
Z =    -0.7500E+00   0.1000E+01  F(Z) =    -0.4639E+01  0.1029E+01
Z =    -0.1000E+01   C.1000E+01  F(Z) =    -0.7221E+01 -0.1596E+01
PJUMP = F    Z(1) =   0.0          0.1000E+01     ADIFF = 0.2778E+00    ADIFFI = 0.6064E+00    NJUMP = 1    LEVEL = 1
Z =    -0.1000E+01   0.1000E+01  F(Z) =    -0.7221E+01 -0.1596E+01
Z =    -0.1000E+01   C.5000E+00  F(Z) =    -0.1042E+01 -0.3396E+01
Z =    -0.1000E+01   0.0         F(Z) =     0.1987E+01 -0.9750E+00
Z =    -0.1000E+01  -C.5000E+00  F(Z) =     0.9167E+01  0.2104E+01
Z =    -0.1000E+01  -C.1000E+01  F(Z) =    -0.3704E+01  0.2279E+01
PJUMP = F    Z(1) =  -0.1000E+01  0.1000E+01     ADIFF = 0.4731E+00    ADIFFI = 0.1085E+02    NJUMP = 1    LEVEL = 0
Z =    -0.1000E+01   0.1000E+01  F(Z) =    -0.7221E+01 -0.1596E+01
Z =    -0.1000E+01   C.7500E+00  F(Z) =    -0.3855E+01 -0.3246E+01
Z =    -0.1000E+01   0.5000E+00  F(Z) =     0.1987E+01 -0.9750E+00
Z =    -C.1000E+01   0.2500E+00  F(Z) =     0.9612E+01 -0.2490E+01
Z =    -0.1000E+01   0.0         F(Z) =    -0.3704E+01  0.2279E+01
PJUMP = F    Z(1) =  -0.1000E+01  0.1000E+01     ADIFF = 0.2829E+00    ADIFFI = 0.6096E+00    NJUMP = 1    LEVEL = 1
Z =    -0.1000E+01   0.0         F(Z) =    -0.7221E+01 -0.1596E+01
Z =    -0.1000E+01  -0.2500E+00  F(Z) =     0.1965E+01  0.7049E+00
Z =    -0.1000E+01  -0.5000E+00  F(Z) =     0.1987E+01 -0.9750E+00
Z =    -0.1000E+01  -0.7500E+00  F(Z) =    -0.1043E+01  0.2777E+01
Z =    -0.1000E+01  -0.1000E+01  F(Z) =    -0.3704E+01  0.2279E+01
PJUMP = F    Z(1) =  -0.1000E+01  0.0            ADIFF = 0.2265E+00    ADIFFI = 0.5942E+00    NJUMP = 1    LEVEL = 1
Z =    -0.1000E+01  -0.1000E+01  F(Z) =    -0.3704E+01  0.2279E+01
Z =    -0.5000E+00  -0.1000E+01  F(Z) =    -0.9583E+00 -0.7917E+00
Z =     0.0         -0.1000E+01  F(Z) =     0.7250E+00 -0.1958E+00
Z =     0.5000E+00  -0.1000E+01  F(Z) =     0.3333E-01  0.1267E+01
Z =     0.1000E+01  -C.1000E+01  F(Z) =    -0.2846E+01  0.7958E+00
PJUMP = F    Z(1) =  -0.1000E+01 -0.1000E+01     ADIFF = 0.1964E+01    ADIFFI = 0.1258E+02    NJUMP = 2    LEVEL = 0
Z =    -0.1000E+01  -0.1000E+01  F(Z) =    -0.3704E+01  0.2279E+01
Z =    -0.7500E+00  -0.1000E+01  F(Z) =    -0.2339E+01  0.1104E+00
Z =    -0.5000E+00  -0.1000E+01  F(Z) =     0.7250E+00 -0.1958E+00
Z =    -0.2500E+00  -0.1000E+01  F(Z) =     0.1333E+00 -0.7771E+00
Z =     0.0         -C.1000E+01  F(Z) =    -0.2846E+01  0.7958E+00
PJUMP = T    Z(1) =  -0.1000E+01 -0.1000E+01     ADIFF = 0.1472E+00    ADIFFI = 0.6107E+00    NJUMP = 2    LEVEL = 1
```

AP-26

AVAILABILITY: LSQNK1 and LSQNK2 are available in load module form in the library SYS5.MATHLIB.SUBR and in source form in SYS5.MATHLIB.SOURCE. For further information about the use of these libraries refer to AP-60 or consult the Programming Assistants, Room 39-219.

CORE
REQUIREMENTS: LSQNK1 uses 19,068 bytes (4A7C in hexadecimal) of core storage. LSQNK2 uses 19,588 bytes (4C84 in hexadecimal) of core storage. This does not include the space required by the user-supplied CURVE and FUN function subprograms.

REFERENCES: LSQNK1 and LSQNK2 were written by Dorothy Zaborowski, an IPC staff member, with advice from Dr. James Rome of the M.I.T. Electrical Engineering Department, currently with the Oak Ridge National Laboratory, Oak Ridge, Tennessee.

LSQNK1 and LSQNK2 use Method B in the publication: Delves, L.M. and Lyness, J.N. "A Numerical Method for Locating the Zeros of an Analytic Function," Mathematics of Computation, Vol. 21, 1967.

The original articles for SQUANK are:

Lyness, J.N. ACM Algorithm 379. Communications of the ACM, Vol. 13 (April 1970), page 260.

Lyness, J.N. "Notes on the Adaptive Simpson Quadrature Routine," Journal of the ACM, Vol. 16, No. 3 (July 1969), pages 483-495.

ROOT4 was supplied by C.O. Beasley, Oak Ridge National Laboratory.

APPENDIX C

Domain of Analyticity of $\mathcal{D}(k)$

The dispersion relationship $\mathcal{D}(k)$ possesses branch lines where $Re(\gamma)$, with $\gamma = \left[(k^2 + k_\theta^2) \dfrac{\sigma_{II}^2 - N^2}{\sigma_{II}^2} + \dfrac{1}{4H^2} \right]^{1/2}$, changes sign. This is because we have chosen γ such that $Re(\gamma) > 0$. If we write $\gamma = |\gamma| e^{i(\theta + n\pi)}$, then the value n takes on will depend on the value θ such that $Re(\gamma) = |\gamma| \cos(\theta + n\pi) > 0$. Hence, in order to use SUBROUTINE LSQNK2, the contour in the k-plane must be chosen such that it does not include the branch lines.

To determine the position of the branch lines in the k-plane, we first write

$$\gamma = (k^2 A)$$

where $\kappa^2 = k^2 + k_\theta^2$ and $A = \dfrac{\sigma_{II}^2 - N^2}{\sigma_{II}^2} = |A| e^{i\phi}$ and determine the branch lines in the κ-plane. Since H is large, we shall neglect $1/4H^2$.

We write:

$$\kappa = |\kappa| e^{i\theta}$$

$$\gamma = \left(\kappa^2 A\right)^{1/2} = |\kappa| |A|^{1/2} e^{i\left(\theta + \frac{\phi}{2} + n\pi\right)}$$

so that $Re(\gamma) = |\kappa| |A|^{1/2} \cos\left(\theta + \frac{\phi}{2} + n\pi\right)$

We see that in order to have $Re(\gamma) > 0$

then $n = 0$ or even $\quad$ if $\left| \theta + \frac{\phi}{2} \right| < \frac{\pi}{2}$

$n = 1$ or odd $\qquad$, if $\left| \theta + \frac{\phi}{2} \right| > \frac{\pi}{2}$

Thus the branch lines in the κ-plane are at

$$\theta = \frac{\pi}{2} - \frac{\phi}{2}$$

and

$$\theta = -\frac{\pi}{2} - \frac{\phi}{2}$$
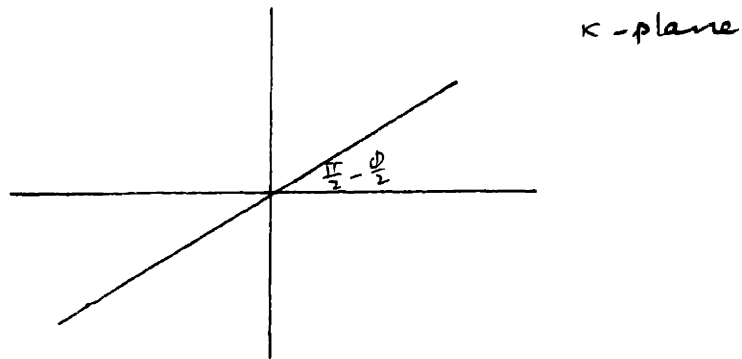
κ -plane

and the branch lines in the κ^2-plane are at

$$2\theta = \pi - \phi$$

and

$$2\theta = -\pi - \phi$$
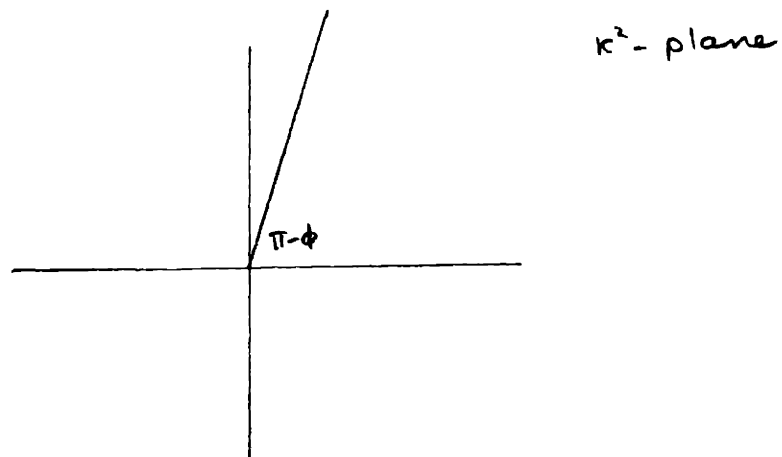
κ^2- plane

Since $k^2 = \kappa^2 - k_\theta^2$, the branch line in the k^2-plane is

k^2-plane

$\pi - \phi$

$k_\theta^2 \tan(\pi - \phi) = k_\theta^2 \tan \phi$

k_θ^2
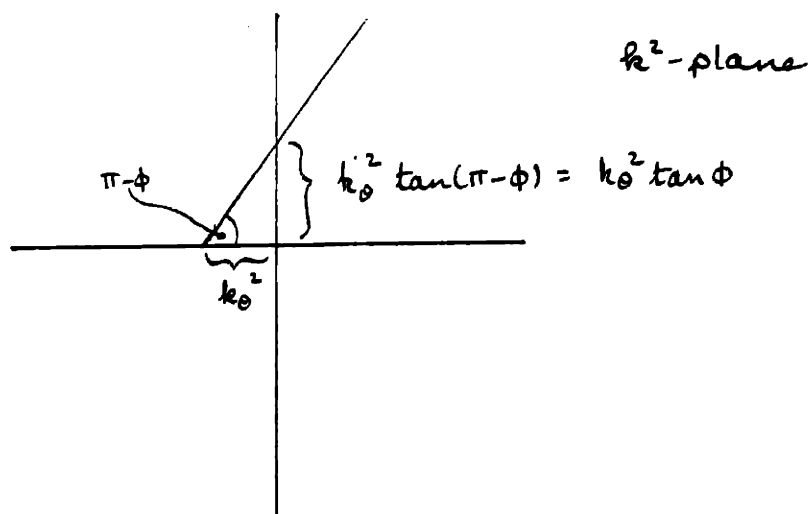
which translates to, on the k-plane:

k - plane

k_θ

$\frac{\pi}{2} - \frac{\phi}{2}$
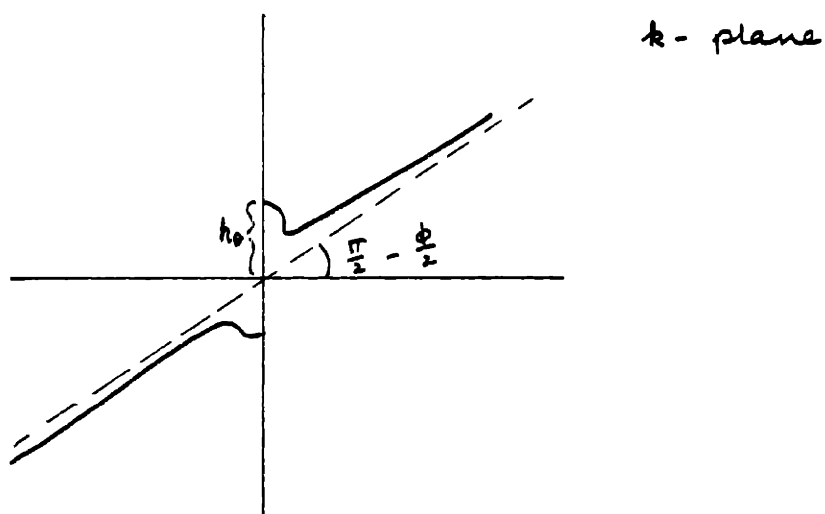
The branch line asymptotes to $\theta = \frac{\pi}{2} - \frac{\phi}{2}$ for large k.

Thus we choose the contour in the k-plane which avoids the branch lines:

k-plane

APPENDIX D

Asymptotic form of the parabolic cylinder function

Reference: Whittaker and Watson, A Course of Modern Analysis, Section 16.5

The parabolic cylinder function $D_n(\xi)$ is a solution of Weber's Equation

$$\frac{d^2 D_n(\xi)}{d\xi^2} + \left(n + \tfrac{1}{2} - \tfrac{1}{4}\xi^2\right) D_n(\xi) = 0 \qquad (D.1)$$

The other solution of Weber's Equations is $D_{-n-1}(i\xi)$.

We summarize below the asymptotic form of $D_n(\xi)$ for large ξ and different arguments of ξ :

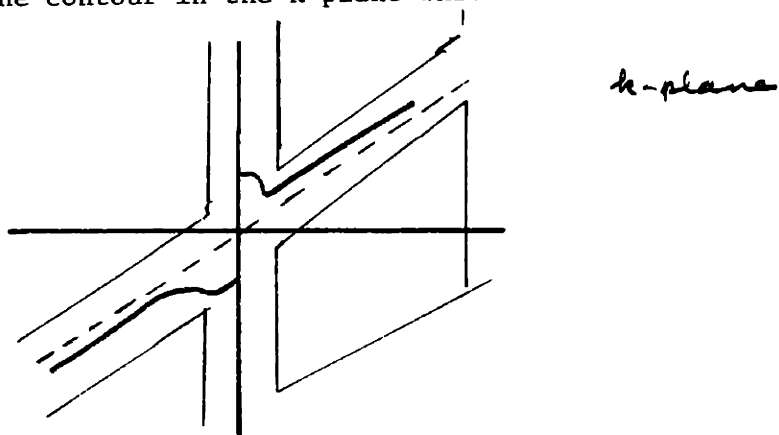$$D_n(\xi) \sim e^{-\frac{1}{4}\xi^2} \xi^n ; \qquad |\arg \xi| < \tfrac{3}{4}\pi \qquad (D.2)$$

$$D_n(\xi) \sim e^{-\frac{1}{4}\xi^2} \xi^n - \frac{\sqrt{2\pi}}{\Gamma(-n)} e^{n\pi i} e^{\frac{1}{4}\xi^2} \xi^{-n-1} ,$$
$$\tfrac{1}{4}\pi < \arg \xi < \tfrac{5}{4}\pi \qquad (D.3)$$

$$D_n(\xi) \sim e^{-\frac{1}{4}\xi^2} \xi^n - \frac{\sqrt{2\pi}}{\Gamma(-n)} e^{-n\pi i} e^{\frac{1}{4}\xi^2} \xi^{-n-1} ;$$
$$-\tfrac{5}{4}\pi < \arg \xi < \tfrac{1}{4}\pi \qquad (D.4)$$

LIST OF FREQUENTLY USED SYMBOLS

Symbol	Defined or first used	Definition
$A(r_1)$	4.4.8	coefficient of solution for $w_1^{(o)}$
$B(r_1)$	4.4.8	coefficient of solution for $w_2^{(o)}$
b	2.4.6	buoyancy $= \dfrac{\theta'}{\bar{\theta}} \dfrac{gD}{U^2}$
$C(r_1)$	4.4.8	coefficient of solution for $w_3^{(o)}$
c	3.1.4	mean circulation of hurricane
D	2.2.7	scale height of boundary layer $= \sqrt{\nu/f}$
D_2	3.4.14	depth of middle layer
$\mathcal{D}(k)$	4.2.5	dispersion relationship
f	2.2.1	Coriolis parameter
g	2.2.1	acceleration due to gravity
$\mathcal{G}(\omega;m)$	4.5.32	global dispersion relationship
H_1	3.4	height of lowest layer
H_2	3.1.1	height of top of boundary layer
$\mathcal{H}$	3.1.1	density scale height of atmosphere
i		$\sqrt{-1}$
$k(r_1)$	2.2.9	radial wave number
L	2.2.7	overall radial scale of hurricane
m	4.1.2	azimuthal wave number
N^2	2.4.6	Brunt-Vaisala frequency, squared
p	2.2.7	pressure (see under u for details)
r	1.1.1	radial coordinate
r_o	2.2.9	"fast" radial coordinate

r_1	2.2.8	"slow" radial coordinate
Re	2.2.11	Reynolds number
R_o	1.1.1	radius of eyewall
Ro	2.2.11	Rossby number
S_j	3.4.14	shear in j^{th} layer
t	2.2.1	time
u_*	2.2.1	radial velocity, dimensional perturbation
u', u	2.2.7	radial velocity, non-dimensional
u_j	3.4.3	u in j^{th} layer
$\overline{U}$	2.2.7	mean radial velocity
$\overline{U}_j$	3.4.1	$\overline{U}$ in j^{th} layer
$\overline{U}_I, \overline{U}_{II}$	3.4.1	$\overline{U}$ at $z = H_1$, $z = H_2$ respectively
U	2.2.7	velocity scale
$U_\perp$	3.4	velocity component perpendicular to wavefront
v	2.2.1	tangential velocity (see under u for details)
$\overline{V}_\infty$	3.1.4	$\overline{V}$ in hurricane interior
w	2.2.1	vertical velocity (see under u for details)
z	2.2.1	vertical coordinate
α	1.1.1	crossing angle
γ	4.4.9	vertical wavenumber in stratified layer
ε	2.2.8	small parameter = D/L
θ	1.1.1	azimuthal coordinate
Θ	2.2.1	potential temperature (see under u for details)
κ	3.4.9	horizontal wave number
ν	2.2.1	eddy coefficient of viscosity

ω	3.4.9	frequency
Ω	3.2.17	Earth's rate of rotation
ρ	2.2.1	density of air (see under u for details)
ρ_o	2.2.7	scaling parameter for ρ
σ	3.4.14	Doppler shifted frequency (see under u for details)

REFERENCES

Abdullah, A. J. (1966). The spiral bands of a hurricane: A possible dynamic explanation. J. Atmos. Sci., 23, 367-375.

Anthes, R. A., S. L. Rosenthal and J. W. Trout (1971). Preliminary results from an asymmetric model of the tropical cyclone. Mon. Wea. Rev., 99, 744-758.

Anthes, R. A. (1972). Development of asymmetries in a three-dimensional numerical model of the tropical cyclone. Mon. Wea. Rev., 100, 461-476.

Büdewadt, U. T. (1940). Die Drehströmung über festem Grunde. Z. angew. Math. Mech., 20, 241-253.

Carrier, G. F., A. L. Hammond, and O. D. George (1971). A model of the mature hurricane. J. Fluid Mech., 47, 145-170.

Charney, J. G. and J. Pedlosky (1963). On the trapping of unstable planetary waves in the atmosphere. J. Geophys. Res., 68, 6441-6442.

Charney, J. G. and A. Eliassen (1964). On the growth of the hurricane depression. J. Atmos. Sci., 21, 68-75.

Diercks, J. W. and R. A. Anthes (1976a). A diagnostic study of spiral bands in a nonlinear hurricane model. J. Atmos. Sci., 33, 959-975.

(1976b). A study of spiral bands in a linear model of a cyclonic vortex. J. Atmos. Sci., 33, 1714-1729.

Faller, A. J. (1961). An experimental analogy to and proposed explanation of hurricane spiral bands, Proc. 2nd Tech. Conf. on Hurricanes, June 1961, Nat. Hurricane Res. Proj., 50, 307-313.

(1963). An experimental study of the instability of the laminar Ekman boundary layer. J. Fluid Mech., 15, 560-576.

Faller, A. J. and R. E. Kaylor (1966). A numerical study of the instability of the laminar Ekman boundary layer. J. Atmos. Sci., 23, 466-480.

(1972). Instability of the stratified Ekman boundary layer and the generation of internal waves. J. Atmos. Sci., 29, 497-509.

Fletcher, R. D. (1945). The general circulation of the tropical and equatorial atmosphere. J. Met., 8, 167-174.

Hamming, R. W. (1962). Numerical Methods for Scientists and Engineers, 2nd ed., McGraw-Hill Book Company, New York, 721 pp.

Hawkins, H. and D. T. Rubsam (1968). Hurricane Hilda, 1964, II. Structure and budgets of the hurricane in October 1, 1964. Mon. Wea. Rev., 96, 617-636.

LaSeur, N. E. (1961). On the role of convection in hurricanes. National Hurricane Research Project Report No.50, pp.323-334.

Kessler, E., III and D. Atlas (1956). Radar Synoptic Analysis of Hurricane Edna, 1954. Geophysical Research Papers, No.50, Air Force Cambridge Research Center, 1956, 113 pp.

Krishnamurti, T. N. (1961). On the vertical velocity field in a steady symmetric hurricane. Tellus, 13, 171-180.

Kuo, H. L. (1971). Axisymmetric flows in the boundary layer of a maintained vortex. J. Atmos. Sci., 28, 20-41.

Kurihara, Y. and R. E. Tuleya (1974). Structure of a tropical cyclone developed in three-dimensional numerical simulation model. J. Atmos. Sci., 31, 893-919.

Kurihara, Y. (1976). On the development of spiral bands in a tropical cyclone. J. Atmos. Sci., 33, 940-958.

Lau, Y. Y., C. C. Lin and J. W.-K. Mark (1976). Unstable spiral modes in disk-shaped galaxies, Proc. Nat'l Acad. Sci., USA, 73, 1379-1381.

Ligda, M. G. H. (1955). Analysis of motion of small precipitation areas and bands in the hurricane, August 23-28, 1949. M.I.T. Weather Radar Research Technical Note Number 3.

Lilly, D. K. (1966). On the instability of the Ekman boundary layer. J. Atmos. Sci., 23, 481-494.

Lin, C. C. (1955). The Theory of Hydrodynamic Stability, Cambridge University Press, London, 155 pp.

(1966). On the mathematical theory of a galaxy of stars. J. SIAM , 14, No.4, July 1966.

(1970). Theory of spiral structure. International Astronomical Union, Highlights of Astronomy, 2, 88-121.

Lin, C. C. and F. H. Shu (1964). On the spiral structure of disk galaxies. Astrophys. J., 140, 646-655.

Malkus, J. S., C. Ronne and M. Chaffee (1961). Cloud patterns in Hurricane Daisy. Tellus, 13, 8-30.

Mark, J. W.-K. (1977). On density waves in galaxies: Maintenance of spiral structure and discrete normal modes. Astrophys. J. (in press).

Mathur, M. B. (1975). Development of banded structure in a numerically simulated hurricane. J. Atmos. Sci., 32, 512-522.

Morse, P. M. and H. Feshbach (1953). *Methods of Theoretical Physics*, Part I, McGraw-Hill Book Co., Inc., New York, 997 pp.

Nayfeh, A. H. (1973). *Perturbation Methods*, J. Wiley & Sons, New York, 425 pp.

Oort, J. H. (1962). Spiral Structure, in *Interstellar Matter in Galaxies*, L. Woltjer, ed., Benjamin, New York, pp.234-244.

Rayleigh, Lord (1880). On the stability, or instability, of certain fluid motions. London Math. Soc. Proc., 11, 57-70. [*Scientific Papers*, 1, 474-487, Cambridge University Press].

(1887). On the stability or instability of certain fluid motions, II. London Math. Soc. Proc., 19, 67-74. [*Scientific Papers*, 3, 17-23, Cambridge University Press].

Rivas, E. K.- (1975). A numerical scheme to solve unstable boundary layer problems. Submitted to *J. Comp. Phys*.

Schlichting, H. (1960). *Boundary Layer Theory*, 4th ed., McGraw-Hill Book Co., Inc., New York, 647 pp.

Senn, H. V., H. W. Hiser and R. C. Bourret (1957). Studies of hurricane spiral bands as observed by radar. NHRP Report 12.

Senn, H. V. and H. W. Hiser (1958). The origins and behavior of hurricane spiral bands as observed on radar. Proc. of Seventh Weather Radar Conference, Am. Met. Soc., K46-K55.

(1959). On the origin of hurricane spiral rainbands. *J. Met.*, 16, 419-426.

Smith, R. K. (1968). The surface boundary layer of a hurricane, *Tellus*, 20, 473-484.

Tatehira, R. (1961). A mesosynoptic and radar analysis of typhoon rain band. Proc. of the Second Technical Conference on Hurricanes, June 27-30, 1961, Miami Beach, Fla., NHRP Report 50, 115-126.

Tatro, P. R. and E. Mollô-Christensen (1967). Experiments on Ekman layer instability. *J. Fluid Mech.*, 28, 531-544.

Tepper, M. (1958). A theoretical model for hurricane radar bands. Proc. of the Seventh Weather Radar Conference, Miami Beach, Fla., Nov.17-20, 1958, Am. Met. Soc., K56-K65.

Wexler, H. (1947). Structure of hurricane as observed by radar. Annals of N.Y. Academy of Sciences, 48, Art.8, September 15, 1947, 821-844.

Whittaker, E. T. and G. N. Watson, *A Course of Modern Analysis*, 4th ed., Cambridge University Press, 608 pp.

Yamamoto, R. (1963). A dynamical theory of spiral rain band in tropical cyclones. Tellus, 15, 151-161.

BIOGRAPHICAL NOTE

I was born on April 11, 1949, in Hong Kong, and attended secondary school there. After one year at the Utica College of Syracuse University, I transferred to M.I.T., where I received my S.B. in Applied Mathematics in 1971. In the fall of 1971, I entered the Department of Meteorology.

I was married on December 30, 1976 to Jim Bishop.